Ricardo Jorge Sousa da Silva

Mestre em Engenharia Química e Bioquímica

Compact simulated countercurrent chromatography for downstream processing of (bio)pharmaceuticals

Dissertação para obtenção do Grau de Doutor em
Engenharia Química e Bioquímica

Orientador:
Prof. Doutor José Paulo Barbosa Mota, Prof. Catedrático
Faculdade Ciências e Tecnologia

FACULDADE DE
CIÊNCIAS E TECNOLOGIA
UNIVERSIDADE NOVA DE LISBOA

Setembro de 2013

to Ângela, who always believed in me, even more than I ever did, and kept me moving forward

essentially, all models are wrong, but some are useful
George P. Box (1987)

Acknowledgements

Completing my PhD was one of the most challenging things I ever done. The best part of this journey is to look back and remember all the friends made, the (un)finished work, and all the good and bad experiences. This journey wouldn't be possible to accomplish without the support and encouragement of a great number of people over the past four years.

My first debt of gratitude must go to my advisor, Prof. José Paulo Mota, for the challenges and opportunities presented. His insight, encouragement, friendship and hard questions provided me the vision necessary to complete my PhD.

I would like to acknowledge Fundação para a Ciência e Tecnologia (FCT/MCTES) for the financial aid in the form of a PhD grant.

To my friends and colleagues at FCT/UNL, to Isabel Esteves for all your help, insight, friendship along these years and support in the tough times; to Prof. Mário Eusébio, Andriy Lyubchik, Fernando Cruz; to my recent colleagues Rui Ribeiro, Eliana, Barbara, and João; and specially to Rui Rodrigues, who in the first years of my PhD provide me with the experimental knowledge needed to accomplish this challenge. I would also like to acknowledge Dr. Cristina Peixoto and Piergiuseppe Nestola from IBET.

I am deeply grateful to my parents, for all the support and sacrifices that you've made for me. I can only hope that one day match the example you have set. To my sister, who was never short of words, and patience.

To Ângela, who I can't thank enough for encouraging me through this journey and for all the time lost that I will try to make up.

Table of Contents

List of Figures

List of Tables

Resumo

A recente redução de escala da tecnologia de Leito Móvel Simulado (LMS) possibilitou o aparecimento de novas aplicações, como a purificação de produtos de química fina, ácidos orgânicos, produtos de índole farmacêutica, anticorpos monoclonais e proteínas recombinantes. O nosso grupo desenvolveu recentemente uma nova classe de processos LMS semi-contínuos que utilizam duas colunas cromatográficas em anel aberto. Estes processos exploram os benefícios do processo LMS mas, utilizando uma configuração de nodos flexível, uma operação robusta das bombas e modulação cíclica dos caudais. A grande vantagem do processo sugerido é a sua simplicidade de operação pois, independentemente do número de colunas, são apenas necessárias duas bombas – uma para a adição de alimentação e outra para a adição de dessorvente – bem como válvulas simples com uma operação on-off, por forma a controlar os caudais de fluidos retirados do sistema. A performance do nosso processo foi testada com sucesso numa separação enantiomérica não linear, usando duas estratégias de eluição.

O princípio de operação do processo de duas colunas mencionado anteriormente, descarta a divisão do fluxo de caudal em duas ou mais correntes num determinado porto de colecta: a fracção de produto, resíduo, ou passíveis de reciclo são sempre obtidas pelo direccionamento do efluente, durante um determinado período do ciclo produtivo, para um destino apropriado. Esta estratégia de gestão dos portos de colecta é também explorada no processo Relay-SMB (R-SMB). Neste processo a analogia com o LMS padrão em termos de volumes eluídos é mantida, evitando contudo o uso de controladores de caudal ou bombas adicionais. Neste processo o efluente de uma zona (ou coluna) encontra-se sempre num dos seguintes estados: (i) estagnado, (ii) direccionado completamente para a zona (ou coluna) seguinte, ou (iii) direccionado completamente para uma linha de colecta de produto. Para esta classe de processos foi desenvolvido um processo análogo ao LMS – o processo R-SMB e demonstrado de acordo com a teoria do equilíbrio que este último tem a mesma região separativa que o processo de LMS padrão para um sistema de adsorção linear. De acordo com a teoria do equilíbrio, os resultados demonstram que o R-SMB é composto por dois ciclos distintos que apenas diferem num passo intermédio, que é dependente da selectividade da separação a considerar.

Em muitos dos problemas de purificação de produtos biológicos, o composto desejado encontra-se numa posição intermédia entre dois grupos de impurezas - menos ou mais adsorvidas. Um corte central é, então, uma alternativa viável para a recuperação do produto de interesse. O processo de reciclo em estado estacionário com gradientes (GSSR) é composto com um sistema multi-coluna em anel aberto com um gradiente de solventes e uma operação em estado estacionário cíclico. É especialmente indicado para separações ternárias, visto que possibilita a existência de três fracções ou produtos, sendo o produto de interesse contido na fracção intermédia. Uma descrição detalhada do processo GSSR é fornecida, realçando a sua versatilidade, flexibilidade e simplicidade de operação. A validação experimental numa unidade piloto é também fornecida, usando para este fim a separação de uma mistura de proteínas em fase reversa como referência e caso de estudo.

Embora a operação em estado contínuo de sistemas cromatográficos seja significativa, a indústria biofarmacêutica encontra-se ainda cética quanto à adoção de processos cromatográficos multi-coluna. Isto é, em parte, devido à complexidade acrescida da validação do processo. Contudo, a implementação de tecnologias de utilização única e descartável estão neste momento a mitigar este ceticismo, havendo assim espaço para o desenvolvimento de um processo cromatográfico semi-contínuo, compacto e eficiente. Neste sentido, foi estudada a possibilidade de utilização de um sistema cromatográfico em contra-corrente, composto por duas colunas em anel aberto. A separação de um adenovírus, utilizando cromatografia de exclusão em condições isocráticas foi conseguida com sucesso e é também reportada.

Abstract

The recent scale-down of the Simulated Moving Bed (SMB) technology led to new applications, including the purification of fine chemicals, organic acids, pharmaceutics, monoclonal antibodies, and recombinant proteins. We developed a novel class of semi-continuous, two-column, open-loop SMB systems. These processes exploit the benefits of the SMB but with a flexible node design, robust pump configuration, and cyclic flow-rate modulation. The major advantage of our design is the simplicity of its physical realization: regardless of the number of columns, it uses only two pumps — one to supply feed and another to supply desorbent — and simple two-way valves to control the flow rates of liquid withdrawn from the system. The performance of our process was successfully tested on a nonlinear enantiomeric separation, using two types of elution strategies.

The operating principle of our two-column SMB systems discards the splitting of the flow into two or more streams at an active outlet: the product, waste, or recycled fractions are always obtained by completely directing the effluent over a certain period of the cycle to the appropriate destination. This strategy of handling the product outlets was also explored in the Relay SMB. In this process, the analogy with the standard SMB in terms of displaced volumes of fluid per switch interval is maintained, whilst avoiding the use of flow controllers or an extra pumps. In this process the flow through a zone (or column) is always in one of the three states: (i) frozen, (ii) completely directed to the next zone (or column), or (iii) entirely diverted to a product line. For this class of processes we derive a SMB analog — the R-SMB process and demonstrate, under the framework of the equilibrium theory, that this process has the same separation region as the classical SMB for linear adsorption systems. In addition, the results from the equilibrium theory show that the R-SMB process consists of two distinct cycles that differ only in their intermediate sub-step depending on the selectivity of a given separation.

For many biopurification problems, the desired product is intermediate between weakly and strongly adsorbing impurities, and a central cut is thus required to get the desired product. The Gradient Steady State Recycling (GSSR) process comprises a multi-column, open-loop system with a solvent gradient and cyclic steady-state

operation. It is particularly suited for ternary separations: it provides three main fractions or products, with a target product contained in the intermediate fraction. A comprehensive description of the GSSR process is given, highlighting the versatility, flexibility, and ease of operation of the process. The experimental validation in a pilot unit is provided, using the purification of a crude peptide mixture by reversed phase as a benchmark and case study.

Despite the advantages of a continuous chromatography, biopharmaceutical industry is somehow skeptical about moving to multi-column chromatography. This is, in part due to the increase in complexity in terms of process validation. However, the implementation of single use and ready to process technologies are mitigating these issues, therefore there is room for exploring a single compact and efficient multi-column chromatographic process. In this sense, the use of a simple semi-continuous, open-loop, two-column, countercurrent chromatographic process was studied. The separation of adenovirus serotype 5 (Ad5) was successfully accomplished by size-exclusion chromatography under isocratic elution conditions.

1 Introduction

1.1 Relevance and Motivation

Chromatography is one of the simplest, yet effective, separation methods, able to separate any soluble or volatile component if the right column configuration, operating conditions, mobile phase, and stationary phase are employed. Batch chromatography, because of its ease of operation and low capital investment, is a well-established process used in many large-scale industries, like sugar processing, and to some extent in the hydrocarbon industry; also chromatography proven to be very useful, as both an analytical and preparative or process-scale purification, in small-scale applications such as the pharmaceutical, biotechnology, fine chemistry, and food processing industries. Although batch chromatography can be very flexible, allowing the recovery of several fractions from a feed mixture in a single operation, it suffers from the drawbacks of batch operation, the products are recovered at a high dilution rate, the stationary phase is not efficiently used, and the purity of the recovered fractions is extremely dependent on the selectivity of the chromatographic system.

One way to overcome the above mentioned problems and to improve the separation efficiency is to operate the process in countercurrent mode, with the mobile phase circulating in opposite direction relative to the stationary phase. This is the operating principle of a moving-bed system, with the True Moving Bed's being the best idealization of the concept of continuous countercurrent adsorption chromatogra-

phy (not to be confused with liquid-liquid countercurrent chromatography). In a binary separation, the moving bed achieves of high purity, even if the resolution of the system is not excellent, because only the purity at the two tails of the concentration profiles, where the withdrawal ports are located, is of interest. This is contrary to batch chromatography where the purity of the products is dependent of the system resolution. It is also clear that the loading of the stationary phase is higher in a moving bed than in a fixed bed system, which leads to a higher productivity per unit mass of stationary phase. However, the advantages of the *TMB* process are rapidly overcome by the difficulty of its physical realization; therefore, in practice the continuous movement of the stationary phase is simulated in a discrete way by replacing the moving bed by a circular train of fixed beds packed with the stationary phase and periodically moving the inlet and outlet ports in the same direction as the fluid flow—this is the Simulated Moving Bed (SMB) process.

The first large-scale commercial application of continuous simulated countercurrent adsorption was developed by *UOP* (Universal Oil Products, Des Plaines, Illinois, USA) in the early 1960s, under the generalized name of Sorbex.

In the last decades, the scaling-down of the SMB technology led to a new set of applications, especially in the purification of fine chemicals, organo acids, pharmaceutics, monoclonal antibodies, or recombinant proteins. A new trend in SMB processes emerged from the demands of these new type of applications. Smaller and more versatile configurations are preferred, no longer making use of the initial process configuration where several columns with large dimensions were employed. The moving trend is supported by an increase in complexity, which in most cases requires highly versatile equipment and advanced optimization tools.

Although the SMB process increases throughput, purity, and yield relative to batch chromatography, the batch process still presents the obvious advantages of being easy to operate, requiring a low capital investment, and being easily prone to the application of solvent gradients or center-cut separations.

The development of new chromatographic processes that attempt to combine the ”best of both worlds” of batch and SMB operation poses a challenge, whose solution can bring economical advantages to the industry and lead to new applications in the field of chromatographic separations.

1.2 Objectives and Outline

This thesis is organized into nine chapters. The present chapter describes the relevance and motivation of the work as well as the structure of the thesis.

Chapter 2 introduces the principles of TMB and SMB chromatography. Moreover, a brief review of the state of the art on the SMB processes and applications is included. This chapter finalizes with an introduction to chromatographic separation techniques used for the separation of biological products.

Chapter 3 presents a proof of concept of the application of a streamlined, two-column SMB system, developed by our group, to a nonlinear chiral separation problem. In this chapter we also present two different elution strategies that can be implemented in the two-column system. These strategies are analyzed numerically and compared to the reference cases of batch chromatography and steady-state recycling. This chapter is based on the submitted paper to Journal of Chromatography A:

- R.J.S. Silva, R.C.R. Rodrigues, J.P.B Mota, Two-column streamlined simulated moving bed applied to a nonlinear chiral separation.

Chapter 4 deals with the concept and design criteria for a new class of multicolumn chromatographic processes that change the classical way of handling the product outlets of simulated moving-bed (SMB) chromatography to avoid the use of flow controllers or an extra pump. Despite the simplified manipulation of the zone flow rates, the R-SMB process maintains the analogy with the SMB in terms of displaced volumes of fluid per switch interval. This chapter is based on work published in

- Ricardo J.S. Silva, Rui C.R. Rodrigues, José P.B. Mota, Relay simulated moving bed chromatography: Concept and design criteria, Journal of Chromatography A, 1260 (2012),132-142.

Chapter 5 presents the experimental validation of the Relay simulated moving bed concept, presented in the previous chapter. This chapter is an extension of the previous work done in this field

Chapter 6 reports the process rationalization and pilot unit validation used for the proof of concept of the Gradient with Steady State Recycling (GSSR) process for center-cut separation of multicomponent mixtures. This chapter is based on the work published in

- Ricardo J.S. Silva, Rui C.R. Rodrigues, Hector Osuna-Sanchez, Michel Bailly, Eric Valéry, José P.B. Mota, A new multicolumn, open-loop process for center-cut separation by solvent-gradient chromatography, Journal of Chromatography A, 1217 (2010), 8257-8269.

Chapter 7 deals with the model-based analysis of the process and the optimal cycle design. We also report on the experimental validation of this process. The work described in the previous chapter and in the present one is summarized and some conclusions are drawn.

Chapter 8 describes the application of the two column simulated moving bed system, using size exclusion chromatography, in the purification of adenovirus. This chapter is based on the paper submited to Journal of Chromatography A:

- Piergiuseppe Nestola, Ricardo J.S. Silva, José P.B. Mota, Adenovirus purification by two-column, size-exclusion, simulated countercurrent chromatography.

In Chapter 9, a few remarks and ideas for future work are presented, before summarizing the work and drawing final conclusions.

2

Simulated Moving Bed technology: a brief review

2.1 Introduction

The Simulated Moving Bed (SMB) is a multicolumn, continuous, countercurrent adsorption separation process that, generally speaking, increases throughput, purity, and yield. The first large-scale commercial application of continuous simulated counter-current adsorption was developed by UOP (Universal Oil Products) in the early 1960s, since then, the SMB technology has been widely used in the petrochemical (xylene isomer separation) and food industries (glucose-fructose separation) on a multi-ton scale. In the last two decades, with the advent of stable bulk stationary phases for chromatographic enantioseparation, the SMB principle has been successfully transferred to the pharmaceutical industry.

The most recent applications of SMB technology, such as the purification of fine chemicals, organic acids, pharmaceuticals, monoclonal antibodies, or recombinant proteins, no longer make use of the original configuration, where several columns with large dimension are employed. Today it is possible to build SMB systems with column sizes ranging from 4 to 1000 mm inner diameter and to produce pharmaceuticals on a small scale as well as on a 100-ton scale. This has opened the opportunity for smaller and more versatile configurations, which are however more complex to operate, thus making an empirical design quite difficult and requiring

modeling and simulation for reliable process design and optimization.

2.2 Principle of SMB Technology: the concept of True Moving Bed

The operation of a SMB unit can be best understood by means of the ideal concept of the TMB, which involves the actual circulation of the solid at a constant flow rate in opposite direction to the fluid phase. Furthermore, liquid and adsorbent streams are continuously recycled as shown in figure 2.1. The feed is continuously injected into the middle of the system and two product lines are collected: the extract, rich in the more retained components, and preferentially carried with the solid phase, and the raffinate, rich in the less retained components that move with the liquid phase. Also, pure solvent is continuously injected at the beginning of section I and admixed with the liquid recycled from the downstream end of section IV.

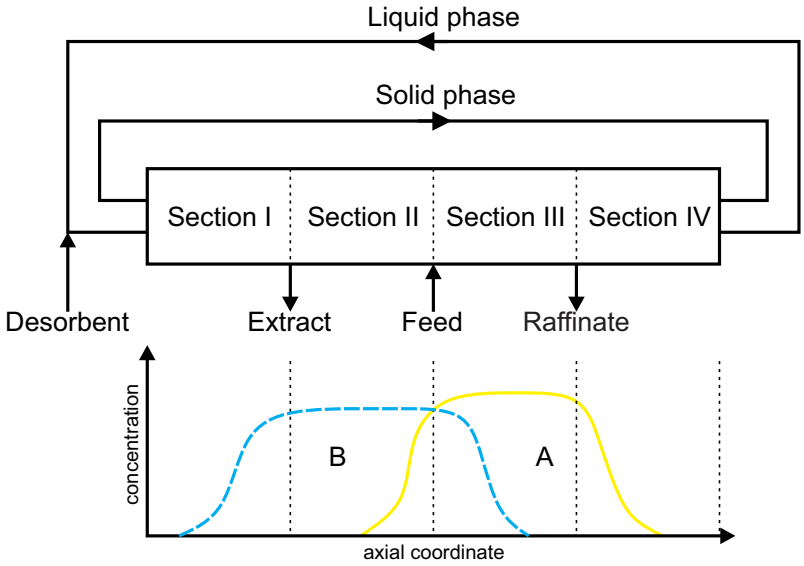

Figure 2.1: Schematic of a four-section TMB. The separation A and B is carried out in sections II and III. The collection of products A and B is performed in the extract and raffinate streams, respectively.

Because of the addition and withdrawal of the four streams, the TMB unit can be divided into four sections or zones with different flow rates of the liquid phase, where each section plays a specific task in the separation. The separation of components A and B is performed in sections II and III, where the more retained component B has to be adsorbed and carried towards the extract port through the movement of the solid, while the less retained component A has to be desorbed

and carried by the mobile phase in the direction of the raffinate port. In section I the solid is regenerated by desorption of the strongly adsorbed component with fresh eluent stream. Finally, in section IV the liquid is regenerated by adsorption of the less retained component that was not collected in the raffinate. With this arrangement it is possible to recycle back both the solid and liquid phase to sections IV and I, respectively. With a proper choice of the internal flow rates and solid phase velocity, the feed mixture can be completely separated into two pure products, even if the resolution of the system is not excellent because only the purity at the tails of the concentration profiles, where the withdrawal ports are located, is of interest. This is contrary to batch chromatography, where high resolution is vital in order to achieve high purity. It is also evident that a larger portion of the stationary phase is loaded in the moving-bed system than in a fixed-bed system. This will ultimately lead to a higher productivity per unit mass of stationary phase.

However, the movement of the adsorbent particles, which are in most cases within the micrometer range, is technically unfeasible as a result of particle attrition and backmixing. Therefore, in practice the movement of the solid phase is simulated by using fixed beds of adsorbent (chromatographic columns) and periodically moving the inlet and outlet ports in the same direction as the fluid flow. The simulated countercurrent behavior of the process becomes obvious when the relative movement of the packed beds with respect to the inlet and outlet streams is followed over several switching intervals (a switching interval is the time interval between consecutive switches of the positions of the inlet and outlet ports). After a number of switching intervals equal to the number of columns in the system, one cycle is completed and the initial positions of all external streams are reestablished.

Due to the continuous nature of countercurrent operation, after the initial transient start-up a TMB unit attains a steady state. On the contrary, the steady regime attained by the discrete movement of the solid in a SMB unit is periodic, that is, it exhibits the same time-dependent behavior over every switching interval.

The equivalence between the concepts of TMB and SMB becomes stronger as the number of SMB columns increases and their size decreases accordingly so as to maintain the same amount of adsorbent. Thus, if the number of SMB columns is not too small, say more than 5 columns, the simpler model of the TMB unit can be employed to predict the separation performance of the equivalent SMB unit, provided that some geometric constraints and conversion rules are fulfilled. The equivalence rules between the TMB and SMB are given by the following

relationships:

$$V_j = N_j V \tag{2.1}$$

$$\frac{V}{\tau} = \frac{Q_S}{1-\epsilon} \tag{2.2}$$

$$Q_j^{SMB} = Q_j^{TMB} + \frac{Q_S}{1-\epsilon} \tag{2.3}$$

Here V is the volume of a SMB column whereas V_j is volume of the j^{th} section of the TMB unit; N_j is the number of subsections in the j^{th} section of the SMB unit, τ is the length of the switching interval of the SMB unit, ϵ is the void fraction of the adsorbent bed, Q_S, is the volumetric solid flow rate in the TMB unit, and Q_j^{SMB} and Q_j^{TMB} are, respectively, the volumetric fluid flow rates in the equivalent SMB and TMB units.

2.3 SMB process

Classical SMB systems are characterized by the synchronous and downstream shifting by one column of all inlet and outlet lines after a defined switching interval τ. As mentioned above, in a classical SMB it is possible do distinguish four different sections defined by different liquid flow rates (figure 2.2). The number of columns may be evenly distributed or not over the four sections; however, by definition each section has an integer number of columns, $N_I/N_{II}/N_{III}/N_{IV}$, and the sum of the number of columns over the four sections is equal to the total number of columns. Fig. 2.2 shows an example of a SMB system with a $1/2/2/1$ column configuration.

2.4 SMB operation with variable parameters

The scale-down of the original SMB process into smaller SMB units has been gaining an increasing interest over the last two decades. The recent rapid growth of these newly emerging SMB applications has been accompanied by the development of novel SMB schemes that are based on the conventional SMB process, but function with time-variable operating parameters. The following modes of SMB operation presented in this chapter aim to extend the potential of the standard SMB process. It is worth noting that, for sake of brevity, only the operation in liquid phase is

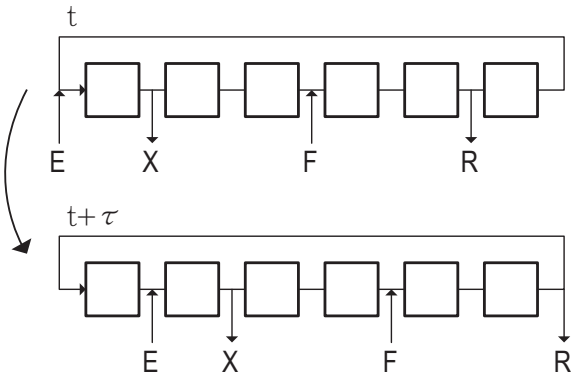

Figure 2.2: Schematic diagram of a four-section SMB unit for two consecutive switching intervals, where the upper diagram depicts the instant t, and the bottom diagram depicts the instant $t + \tau$ where the input and withdrawl ports are moved one column ahead. The position of eluent (E), feed (F), extract (X), and raffinate (R) ports are identified by arrows.

considered.

2.4.1 Varicol

The Varicol process [1, 2] generically consists of performing a predetermined sequence of asynchronous port switchings over every switching interval, resulting in a time-periodic modulation of the zone lengths. When the process dynamics is averaged over a complete cycle the Varicol scheme is equivalent to a non-integer allocation of the number of columns per section. The possibilities for asynchronous port switching are endless; for example, in principle it is possible that a port may shift more than once during the switching interval, either forward or even backwards. As a result, Varicol schemes can have an infinite number of column configurations though only a small subset of them will give rise to high-performance processes.

In Fig. 2.3 we show the example of a standard SMB operation, where the topmost configuration $(1/2/2/1)$ is kept constant during the whole switching interval $t \leq \tau$; when $t = \tau$ all ports are switched forward by one column in the direction of fluid flow. In the Varicol process the ports are switched asynchronously. For example, after a fraction $\alpha < 1$ of the switching interval the position of the feed port is moved forward by one column, giving rise to the middle configuration, which has increased zone II by one column $(1/3/1/1)$; at the end of the switching interval all ports have moved forward by one column like in the standard SMB scheme, and the process returns to the original zone configuration $(1/2/2/1)$.

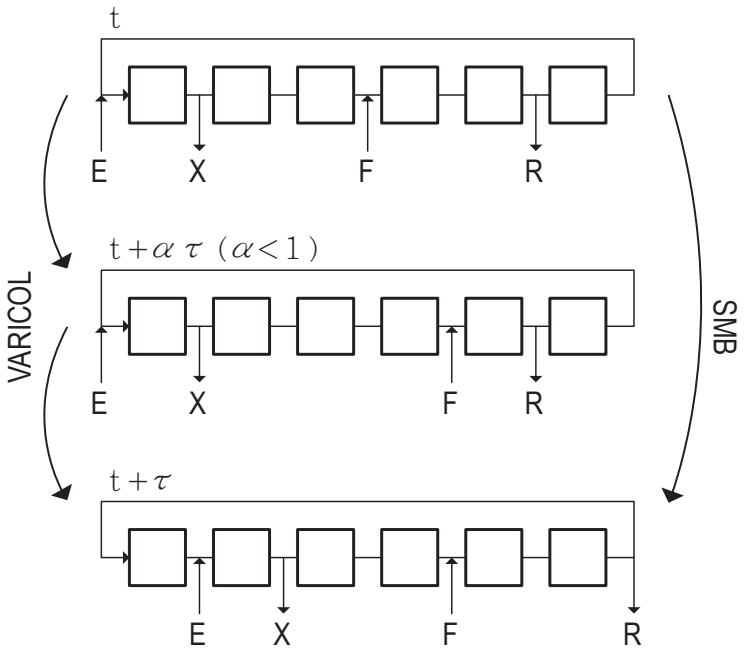

Figure 2.3: Simplified scheme of the Varicol process. The position of eluent (E), feed (F), extract (X), and raffinate (R) ports are identified by arrows.

2.4.2 PowerFeed

This concept was originally introduced by Kearny and Hieb [3], and studied in more detail by other authors [4–6]. Like the conventional SMB process, the switching of the external ports are kept constant, in contrast to the Varicol process. The additional performance improvement is created by the modulation of some or all flow rates during each switching interval. Consequently, the internal flow rates also change within a switching period. Fig. 2.4 shows an example of the Powerfeed process, where the shaded areas are proportional to the flow rate in the corresponding section.

2.4.3 ModiCon

Another variant of the classical SMB process is the ModiCon process [7, 8]. Like in the standard SMB operation, the Modicon process is synchronous and also characterized by a constant flow rate in each section; the performance improvement is achieved by time modulation of the feed concentration over the switching interval. One drawback of this scheme is that it only works for nonlinear separations and is only effective for separations where the feed concentration is limited by technical reasons and not by the solubility of the components in the used solvent.

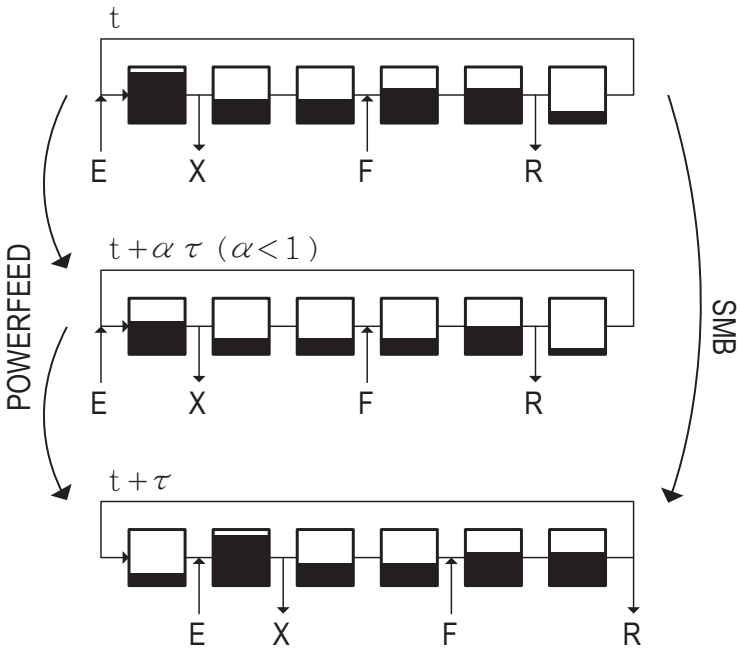

Figure 2.4: Simplified scheme of the PowerFeed process. The position of eluent (E), feed (F), extract (X), and raffinate (R) ports are identified by arrows. The height of each shaded area is proportional to the flow-rate through the corresponding section. The standard SMB scheme keeps the topmost configuration constant over the whole switching interval τ; all ports are then switched forward by one column in the direction of fluid flow. In PowerFeed operation, which is illustrated by the intermediate step, the flow-rates are varied over a fraction of the switching interval but the ports are only moved forward by one column at the end of the step like in the standard SMB process.

2.4.4 Improved-SMB or Intermittent-SMB

The main application area of the ISMB [9, 10] (Improved-SMB or Intermittent-SMB) concept is the sugar industry [11]. In this process the switching interval is partitioned as follows: in the first part of the period, all external lines (desorbent and feed inlets as well as extract and raffinate outlets) are distributed as in a standard SMB scheme. However, in contrast to a classical SMB unit, the outlet of section IV is not recycled during this part of the switching interval and, consequently, the flow rate in section IV is zero. During the second part of the switching interval all external ports are closed and recirculation is performed with a constant flow rate in all sections of the plant. This SMB scheme allows a separation to be carried out with a rather small number of columns, which of course has a positive impact on investment costs.

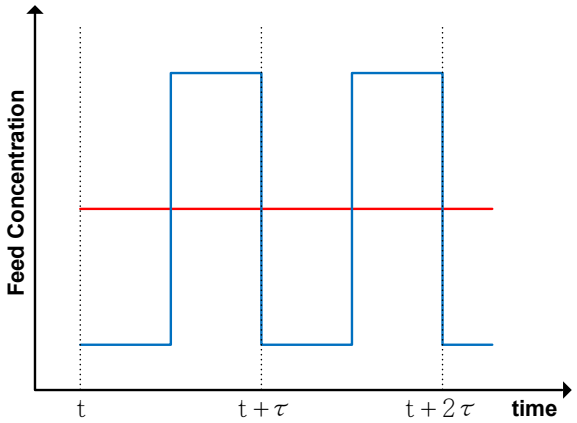

Figure 2.5: Temporal profiles of the Feed concentration in the standard SMB (in red) and Modicon (in blue) over two consecutive switching intervals. Both processes are characterized for a fixed section configuration over the switching intervals. In the exemplified case a period of the switching interval is characterized by a pure eluent feed (cF = 0), followed by a step wave where cF is two times the feed concentration of the equivalent SMB process.

2.4.5 Partial-Feed, Partial-Withdrawal/Discard and Outlet-Swing Stream SMB

In the classical SMB process the composition and flow rate of the feed is constant over the whole switching interval. The approach in the Partial-Feed [12] process introduces two more degrees of freedom, the feed duration and feed time. Fig. 2.7 depicts the flow-rate of the feed and raffinate ports in a Partial-Feed operation. As one can easily understand, in order to fulfill the mass balance constraints the raffinate flow rate changes according to the variation of the feed flow. In the case of the Partial-Feed operation the duration of the feed is shorter, but the introduced flow rate is higher. By this procedure the total amount of feed is kept constant, while productivity and eluent consumption may increase.

The concept of partial withdrawal [13], which is based on the variation of the raffinate flow rate in a three-zone SMB, can be used to withdraw the more concentrated part of the profile or to leave inside the system the most diluted part, respectively. As a consequence, the eluent consumption can be decreased for a given purity requirement. An analogous operation is the so-called partial-discard. In this case, although the recovery of the two product outlets is complete, only a part of the outlet is kept in order to improve the overall purity and the remaining is discarded [14] or recirculated back to the feed [15, 16].

The outlet swing stream-SMB (OSS-SMB) [17] is somewhat similar to the partial-withdrawal techniques. With this type of operation it is possible to expand or

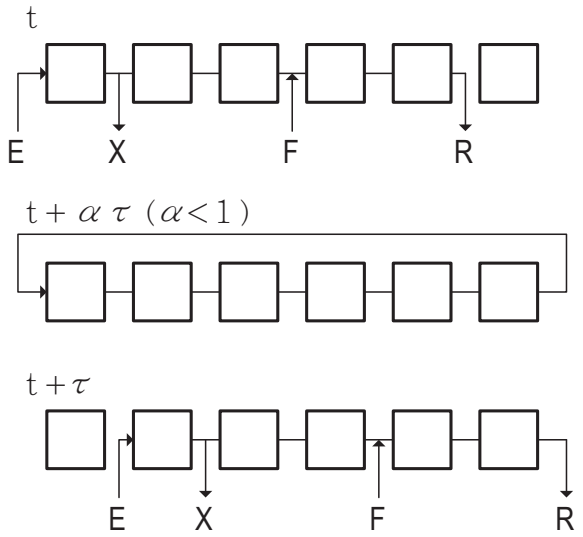

Figure 2.6: Port configuration of an I-SMB scheme for two consecutive switching intervals. In this process, the inlet and outlet ports are only active in a certain period of the switching interval, this is followed by a step of internal recycling at a discrete flow-rate.

contract the product fronts near the withdrawal points, by manipulating the outlet flow rates, thus allowing the variation of flow rates in sections I and IV while keeping the flow rates in sections II and III constant by modulating the eluent flow rate.

2.4.6 Other examples of non-standard SMB operation

The 3-zone SMB scheme is probably one of the simplest schemes that deviates from the classical 4-zone SMB [18]. This configuration relies on the removal of zone IV, letting all fluid coming from zone III to be collected as raffinate, which prevents any contamination of the extract coming from the recirculation line.

More recently, Jin and Wankat [19] theoretically derived a 2-zone SMB for binary separation in which they incorporate a storage tank to temporarily hold the solvent for later use. One-column processes that reproduce the cyclic behavior of the multicolumn SMB chromatography by means of a recycle lag have also been proposed [20, 21]. This setup exploits the cyclic behavior of the SMB where all columns are subjected to the same inlet/outlet concentration waveform every $N\tau$ time units.

The original SMB process is only suitable for binary separations: the partitioning of one or more less retained components (raffinate) from one or more retained components (extract). However, in most separation cases the mixture is composed

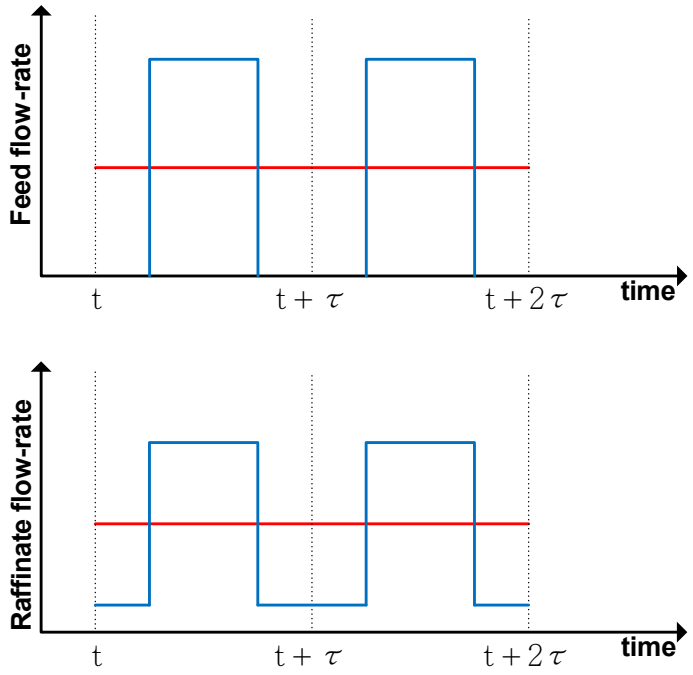

Figure 2.7: Feed and Raffinate flow-rates of a Partial-Feed operation for two consecutive switching intervals.

of more than two components and the goal is, in many cases, to isolate one component that is intermediately retained in the columns. The first logical step to achieve a "center-cut" separation is to implement a cascade of two [22, 23] or even more [24] SMB units, making a series of partitions to isolate the desired product. Although this is a very straightforward solution, it has an economical drawback since the need of several SMB units implies the use of much more equipment.

2.4.7 Gradient elution in SMB processes

One characteristic of the SMB processes described so far is that they are all operated under isocratic, isothermal conditions with nearly-incompressible liquid phases where the thermodynamic effect of pressure changes is negligible. During the selection of both stationary and fluid phase, one of the main goals is to find a separation method where the first component is fairly well adsorbed on the stationary phase while the second one can still be easily eluted under those conditions. The elution strength can be controlled by changing the composition of the solvent or desorbent. A solvent gradient can improve the SMB separation if the selectivity of the components is small or if the separation under isocratic conditions is impossible.

The multicolumn counter-current solvent gradient purification (MCSGP) process is

a (semi-)continuous, countercurrent, multicolumn chromatography process capable of performing three-fraction separations by changing the solvent composition along the system [25, 26]. This process can be used either for the purification of a single species from a multicomponent mixture or to separate a three-component mixture in a single operation. As shown in the scheme of Figure 2.8, the continuous 6-column MCSGP process consists of a group of 3 columns that are interconnected and another 3 columns that operate in batch mode; the interconnected columns implement the separation gradient like in batch chromatography; the disconnected columns perform the loading, the elution of the target product, and the elution of strongly adsorbed species plus washing, cleaning-in-place, and re-equilibration. In between the interconnected columns additional inlet streams are used to adjust the required solvent composition in order to reproduce the desired solvent gradient. This process can be operated discontinuously with only three columns [27].

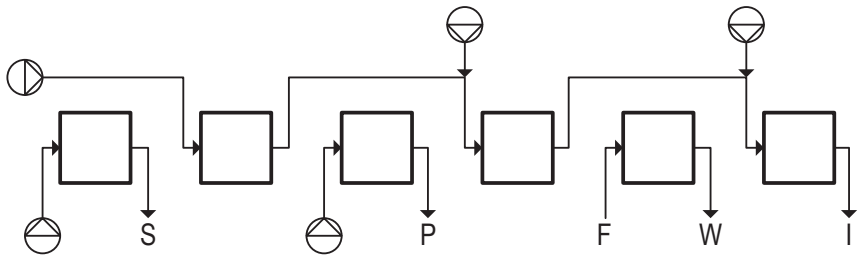

Figure 2.8: A schematic diagram of the MultiColumn Solvent Gradient Process (MCSGP). It is a fully continuous system comprising 6 chromatographic columns using solvent gradient for a three-fraction separation/purifications. Like in the SMB process, the system moves one column ahead every switching interval. S are the strongly adsorbing impurities, P is the target product, W are the weakly adsorbing impurities, I the inerts or very weakly adsorbing impurities and F the feed mixture.

The Gradient with Steady-State Recycle (GSSR) process is particularly suited for ternary separation of bioproducts: it provides three main fractions or cuts, with a target product contained in the intermediate fraction. The process comprises a multicolumn, open-loop system, with cyclic steady-state operation, that simulates a solvent gradient moving countercurrently with respect to the solid phase. However, the feed is always injected into the same column and the product is always collected from the same column as in a batch process; moreover, both steps occur only once per cycle. This process is more extensively discussed in chapters 6 and 7.

References

[1] Philippe Adam, Roger Narc Nicoud, Michel Bailly, and Olivier Ludemann-Hombourger. Process and device for separation with variable-length, October 24 2000. US Patent 6,136,198.

[2] O Ludemann-Hombourger, RM Nicoud, and M Bailly. The varicol process: a new multicolumn continuous chromatographic process. *Separation Science and Technology*, 35(12):1829–1862, 2000.

[3] Michael M Kearney and Kathleen L Hieb. Time variable simulated moving bed process, April 7 1992. US Patent 5,102,553.

[4] E Kloppenburg and ED Gilles. A new concept for operating simulated moving-bed processes. *Chemical engineering & technology*, 22(10):813–817, 1999.

[5] Ziyang Zhang, Marco Mazzotti, and Massimo Morbidelli. Powerfeed operation of simulated moving bed units: changing flow-rates during the switching interval. *Journal of Chromatography A*, 1006(1):87–99, 2003.

[6] Ziyang Zhang, Massimo Morbidelli, and Marco Mazzotti. Experimental assessment of powerfeed chromatography. *AIChE journal*, 50(3):625–632, 2004.

[7] Henning Schramm, Malte Kaspereit, Achim Kienle, and Andreas Seidel-Morgenstern. Improving simulated moving bed processes by cyclic modulation of the feed concentration. *Chemical engineering & technology*, 25(12): 1151–1155, 2002.

[8] H Schramm, A Kienle, M Kaspereit, and A Seidel-Morgenstern. Improved operation of simulated moving bed processes through cyclic modulation of feed flow and feed concentration. *Chemical engineering science*, 58(23): 5217–5227, 2003.

[9] Masatake Tanimura, Masao Tamura, and Takashi Teshima. Method of chromatographic separation, November 12 1991. US Patent 5,064,539.

[10] Kenzaburo Yoritomi, Teruo Kezuka, and Mitsumasa Moriya. Method for the chromatographic separation of soluble components in feed solution, May 12 1981. US Patent 4,267,054.

[11] Florence Lutin, Mathieu Bailly, and Daniel Bar. Process improvements with innovative technologies in the starch and sugar industries. *Desalination*, 148 (1):121–124, 2002.

[12] Yifei Zang and Phillip C Wankat. Smb operation strategy-partial feed. *Industrial & engineering chemistry research*, 41(10):2504–2511, 2002.

[13] Yifei Zang and Phillip C Wankat. Three-zone simulated moving bed with partial feed and selective withdrawal. *Industrial & engineering chemistry research*, 41(21):5283–5289, 2002.

[14] Youn-Sang Bae and Chang-Ha Lee. Partial-discard strategy for obtaining high purity products using simulated moving bed chromatography. *Journal of Chromatography A*, 1122(1):161–173, 2006.

[15] Andreas Seidel-Morgenstern, Lars Christian Keßler, and Malte Kaspereit. New developments in simulated moving bed chromatography. *Chemical engineering & technology*, 31(6):826–837, 2008.

[16] Lars Christian and Seidel-Morgenstern. Method and device for chromatographic separation of components with partial recovery of mixed fractions, August 25 2010. EP Patent 1,982,752.

[17] Pedro Sá Gomes and Alírio E Rodrigues. Outlet streams swing (oss) and multifeed operation of simulated moving beds. *Separation Science and Technology*, 42(2):223–252, 2007.

[18] Douglas M Ruthven and CB Ching. Counter-current and simulated counter-current adsorption separation processes. *Chemical Engineering Science*, 44(5): 1011–1038, 1989.

[19] Weihua Jin and Phillip C Wankat. Two-zone smb process for binary separation. *Industrial & engineering chemistry research*, 44(5):1565–1575, 2005.

[20] José PB Mota and João MM Araújo. Single-column simulated-moving-bed process with recycle lag. *AIChE journal*, 51(6):1641–1653, 2005.

[21] Nadia Abunasser and Phillip C Wankat. One-column chromatograph with recycle analogous to simulated moving bed adsorbers: Analysis and applications. *Industrial & engineering chemistry research*, 43(17):5291–5299, 2004.

[22] Phillip C Wankat. Simulated moving bed cascades for ternary separations. *Industrial & engineering chemistry research*, 40(26):6185–6193, 2001.

[23] Jeung Kun Kim, Yifei Zang, and Phillip C Wankat. Single-cascade simulated moving bed systems for the separation of ternary mixtures. *Industrial & engineering chemistry research*, 42(20):4849–4860, 2003.

[24] Jeung Kun Kim and Phillip C Wankat. Designs of simulated-moving-bed cascades for quaternary separations. *Industrial & engineering chemistry research*, 43(4):1071–1080, 2004.

[25] Lars Aumann and Massimo Morbidelli. Method and device for chromatographic purification, November 2 2006. EP Patent 1,716,900.

[26] Guido Ströhlein, Lars Aumann, Marco Mazzotti, and Massimo Morbidelli. A continuous, counter-current multi-column chromatographic process incorporating modifier gradients for ternary separations. *Journal of Chromatography A*, 1126(1):338–346, 2006.

[27] Lars Aumann and Massimo Morbidelli. A continuous multicolumn countercurrent solvent gradient purification (mcsgp) process. *Biotechnology and bioengineering*, 98(5):1043–1055, 2007.

3

Two-column open-loop system for nonlinear chiral separation

3.1 Introduction

The simulated moving bed (SMB) is a continuous adsorption separation process with numerous applications, many of which are difficult or even impossible to handle using other separation techniques. The SMB process was originally devised as a practical implementation of the true moving bed (TMB) process, where the adsorbent and the fluid phase move counter-currently [1–3].

A binary feed (A/B) may be separated by SMB into two products: an extract product containing mainly solute A (the more strongly adsorbed species, or group of species with similarly strong adsorption properties) and a raffinate containing mainly solute B (the less strongly adsorbed species or group of species). SMB chromatography increases throughput, purity, and yield relative to batch chromatography [4–7].

This technology has been increasingly applied for the separation of pure substances in the pharmaceutical, fine chemistry, and biotechnology industries, at all production scales, from laboratory to pilot to production scale. This led to the development of novel cyclic operating schemes, some of which are substantially different from the conventional process. Broadly speaking, the new operating schemes introduce periodic modulations of selected control parameters into the operating cycle.

Concepts such as asynchronous port switching [8–10], cyclic modulation of feed concentration [11, 12], time-variable manipulation of the flow rates [13–17], and solvent-gradient operation [18–21], have been thoroughly analyzed. The extra degrees of freedom available with these schemes improve the separation efficiency, thus allowing for the use of units with less columns than traditionally used. The advantages are apparent: less stationary phase is used, the set-up is more economic, and the overall pressure drop can be reduced. Furthermore, switching from one mixture to another is easier and takes less time than with more columns.

The classical implementation of the SMB process comprises four zones, with an integer number of columns per zone. Alternatives to this standard operation scheme, with less zones, have also been studied. For example, the three-zone SMB configuration [3, 22, 23] takes the four-zone, open-loop SMB and removes zone IV. If the amount of adsorbent allocated to each zone is properly optimized by means of asynchronous port switching, then a three-zone asynchronous SMB can perform better than a standard (i.e., synchronous) four-zone SMB [24–26]. The advantages and drawbacks of the three-zone SMB have been discussed by Chin and Wang [27]. Another example of a system that uses less zones was proposed by Lee [28], where a two-zone SMB with continuous feeding and partial withdrawal was used for glucose-fructose separation; this process appears to be more suitable for enriching products than for high-purity separations [27]. Another example of a two-zone SMB scheme uses intermittent feeding and withdrawal to achieve ternary separations [29].

Jin and Wankat [30, 31] developed more recently other examples of two-zone SMBs for binary separation, which incorporate a storage tank to temporarily hold desorbent for later use. Their results show that good separation can be achieved but with more desorbent than required by a four-zone SMB. However, partial feed was shown to improve the product purities and recoveries considerably. The system was subsequently extended to ternary separations [32], and a different two-zone SMB system, which does not use a storage tank, was developed for center-cut separation from ternary mixtures [33]. Other processes particulary suitable for ternary separations are the MCSGP [34] and the GSSR [21] processes; these systems incorporate the principle of counter-current operation and the possibility of using solvent gradients. One-column processes that reproduce the cyclic behavior of multicolumn SMB chromatography, by means of a recycle lag, have also been proposed [35–37].

We have recently developed a semi-continuous, two-column chromatograph with a

flexible node design, robust pump configuration, and cyclic flow-rate modulation to exploit the benefits of both batch and simulated counter-current modes [38]. We emphasize the use of two columns rather than two zones, because with three or more columns it is always possible to implement a better SMB scheme which uses more zones with roughly the same ancillary equipment. In fact, running a two-zone configuration with three columns can be detrimental to the separation because the zone lengths become highly asymmetrical [39].

One advantage of our streamlined design is the simplicity of its physical realization: the simplest configuration, with no recirculation step, requires only two pumps to supply feed and desorbent into the system, while the flow rates of liquid withdrawn from the system are controlled by material balance using simple two-way valves. This type of operation implicitly discards the possibility of splitting into two or more streams the flow exiting one column; in this sense, the product, waste, or recycling fractions are always obtained by completely directing the effluent over a certain period of the cycle to the appropriate destination. The different port configurations that can be implemented with our simplest streamlined design are depicted in Fig. 3.1. In the present work a series of two-column open-loop processes

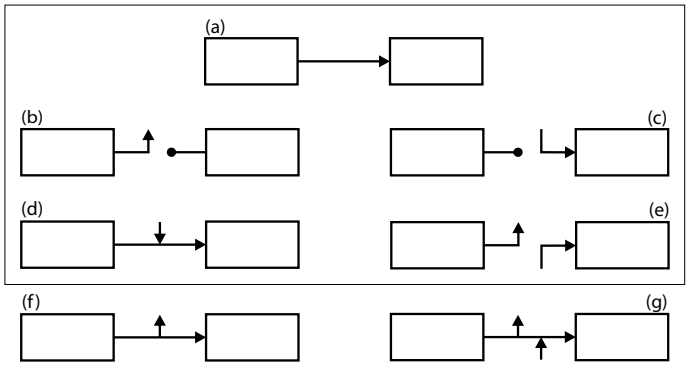

Figure 3.1: Possible port configuration between two consecutive columns, or group of columns: (a) complete direction of flow to the next column; (b) downstream frozen bed; (c) upstream frozen bed; (d) flow addition to circulating stream; (e) complete withdrawal and flow injection at the same node; (f) partial withdrawal, and (g) partial withdrawal and flow addition at the same node. Configurations (f) and (g) are not considered, as they imply partial withdrawal of the exit stream from a column.

for semi-continuous enantiomeric separation are assessed both numerically and experimentally. These schemes are compared against batch chromatography and batch chromatography with recycle for a case of nonlinear adsorption. We explore two cases of elution strategy: continuous elution and discontinuous elution; in the latter case the upstream column is frozen (the flow is halted) while fresh feed is injected into the downstream column.

This chapter is organized as follows. We start by describing the experimental setup where the proofs of concept were realized, discuss the procedure for optimal cycle design, and then the numerical approach used to solve the resulting nonlinear programming problem. We then report on the experimental verification of the performances of the two-column processes, using the nonlinear separation of Tröger's base in Chiralpak AD as a convenient model separation problem. The experiments not only support the discussion of the results but also validate the modeling tools employed in a comparison study of the processes assessed. Finally, the work is summarized before drawing final conclusions.

3.2 Experimental Setup

Fig. 3.2 shows a schematic of the node configuration employed in our prototype apparatus. As stated above, the flow rate of liquid that is withdrawn at each node is controlled by material balance. The versatility of the valves used, allows the easy implementation of the port configurations (a)-(e) depicted in Fig. 3.1. Two-way

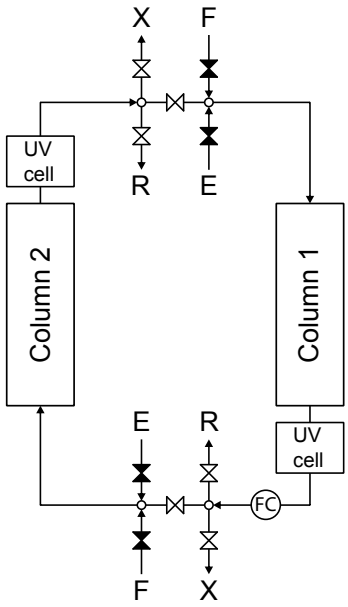

Figure 3.2: Schematic diagram of semi-continuous, two-column, open-loop chromatograph for chiral separation.

valves allow the flow either to go through or not to go through. Each valve is attached to the transfer line between columns by a tee. A two-way valve is placed immediately downstream of the two outlet ports of each column, but preceding the two inlet ports, to control the flow rate of liquid from the column that is circulated

to the other column. This valve is normally open and is only closed when the effluent from the upstream column is totally withdrawn as product or the fluid in the column needs to be temporarily frozen. Overall, each set-up employs 10 two-way valves to control the port switching. The two-way valves are model SFVO from Valco International (Schenkon, Switzerland) with pneumatic actuation. Each valve is automated by means of a single computer-controlled three-way solenoid: application of 50 psi opens the valve; venting the air allows the spring to return the valve to the closed position.

The inlets of the chromatographic unit are represented in detail in Fig.3.3. This valve scheme allows the recycling of the desorbent or feed stream back to the original source tanks by means of a closed loop. This brings also another advantage which is the steady operation of both pumps, thus eliminating the uncertainty in the flow rates.

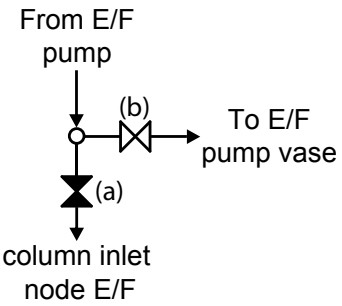

Figure 3.3: Details of the inlets present in the unit described and portrayed in Fig.3.2. The painted valves (a) are the same of Fig.3.2.

3.3 Model based cycle design

The periodic forward movement of the active inlet/outlet ports by one column in the direction of the fluid flow—characteristic of a SMB at the end of a switching interval—is also implemented in our process. Because the two columns are assumed to be identical, the cycle of a two-column system can be divided into two intervals of identical length τ. At the end of each switching interval, i.e. every τ time units, the inlet/outlet ports are switched, and the columns reverse roles. The port configurations (a) to (e) shown in Fig. 3.1 are the building blocks for establishing the cyclic operation of the two-column SMB process assessed in this work.

As described next, the feed and eluent flow rates are initially modulated in time as a convenient means of solving the design problem. This has the fortunate side effect

of providing an optimal cycle with slightly better performance than one operated with constant flow rates. For convenience, the τ-periodic modulations implemented here are piecewise-constant, i.e., the flow rates are kept constant over each step before jumping discretely to different values over the next step. In practice, the switching interval is divided into a given number n_Q of steps, which may have nonuniform lengths, $\tau_n > 0$,

$$\sum_{n=1}^{n_Q} \tau_n = \tau. \tag{3.1}$$

The adopted formulation does not explicitly track the port switching over the cycle; instead, the state of each two-way valve is inferred from the piecewise-constant flow-rate profiles. If in Fig. 3.2, for example, $E_j = 0$ over a given step of the switching interval, then the two-way valve that connects the eluent pump to the inlet of column j is closed, otherwise it is open. Similarly, if $Q_j = 0$ or $X_j + R_j = Q_j$ then the two-way valve located between the inlet/outlet ports downstream of column j is closed, otherwise it is open. This formulation is highly flexible and has the advantage of eliminating the integer nature of the design problem, since the only remaining degrees of freedom are the switching interval and the time-variable flow rates.

A rigorous model-based optimization approach is employed to determine the optimal operating parameters. The purpose of the nonlinear programming problem (NLP) is to guarantee the fulfillment of product and process specifications, such as minimal purities and maximal operating flow rates, while optimizing process performance in terms of productivity and eluent consumption. At each step of the flow-rate modulation, the following basic restrictions must be satisfied:

$$0 \leq E_j \leq Q_{max}, \quad X_j \geq 0, \tag{3.2}$$

$$0 \leq F_j \leq Q_{max}, \quad R_j \geq 0, \tag{3.3}$$

$$Q_j \leq Q_{max}^{'}, \tag{3.4}$$

$$0 \leq (X_j + R_j) \perp (Q_j - X_j - R_j) \geq 0, \tag{3.5}$$

$$0 \leq E_1 \perp E_2 \geq 0. \tag{3.6}$$

Here, j is the column index; Q_{max} is the capacity of the installed pumps; $Q_{max}^{'}$ is the maximum flow rate through the column imposed by an hypothetical pressure drop constraint; E, F, X, and R stand for the flow rates of eluent, feed, extract,

and raffinate, respectively; and $\perp$ is the complementarity operator enforcing at least one of the bounds to be active. The complementarity constraint $0 \leq x \perp y \geq 0$ implies the following [40]:

$$x = 0 \quad or \quad y = 0, \tag{3.7}$$

$$x \geq 0, \quad y \geq 0. \tag{3.8}$$

Here the 'or' operator is inclusive as both variables x and y may be zero.

The constraints defined by Eqs. 3.2–3.6 guarantee that the solution is physically realizable with our experimental set-up. Eq. 3.5 ensures that product withdrawal can be implemented with on-off valves: either nothing is withdrawn as product from column j (clause $X_j + R_j = 0$ is active) and the flow is totally circulated to the other column, or the exit stream from column j is totally withdrawn as product (clause $Q_j - X_j - R_j = 0$ is active). Note that the complementarity constraint implicitly enforces the condition:

$$Q_j \geq X_j + R_j. \tag{3.9}$$

This constraint is of utmost importance, as it prevents the withdrawal of product at a flow rate larger than that provided by the column—otherwise the packed bed would dry out and no longer be saturated with fluid. Eq. 3.6 enforces the use of a single pump for supplying desorbent to the system.

Open-loop configurations can be generated by imposing one of the constraints:

$$E_1 + E_2 + F_1 + F_2 \geq Q_{min} \quad \text{or} \quad X_1 + X_2 + R_1 + R_2 \geq Q_{min}, \tag{3.10}$$

as they enforce at least Q_{min} amount of fluid to be supplied into (or removed from) the system at every step; Q_{min} should be a small, positive constant. Note that Eq. 3.10 is not, by itself, a sufficient condition for open-loop operation; however, when Eqs. 3.5 and 3.10 are applied together, the desired effect is achieved. Our experience with the type of problems under consideration here has shown that Eq. 3.10 offers an efficient method of defining the open-loop condition in a NLP formulation.

Product purity and recovery are enforced through the following constraints:

$$Pur_R \geq Pur_R^{min}, \quad Pur_X \geq Pur_X^{min}, \tag{3.11}$$

$$Rec_R \geq Rec_R^{min}, \quad Rec_X \geq Rec_X^{min}, \tag{3.12}$$

where Pur and Rec denote product purity and recovery, respectively (the 'min' superscripts represent their minimum admissible values), and the subscripts 'R' and 'X' denote the extract and raffinate streams; these performance parameters are defined as follows:

$$Pur_R = \frac{\int_t^{t+\tau} c_{1,j}^{out} R_j dt}{\int_t^{t+\tau} \left(c_{1,j}^{out} + c_{2,j}^{out}\right) R_j dt}, \quad Pur_X = \frac{\int_t^{t+\tau} c_{2,j}^{out} X_j dt}{\int_t^{t+\tau} \left(c_{1,j}^{out} + c_{2,j}^{out}\right) X_j dt}, \tag{3.13}$$

$$Rec_R = \frac{\int_t^{t+\tau} c_{1,j}^{out} R_j dt}{c_1^F \int_t^{t+\tau} F_j dt}, \quad Rec_X = \frac{\int_t^{t+\tau} c_{2,j}^{out} X_j dt}{c_1^F \int_t^{t+\tau} F_j dt}, \tag{3.14}$$

Eqs. 3.13 and 3.14 have been written under the assumption that component 1 is the least retained species and component 2 the more retained one.

In practice, processes with constant flow rates are easier to implement and to control. Because our schemes are semi-continuous, the schematics in Fig. 3.2 must be slightly changed in order to work with fixed-velocity pumps. Instead of allowing a flow rate, say Q, to have a flexible piecewise-constant profile, i.e., taking a different value at each sub-step of the switching interval, say $Q_1, ..., Q_n$, it is constrained to two values only: 0 or Q_{max}. This way, the pump driving the flow is always operated at Q_{max} but when Q must be zero the flow is directed back to the source tank by means of one three-way valve, or two two-way valves, placed at the pump outlet. This has the added advantage of producing a near-perfect step change in the flow rate.

In general, the optimization of a chromatographic process is a multi-objective optimization problem with conflicting interests, because one usually seeks to maximize the productivity or feed throughput while minimizing the solvent consumption [38]. This issue is addressed here by means of Pareto curves, which are curves representing optimal points nondominant with respect to the others in terms of maximization of the feed throughput and minimization of the solvent consumption.

For the sake of brevity, the Pareto curves presented here will be restricted to curves on the (feed throughput)$\times$(eluent consumption) plane, each curve representing a set of optimal solutions for a given column configuration (or operating scheme)

and a fixed set of product specifications (e.g., purity and yield). Special care is taken to subject all the Pareto curves to the same product constraints and same amount of stationary phase so that curves for different column configurations can be directly compared.

In the present work, the objective function, f_{obj}, is chosen to be the maximization of productivity, or feed throughput:

$$F_{av} = \frac{1}{\tau}\int_{t}^{t+\tau} (F_1 + F_2)\, dt = \frac{2}{\tau}\int_{t}^{t+\tau} F_j dt \tag{3.15}$$

where F_{av} is the average feed flow rate per cycle. Given that the solvent consumption is $(F_{av} + E_{av})/F_{av} = 1 + E_{av}/F_{av}$, minimizing the solvent consumption is the same as minimizing E_{av}/F_{av}; for a matter of simplicity we will work on the $(F_{av}) \times (E_{av}/F_{av})$ plane.

To construct a Pareto curve on this plane, we replace the constraints '$0 \leq E_j \leq Q_{max}$' and "$0 \leq F_j \leq Q_{max}$' by a new constraint '$0 \leq E_{av} \leq Q_{max}$', drop out the pressure drop constraint given by Eq. 3.4 (this is done only for a matter of simplicity), and carry out a series of single-objective optimizations that maximize F_{av} for progressively larger values of Q_{max}. Hence we solve:

$$f_{obj} = max\ F_{av}, \quad s.t. \quad E_{av} \leq Q_{max}. \tag{3.16}$$

for increasing values of the parameter Q_{max}. The set of points thus generated gives the desired Pareto curve. Alternatively, we could have solved:

$$f_{obj} = min\ E_{av}, \quad s.t. \quad F_{av} \geq Q_{min}. \tag{3.17}$$

for increasing values of Q_{min}. This procedure would have produced exactly the same Pareto curve.

Each NLP problem defined by Eq. 3.16 is solved directly for steady periodic operation of the process, i.e., for cyclic steady state (CSS) conditions. To this end, the NLP problem is formulated with a single-column analog model that reproduces the CSS of the two-column unit [41, 42], together with a full-discretization approach for steady period dynamics. The method is described in detail elsewhere [25, 43].

Discretization is handled via collocation, using 25 cubic Hermite elements [44] for the spatial domain and 10–15 Radau elements (with two interior points) per substep of the switching interval. The latter type of collocation elements is especially suitable for handling process dynamics with frequent discontinuities in time [45].

The flow rates remain constant over the Radau elements of a step, but are allowed to change discretely to different values across steps.

The complementarity conditions-—Eqs. 3.5 and 3.6—are reformulated as NLP constraints using a relaxed formulation [46]. The nonlinear programming problem obtained after discretization and relaxation of the complementarity conditions is formulated in AMPL [47] and solved with IPOPT 3.10 [48]. This solution strategy has been previously employed with success by our group on a broad class of SMB problems [36], [25] and [26]. IPOPT implements a primal-dual interior-point method, and uses line searches based on filter methods; it directly exploits the first and second derivative (Hessians) information provided by AMPL via automatic differentiation.

3.4 Chromatographic column model

The complexity of the model required to simulate a particular system depends on the nature of that system and on the accuracy required. The dispersed plug-flow model with linear driving-force approximation for mass transfer is a sufficiently general model to provide a realistic representation of the isothermal operation of most liquid-phase chromatographic columns [49].

In general, the LDF model can be reasonably well approximated by an equilibrium-dispersed model. The equilibrium-dispersive model assumes that all contributions resulting from a lack of equilibrium can be lumped into an apparent axial dispersion term. The model provides a very good approximation of the dynamics of a chromatographic column if the adsorption isotherms are linear (Henry's law) and mass transfer is controlled by molecular diffusion. However, the model can also be applied with reasonable accuracy to nonlinear adsorption is the Henry's constant is replaced by the local slope of the adsorption isotherm in the calculation of the local plate height.

The mass balance for a chromatographic column is:

$$\frac{\partial c_i}{\partial \theta} + \beta \frac{\partial q_i}{\partial \theta} = \frac{\tau Q}{\epsilon V_C} \left(\frac{1}{Pe_i} \frac{\partial^2 c_i}{\partial x^2} - \frac{\partial c_i}{\partial x} \right) \qquad \text{for} \quad 0 < x < 1 \tag{3.18}$$

where subscript i is the solute index, $\theta = t/\tau$ and $x = z/L$, the dimensionless temporal and axial coordinates, respectively; c_i and q_i, the liquid phase and adsorbed phase concentrations, respectively; $\beta = (1-\epsilon)/\epsilon$ the phase ratio; V_C, the geometri-

cal column volume; Q, the flow-rate of the fluid phase; and Pe_i the apparent Péclet number.

The concentrations of solute i in the liquid and in the solid phases, c_i and q_i, respectively, are related through the adsorption isotherms:

$$q_i = f\left(c_1, c_2, ..., c_n\right) \quad i = 1, ..., n_{solutes} \tag{3.19}$$

If the adsorption isotherms are linear, the time derivatives $\partial q_i/\partial\theta$ are given by the corresponding Henry constants; if the adsorption isotherms are nonlinear, the time derivatives must be replaced by the total derivatives resulting from the chain rule:

$$\frac{\partial q_i}{\partial \theta} = \sum_{k=1} \left(\frac{\partial q_i^\star}{\partial c_k}\right)\left(\frac{\partial c_k}{\partial \theta}\right) \tag{3.20}$$

Eq.3.18 is subjected to the usual boundary conditions:

$$c_i - \frac{1}{Pe_i}\frac{\partial c_i}{\partial x} = c_i^{in} \qquad \text{for} \quad x = 0, \tag{3.21}$$

$$\frac{\partial c_i}{\partial x} = 0 \qquad \text{for} \quad x = 1. \tag{3.22}$$

where c_i^{in}, the solute concentration in the inlet effluent.

3.5 Materials and methods

To experimentally evaluate and demonstrate the feasibility of the proposed two-column process, the separation of Troger's base enantiomers, using ethanol as pure mobile phase and Chiralpak AD as chiral stationary phase is proposed. The maximum liquid concentration of the racemate used was about 80% of the solubility value described elsewhere [50] and experimentally validated.

The pure enantiomers were purchased from Fluka (Germany), with a purity of 99%, and the racemate was purchased from Sigma-Aldrich (Germany), with a purity of 98% and was recrystallized from ethanol (Panreac, Spain) before use. The stationary phase (Daicel Chemical Industries Ltd, Chiral Technologies, Europe Illkirch, France) was slurry-packed into a thermojacketed Superformance with 10 mm i.d. glass column (Gotec Labortechnik, Germany) to a bed height of 120 mm. The system was operated isothermally at 25°C.

A multi-wavelenght UV detector (USB2000, Ocean Optics, USA) with a light source (Micropack, Ostfildern, Germany), and attenuator, was used to monitor the outlet stream of the chromatographic columns.

The HPLC pumps employed in the experiments are model K-501 from Knauer (Berlin, Germany) with 10 ml and 50 ml pump heads, controlled by RS232 communication protocol. The whole setup is fully automated and driven by our Labview-based software system (BioCTR) for process monitoring and control of chromatographic processes [51].

3.5.1 System characterization

The total bed porosity (ϵ) was determined from the retention time of 1,3,5-tri-tert-butylbenzene (TTBB) (Sigma–Aldrich, Germany); this solute is not retained by the stationary phase but can access its internal porosity. The packing reproducibility was assessed by comparing the peak shapes and retention times of the chromatograms obtained with the two preparative columns; both columns were found to be identically and reasonably well packed. Extra-column volumes in the experimental set-up were estimated from TTBB pulse experiments with and without the two chromatographic columns.

The dimensionless plate height, h_i, governing band broadening for the i^{th} component, can be expressed as [49]

$$\frac{h_i}{2} = \frac{1}{Pe_i} + \alpha_i \frac{Q}{\epsilon V_C} \tag{3.23}$$

which is known as the linearized van Deemter plot. In principle, under normal preparative flow conditions the Péclet number, $Pe_i = vL/D_{iL}$, where D_{iL} is the axial dispersion coefficient for component i, should be independent of the solute index, because $D_{iL} \approx \gamma v d_p$, where d_p is the particle diameter and $\gamma \approx 0.5$–0.7 is a constant dependent only on the characteristics of the packing ($Pe_i \approx L/\gamma d_p$). On the other hand, the slope of the linearized van Deemter plot is given by

$$\alpha_i = \frac{1}{k_i} \frac{\beta H_i^2}{(1+\beta H_i)^2}, \tag{3.24}$$

where H_i is the local slope of the adsorption isotherm and k_i is the LDF coefficient for component i. The intercept and slope of the linearized van Deemter plot for each enantiomer were determined by fitting the experimental dependence of h_i on

Q for diluted pulses of the solutes eluted at different flow rates.

3.5.2 Adsorption isotherms

The experimental determination of adsorption isotherms is of utmost importance for the design and operation of any cyclic adsorption process. This statement holds true for the two-column chromatographic process under consideration, since its operating conditions cannot be properly determined without knowledge of the competitive isotherms of the two enantiomers.

In the present work, the competitive isotherms were estimated with good accuracy by applying a hybrid inverse method [52]. Briefly, a prescribed adsorption isotherm model—in the present case, a bi-Langmuir adsorption model—is plugged into the chromatographic column model described above and then fitted to experimental band profiles from overloaded injections of the racemic mixture and breakthrough data. The numerical constants of the isotherm model are tuned so that the calculated and measured band profiles match as much as possible. The bi-Langmuir adsorption isotherm model can be written as

$$q_i^\star = \frac{a_{i,1} c_i}{1 + \sum_j b_{j,1} c_j} + \frac{a_{i,2} c_i}{1 + \sum_j b_{j,2} c_j} \quad i = A, B \tag{3.25}$$

where the a_i and b_i are the fitting parameters.

For the system characterization two different equipment configurations were used. The first setup, used for parameter scouting, is shown in Fig. 3.4; it uses an injection loop coupled to the six-port valve for pulse injections, using one of the HPLC pumps to fill the loop and the other HPLC pump to elute the column. For longer injections, such as well-defined rectangular pulses, the loop is removed and the flow scheme is altered as described in more detail in Fig. 3.4. This change has three major advantages: the length of the injections can be controlled without any additional change to the experimental setup; the experimental uncertainty due to flow disturbances is reduced because the HPLC pumps are continuously operated in closed loop at prescribed flow rates; and, as the commutation of the six-port valve is almost instantaneous, it is expected to provide a good approximation to the sharp front and rear edges of a rectangular pulse. The data collected from the pulse experiments, used in the calculation of the dimensionless plate height, were grouped with other experiments, namely step injections of 5 ml and 15 ml of racemic mixture at different concentrations.

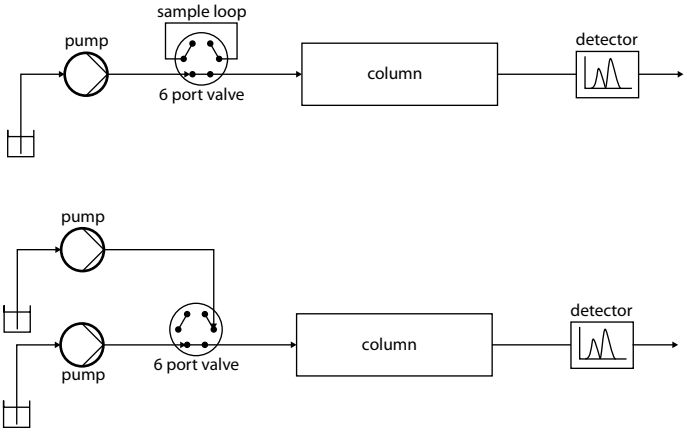

Figure 3.4: Schematic diagram of the single-column SMB analog chromatograph. Pumps, 6-port valve and detector are connected to an automated data acquisition and control unit.

In the cases of longer injections, several fractions were collected during the elution profile and analyzed off-line by HPLC. These data are essential to complement the frontal analysis experiments in which we only monitored the total enantiomeric concentration in the liquid at the outlet of the column. Using the adopted approach, it is possible to gain more insight into the individual profiles of the solutes by comparing the sampled points with the fittings for the individual solutes given by the adjusted model. Table 3.1 summarizes the estimated parameters for the

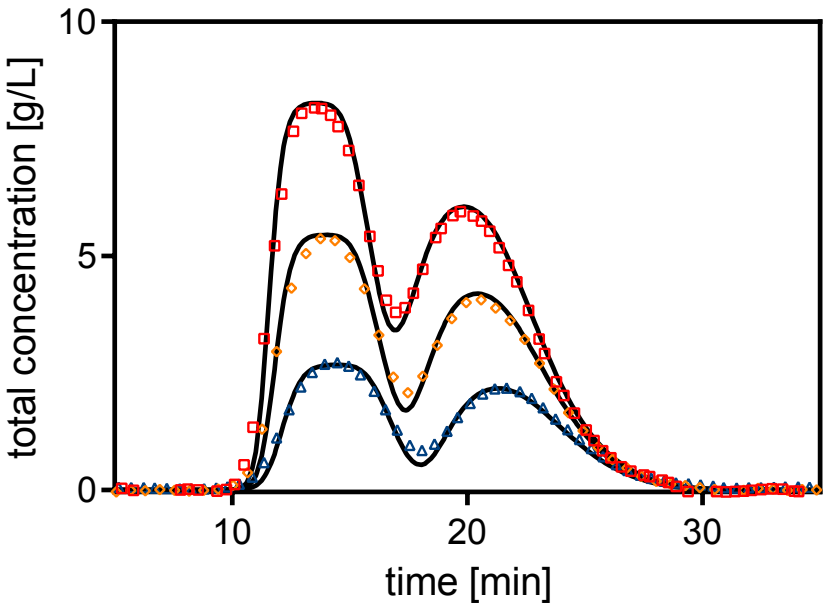

Figure 3.5: Rectangular injections (5 ml) of the racemic mixture at 5.0, 10.0, and 15.0 g/l and flow rate of 1 ml/min; the solid line represents the simulation data of the total enantiomer concentration ($c_A + c_B$); the symbols are the experimental data for each injection.

adsorption system and column characterization.

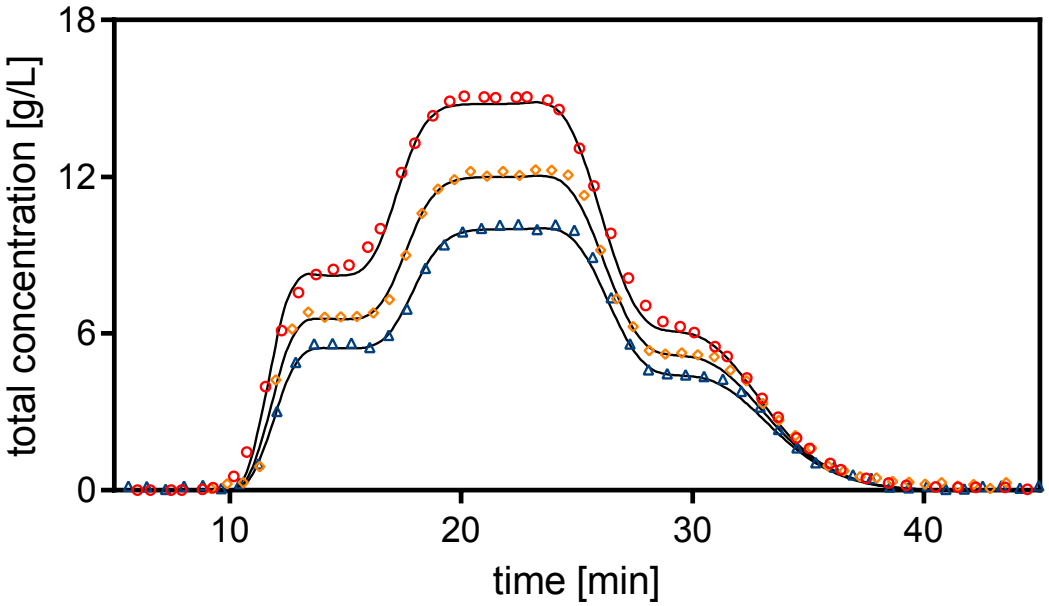

Figure 3.6: Breakthrough experiments of the racemic mixture at 10.0, 12.0, and 15.0 g/l for an injection volume of 15 ml at a flow rate of 1 ml/min; the solid line represents the simulation data for the total enantiomer concentration ($c_A + c_B$); the symbols are the experimental data for each injection(triangles, 10.0 g/l; squares, 12.0 g/l; circles, 15.0 g/l.

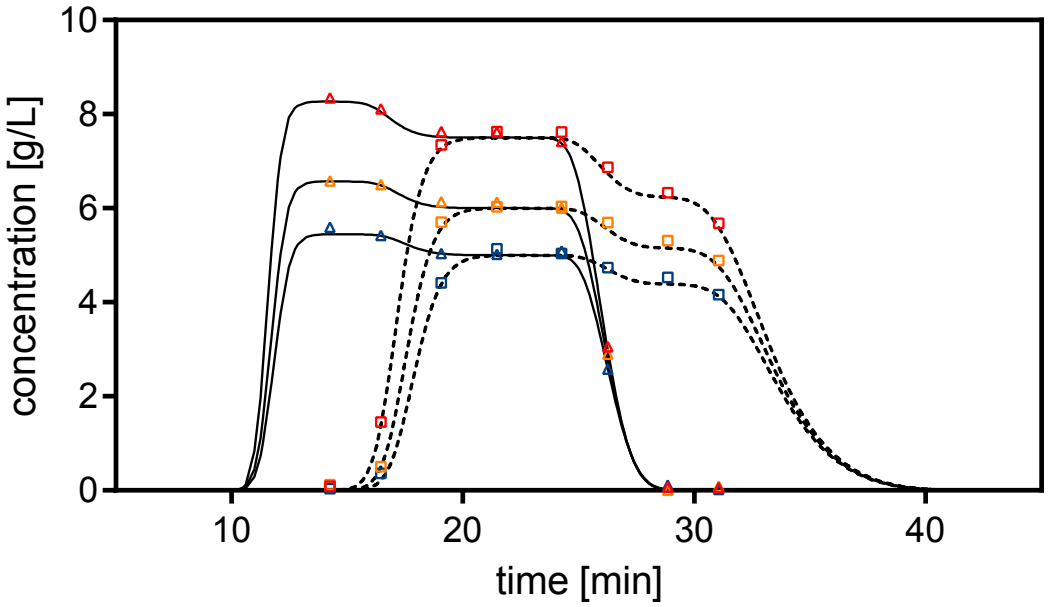

Figure 3.7: Elution profiles of the individual enantiomers from frontal analysis experiments with a racemic mixture of Tröger's base, at total feed concentrations of 10.0, 12.0, and 15.0 g/l, injection volume of 15 ml, and flow rate of 1 ml/min; The solid and dashed lines represent the simulation data for the less (A) and more (B) retained enantiomers, respectively, using the equilibrium-dispersive model with bi-Langmuir isotherms and model parameters given in Table 3.1; triangle square symbols denote the experimental individual enantiomer concentrations determined from the collected fractions of the frontal experiments.

Table 3.1: Column characterization and adsorption parameters for the nonlinear separation of Tröger's base enantiomers on Chiralpak AD and ethanol at 25°C (A and B denote the less and the more retained enantiomers, respectively).

$\epsilon = 0.685$	A	B
Pe_i	754	665
αL [s]	0.517	0.790
$a_{i,1}$	1.673	3.954
$a_{i,2}$	0.304	0.982
$b_{j,1}$ [l/g]	0.013	0.011
$b_{j,2}$ [l/g]	0.136	0.602

3.6 Results and discussion

Using the parameters given in Table 3.1, the methodology presented in Section 3.3 was applied to the optimal design of chromatographic cycles that are realizable with the schematic of Fig. 3.2. The parameter values for the geometrical and physical constraints are $Q_{min} = 0.1$ ml/min and $Q_{max} = Q'_{max} = 10.0$ ml/min. In order to compare fairly the performance of the processes discussed in this section, the amount of stationary phase was kept invariant; it is also important to note that for simplicity of operation of the experimental set-up we were only interested in schemes that work exclusively in open loop. For the purpose of experimental validation, the two processes studied in this work as well as the classical batch process were operated with the same average eluent consumption (E_{av}/F_{av}). Therefore, the value E_{av}/F_{av} was fixed at 2.9 and the corresponding optimal operating point, where the feed flow rate is maximized while still satisfying the constraint given by Eq. 3.4, was determined for each process.

3.6.1 Batch chromatography

Let us first consider the simplest process: batch chromatography without recycle. In order to design this process, the two columns of the experimental set-up are modeled as a single column with a bed height equal to the sum of the heights of the two columns. Moreover, the parameter Pe_i has to be scaled because the batch process uses a single column with twice the bed height; from the definition of the Péclet number, it is easy to scale it according to its dependence on the column length. Although the slope of the linearized van Deemter plot must also be scaled, its scaling factor is already explicitly given in Eq. 3.24 as $1/(\epsilon V_C)$ since α_i is independent of the geometrical dimensions of the column.

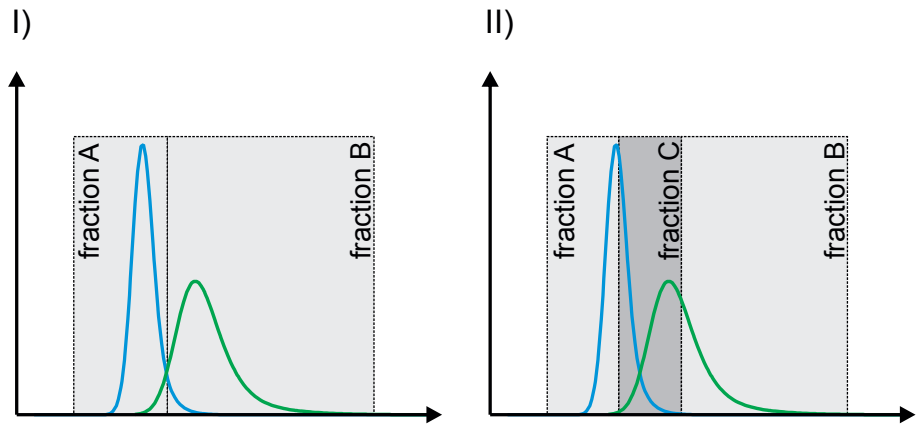

Figure 3.8: Cut strategies in batch operation. In the first case only two fractions, A and B, are generated at each cycle; in the second case three fractions are collected separately in each cycle: two product fractions (A and B) and an intermediate fraction (C) that can be either recycled (as s the case in steady-state recycling) or directed to waste.

In batch chromatography there are two approaches that are generally considered for the cut strategy (Fig. 3.8). In cut strategy I we collect two consecutive fractions, which are both taken as products. In this case, purity and yield are coupled together and cannot be varied independently. When high purity is demanded, which is usually the case in pharmaceutical and fine chemical applications, this cut strategy requires almost baseline separation of the two target components, which in many cases can only be achieved by increasing the column volume and reducing the feed throughput.

Cut strategy II generates an intermediate fraction between the two product fractions, which can be either discarded or processed further. Due to the introduction of this fraction, additional degrees of freedom are available. A high purity demand can be satisfied with this cut strategy by increasing the size of the intermediate fraction but at the expense of reducing the yield of separation.

The choice between the two different strategies depends not only on the column resolution, but also on the costs associated with the extra processing of the intermediate fraction (strategy II). In the present case, we are interested on the first strategy for fractionating the products because the target yield is high and, as stated above, the system is supposed to operate in an open-loop configuration. The design of the cycle for the batch process must take the following points into consideration: (i) the two products are collected alternately at the downstream end of the column, while feed or desorbent are injected into the upstream end of the column; (ii) the positions and lengths of the feed, elution, and the two product collection steps must be correctly sized to optimally satisfy the purity and recovery constraints.

Table 3.2: Optimal operating cycle for the solution of the separation problem defined in Table 3.1 with a batch configuration (Fig. 3.9). The parameter values for the NLP design problem $Q_{max} = Q'_{max}$=10 mL/min,($f_{obj} = maxf$) are: n_Q=3, Q_{min}=0.1 $Pur_R^{min} = Pur_X^{min}$=0.99. The step durations, τ_n, are expressed in minutes; the eluent (E), feed (F), extract (X), and raffinate (R) flow rates are given in mL/min. The first value on the bottom row is the switching interval, $\tau = \sum_n \tau_n$.

Step, n	τ_n	E	F	X	R
1	3.265	0.000	2.572	2.572	0.000
2	7.600	1.719	0.000	1.719	0.000
3	6.567	1.719	0.000	0.000	1.719
Average	17.432	1.385	0.478	1.221	0.642

To enforce the collection of the fractions alternately the following constraint is added to the model: Let's say that the cycle is divided into n_Q steps that do not necessarily have the same length. For step n let $Q^{(n)} \geq 0$ be the column flow rate; $E^{(n)}$ $ge0$ and $F^{(n)} \geq 0$ the flow rates of eluent and feed injected at the upstream end of the column, respectively; and $X^{(n)} \geq 0$ and $R^{(n)} \geq 0$ the flow rates of extract and raffinate fractions collected at the downstream end of the column. Obviously,

$$Q^{(n)} = E^{(n)} + F^{(n)} = X^{(n)} + R^{(n)}, \quad n = 1, ..., n_Q. \tag{3.26}$$

$$X^i R^i = 0, \quad i = 1, ..., n_Q. \tag{3.27}$$

Also we are interested in a steady operation of both the desorbent and feed pump. This can be traduced in the following:

$$E^1 = ... = E^{n_Q} = E, \quad E \leq Q_{max} \tag{3.28}$$

$$F^1 = ... = F^{n_Q} = F, \quad F \leq Q_{max} \tag{3.29}$$

The optimal solution of the NLP problem defined in Table 3.1 resulted in $n_Q = 3$, i.e., three subdivision of the cycle. The optimal solution is reported in Table 3.2. Analyzing the cycle one can see that we start by eluting the extract from the injection performed on a previous cycle, also, the duration of the feed step is shorter than the collection of extract. Because of this, a second step of elution is necessary to recover the remaining of the extract band, after that, in the next step we recover the raffinate fraction.

The cycle was implemented on the unit shown in Fig.3.2, using only the first column node. Both columns were coupled together, using a zero-volume coupling.

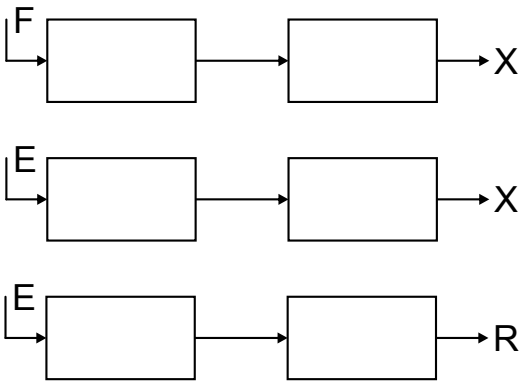

Figure 3.9: Schematic of the operating cycle for the batch process. E denotes de eluent inlet, F the feed inlet, X the extract outlet and R the raffinate outlet.

The cyclic operation was performed for five cycles. In Fig. 3.10 is represented the experimental data and the dynamic model simulation. The concordance between experimental and simulated profiles is fairly good.

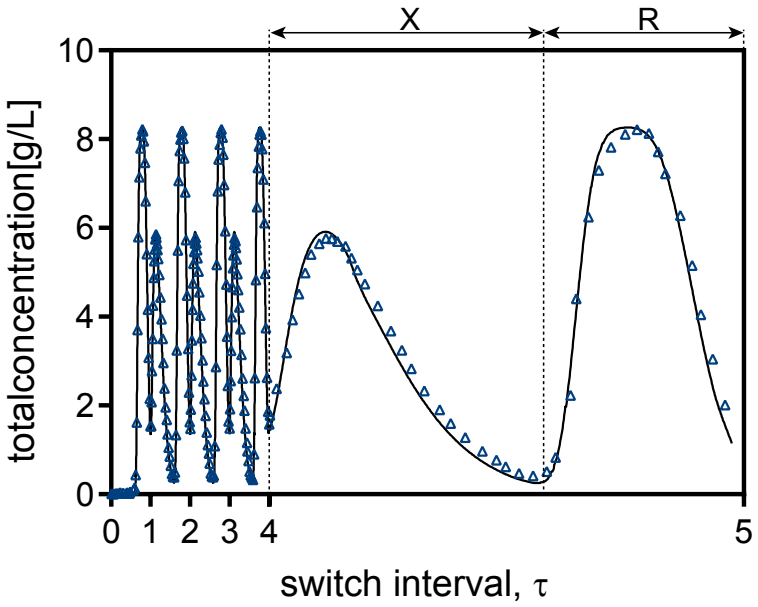

Figure 3.10: Solute concentration profile at the outlet of the system, for the batch-wise operation defined in Table 3.2. Symbols denote the experimental data $(c_1 + c_2)$, whereas the solid line represent the dynamic process model.

Previously we discussed the importance of adding an extra fraction to a batch elution, and the option to further process it or not. The recycling step is normally used to recycle an impure fraction back to the system, but it can also be used to replace the role of the desorbent, in terms of the progression of the band in the interior of the column. Fig. 3.11 shows an optimized cycle for a steady state recycling process, and Fig. 3.12 depicts the axial composition profiles of the fluid phase at four different periods of the cycle. As stated before, the recycling

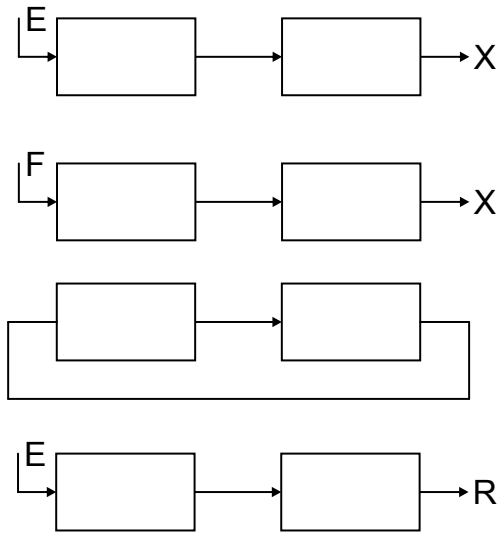

Figure 3.11: Schematic of the operating cycle for the SSR process. E denotes de eluent inlet, F the feed inlet, X the extract outlet and R the raffinate outlet.

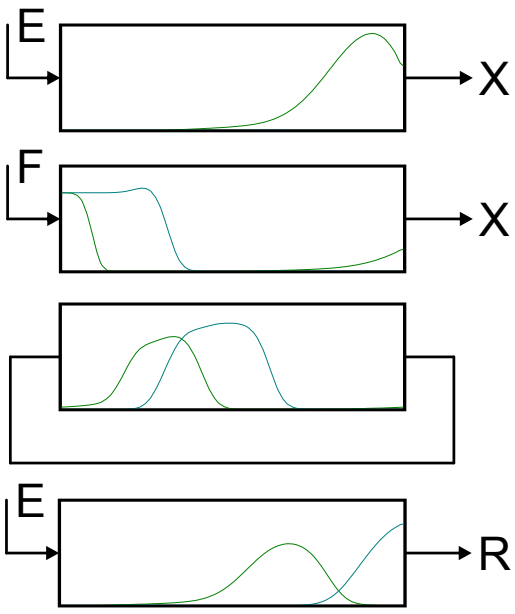

Figure 3.12: Axial composition profiles in the fluid phase at four intervals of the cycle. The green and blue lines represent solute 1 and 2 respectively.

step is being used for reducing the desorbent consumption, fact that is supported by analyzing Fig. 3.13 - Pareto optimal curves for batch and SSR processes. In this figure is possible to see that the range of productivity, represented by F_{av} is slightly increased, and the desorbent consumption is decreased for the SSR process. Generally speaking the performance of single column batch process can be enhanced by adding a recycle step. However, the biggest leap in productivity is obtained when the stationary phase is split into two columns, and we take advantage on the simulated counter-current movement of the solid phase, as we

discuss next.

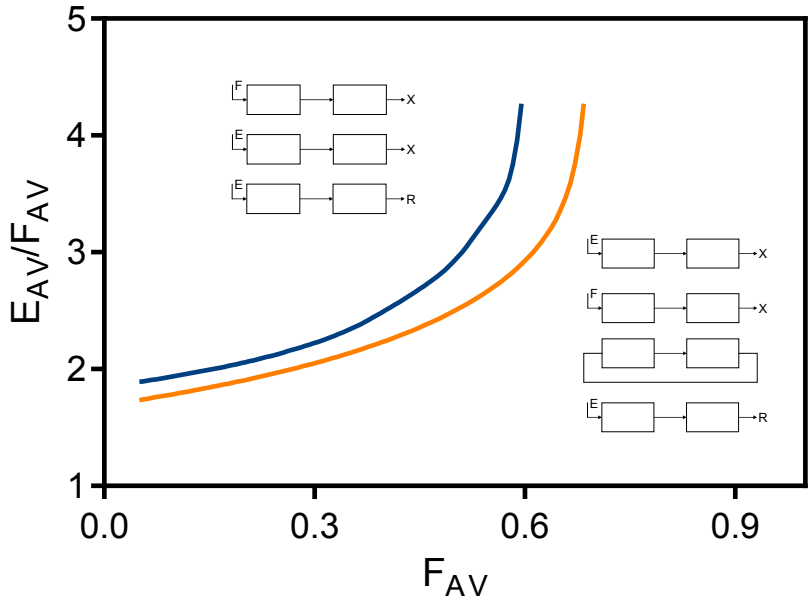

Figure 3.13: Optimal (Pareto) curves of eluent consumption (E_{av}/F_{av}) versus average feed flow rate (F_{av}), for solution of the separation problem defined in Table 3.1 with the batch and SSR configuration of Figs. 3.9 and 3.11. The blue solid line represents the solutions obtained for the batch configuration, whereas the orange line represent a case of SSR operation. The parameter values of the NLP design problem ($f_{obj} = maxf$) are: n_Q=3, $Q_{max} = Q'_{max}$=10 mL/min, Q_{min}=0.1 mL/min $Pur_R^{min} = Pur_X^{min}$=0.99.

3.6.2 Two-column open-loop SMB: continuous and discontinuous elution

Considering the possibilities for port configuration between two consecutive columns, given by Fig. 3.1 from (a) to (f), and that we want now to exploit the simulated counter-current movement of the solid phase, the cycles reported next follow the same approach that we see in a standard SMB process. The sequence of operations that applied to a specific column, is repeated to the next column, following the direction of the fluid phase. A complete cycle is finished when all the columns suffer the same sequence of operations.

3.6.3 Two-column open-loop SMB with continuous elution

Let us consider a cycle that can be implemented with the schematic of Fig. 3.2: a two-column, open-loop configuration. In order to design such cycle, the first

condition in Eq. 3.10 is enforced at each sub-step, of the switching interval for generating an open-loop configuration. Also, we are interested in keeping the system as simple as possible, namely to keep the desorbent and feed pumps in a steady operation. This can be obtained by the following constraint:

$$E_1^{(1)} = E_1^{(2)} = E_1^{(3)} = E, \quad E \leq Q_{max.} \tag{3.30}$$

The optimal solution for $n_Q = 3$, i.e., for three sub-division of the switching interval is given in Table 3.3 and a schematic of the cycle is depicted in Fig. 3.14.

Table 3.3: Optimal operating cycle for the solution of the separation problem defined in Table 3.1 with a two-column, open-loop configuration with continuous elution (Fig. 3.14). The parameter values for the NLP design problem ($f_{obj} = maxf$) are: n_Q=3, Q_{min}=0.1 mL/min, $Q_{max} = Q'_{max}$=10 mL/min, $Pur_R^{min} = Pur_X^{min}$=0.99. The step durations, τ_n, are expressed in minutes; the eluent (E), feed (F), extract (X), and raffinate (R) flow rates are given in mL/min. The first value on the bottom row is the switching interval, $\tau = \sum_n \tau_n$.

Step, n	τ_n	E	F	X	R
1	4.144	2.615	0.000	2.615	0.000
2	0.603	2.615	7.385	0.000	10.000
3	0.195	2.615	0.000	0.000	2.615
Average	4.942	2.615	0.901	2.193	1.323

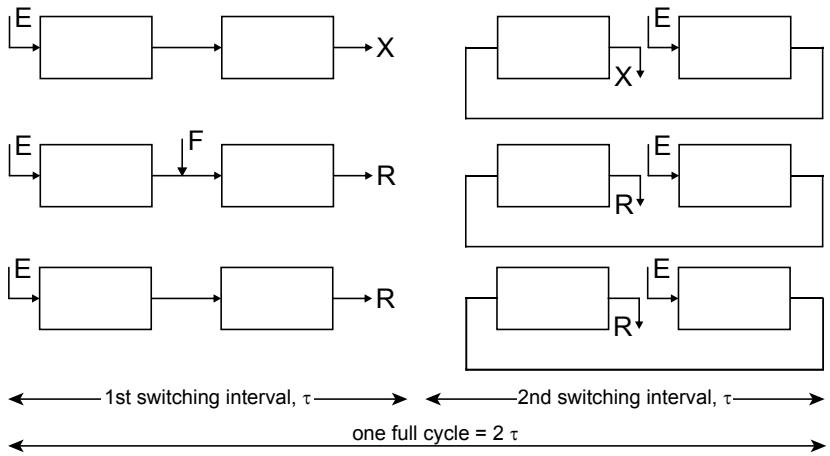

Figure 3.14: Schematic of the operating cycle (2τ) for the two-column, open-loop process with continuous elution. E denotes de eluent inlet, F the feed inlet, X the extract outlet and R the raffinate outlet.

The cycle was implemented on the unit shown in Fig.3.2. Upon completion of the fourth cycle, a cyclic steady state was visible, after which a few more cycles were carried out. In the last cyclic operation the fraction collector was used to recover 100 μL samples, which were analyzed by HPLC, and are represented in Fig. 3.15. The agreement between experimental and simulated profiles is reasonably good.

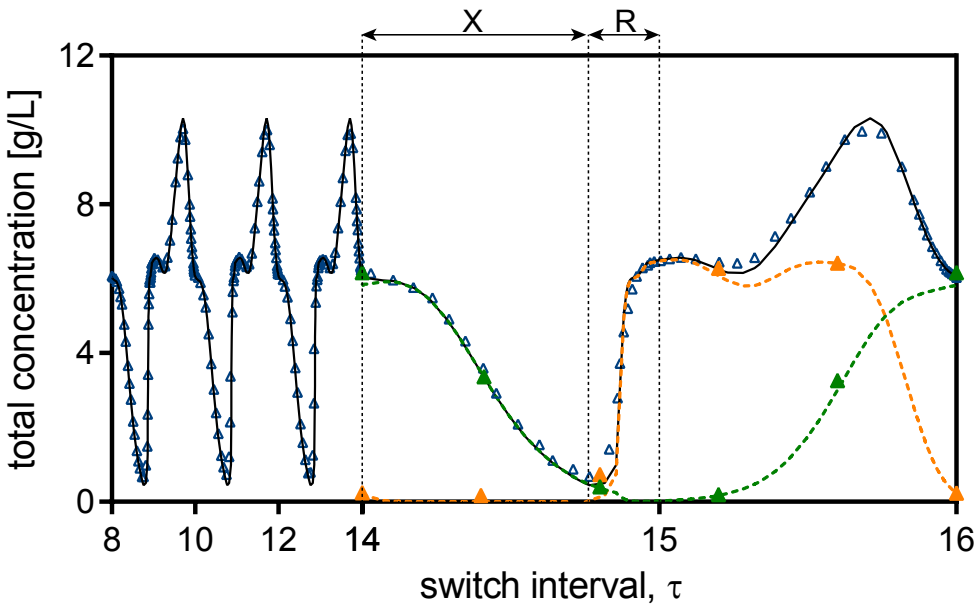

Figure 3.15: Solute concentration profile at the outlet of the system, for the two-column, open-loop operation with continuous elution defined in Table 3.3. The solid line represents the dynamic process model $(c_1 + c_2)$ and the blue triangles denotes the experimental data; the traced green and orange lines represent the model solution for solutes 1 and 2 respectively whereas the green and orange triangles are the analyzed fractions collected in the last operating cycle.

Fig. 3.16 shows the cyclic steady state of the axial composition profiles in the liquid phase for the first switching interval of the cycle. Over the second switching interval the columns undergo the same steps, but their positions are reversed.

The cycle is defined by two characteristics: (i) because of the open-loop nature of the process, both products, extract and raffinate are collected alternately recovered at the downstream of the column end of the unit, while desorbent is supplied into the upstream of the system; (ii) like in any counter-current process, the feed injection is done in the point of the system where the composition of the fluid is closest to that on the feedstock.

The position and timing of the feed injection in the system is an intrinsic component of the design procedure, and depends on the selectivity of the separation. Because we are operating the desorbent pump in a steady operation, we need to consider the possibilities for superimpose the feed injection over the fractionation steps. Depending on the volume of the feed injection compared to the fractions of the products, three scenarios can occur while the feed injection is performed: (i) we are recovering the extract; (ii) we are collecting the final part of the extract band, after what we start to recover the raffinate or (iii) we are collecting the raffinate. In the present case the Feed is injected during the raffinate collection. In Fig. 3.16 is

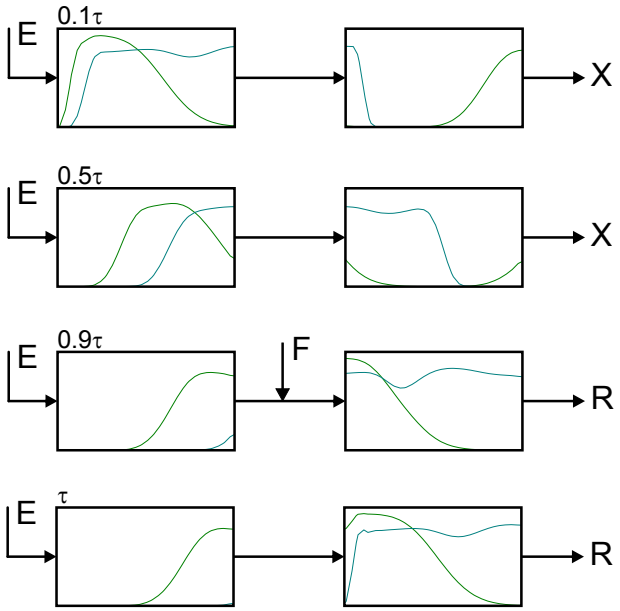

Figure 3.16: Steady periodic solution of the axial composition profile for the first switching interval for the two-column, open-loop operation with continuous elution defined in Table 3.3. The green and blue lines represent solutes 1 and 2 respectively.

possible to see that at the last instants of the switching interval, the first column is occupied primarily by the extract band. The process discussed next takes advantage of this fact, and keeps this band 'parked' in the first column while we use the feed pulse to elute the first part of the raffinate band.

Two-column open-loop SMB with discontinuous elution

This variant of the two-column open-loop presented before has a discontinuous elution, i.e. there is a step of the switching interval, where $E = 0$; as a consequence, the internal axial profiles of the fluid phase are 'frozen'. Experimentally this may be accomplished by two different ways: (i) by switching the eluent pump flow-rate in the determinate step to zero, or (ii) by closing the column valves at both upstream and downstream, and recirculate the desorbent back to the vase, keeping the steady operation of the eluent pump. The second option has the advantage of not only eliminating the uncertainty in the flow-rates, but also the prevent the inertial flow of the band in the interior of the column. To enforce the discontinuous flow in this process, Eq. 3.30 has to be modified,

$$E_1^{(1)} = E_1^{(3)} = E, \quad E \leq Q_{max.} \tag{3.31}$$

$$E_1^{(2)} = 0 \tag{3.32}$$

It is worth noting that this constraint serves only to fulfill the node balance for each of the three sub-divisions of the switching interval, in practice $E_1^{(2)}$ is not set to zero, instead is redirected back to the desorbent vase, by the afore mentioned circuit of valves, that are present in each inlet node.

The optimal solution for $n_Q = 3$, i.e., for three sub-divisions of the switching interval is given in Table 3.4 and a schematic of the cycle is depicted in Fig. 3.17.

Table 3.4: Optimal operating cycle for the solution of the separation problem defined in Table 3.1 with a two-column, open-loop configuration with discontinuous elution (Fig. 3.17). The parameter values for the NLP design problem ($f_{obj} = maxf$) are: n_Q=3, $Q_{min} = 0.1$ mL/min, $Q_{max} = Q'_{max} = 10$ mL/min, $Pur_R^{min} = Pur_X^{min} = 0.99$. The step durations, τ_n, are expressed in minutes; the eluent (E), feed (F), extract (X), and raffinate (R) flow rates are given in mL/min. The first value on the bottom row is the switching interval, $\tau = \sum_n \tau_n$.

Step, n	τ_n	E	F	X	R
1	4.069	2.669	0.000	2.669	0.000
2	0.444	0.000	10.000	0.000	10.000
3	0.758	2.669	0.000	0.000	2.669
Average	5.271	2.444	0.843	2.060	1.227

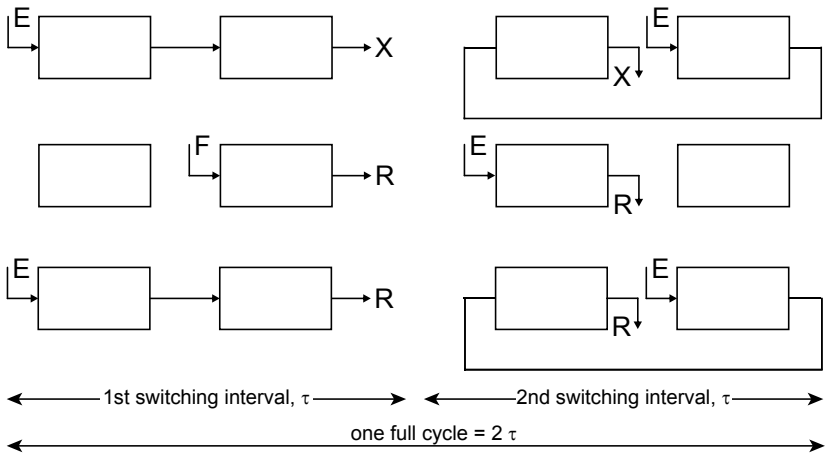

Figure 3.17: Schematic of the operating cycle (2τ) for the two-column, open-loop process with discontinuous elution. E denotes de eluent inlet, F the feed inlet, X the extract outlet and R the raffinate outlet.

The cycle was implemented on the unit shown in Fig.3.2. Upon completion of the

fifth cycle, a cyclic steady state was visible, after which a few more cycles were carried out. In the last cyclic operation the fraction collector was used to recover 100 μL samples, which were analyzed by HPLC, and are represented in Fig. 3.18.

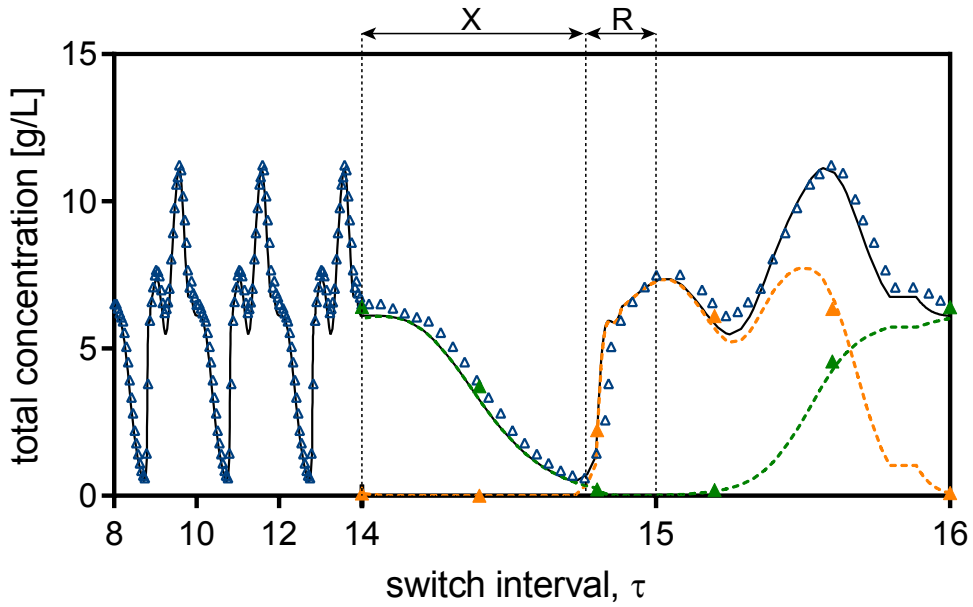

Figure 3.18: Solute concentration profile at the outlet of the system, for the two-column, open-loop operation with continuous elution defined in Table 3.4. The solid line represent the dynamic process model $(c_1 + c_2)$ and the blue triangles denotes the experimental data; the traced green and orange lines represents the model solution for solutes 1 and 2 respectively whereas the green and orange triangles are the analyzed fractions collected in the last operating cycle.

3.6.4 Optimal Pareto curves for the cases reported

Fig. 3.20 compares the optimal curves of productivity against eluent consumption, $F_{av} \times E_{av}/F_{av}$ plane for the different processes presented, batch, SSR and both of the two-column open-loop schemes. Note that any point above the Pareto curve has worse performance than the points on the Pareto curve, because there is always one element of the Pareto set that has a lower solvent consumption for the same feed throughput. The points located below the Pareto curve are not feasible because the purity constraints are not fulfilled. When moving along the Pareto curve, each point is non-dominant with respect to the others, because it is either less productive, but consumes less solvent, or more productive, but requires more solvent. The choice of the optimal operating point depends also on other factors, such as the economics of the process that are not contemplated in this analysis.

The Pareto curves of Figs. 3.13 and 3.20 were created on the assumption that

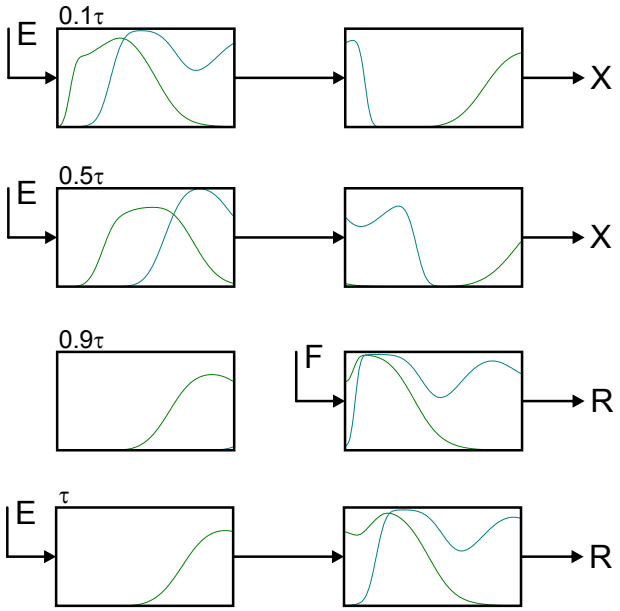

Figure 3.19: Steady periodic solution of the axial composition profile for the first switching interval for the two-column, open-loop operation with discontinuous elution defined in Table 3.3. The green and blue lines represents solutes 1 and 2 respectively.

the respective processes are constrained by the combined effects of dispersion and mass-transfer resistances on band broadening and not by the pressure drop.

The analysis of Fig. 3.20 reveals that the two-column, open-loop processes should perform better in terms of productivity and solvent consumption when compared to the simpler single column processes, in fact if we look to Fig. 3.16 and comparing it against the equivalents on the batch and SSR processes, we can clearly see why the counter-current movement of the solid is so beneficial for the separation. In all processes the amount of stationary phase used was kept constant, however if we look to the internal axial composition profiles we can see that in the case of both two-column open-loop processes the stationary phase is much more loaded with solutes.

Looking closer to the two-open-loop processes, we can see that the discontinuous elution slightly decreases the eluent consumption in the mid-range productivity zone. Also, we can see that the extension in the productivity range, that the continuous elution process offers comes at a cost, a higher eluent consumption.

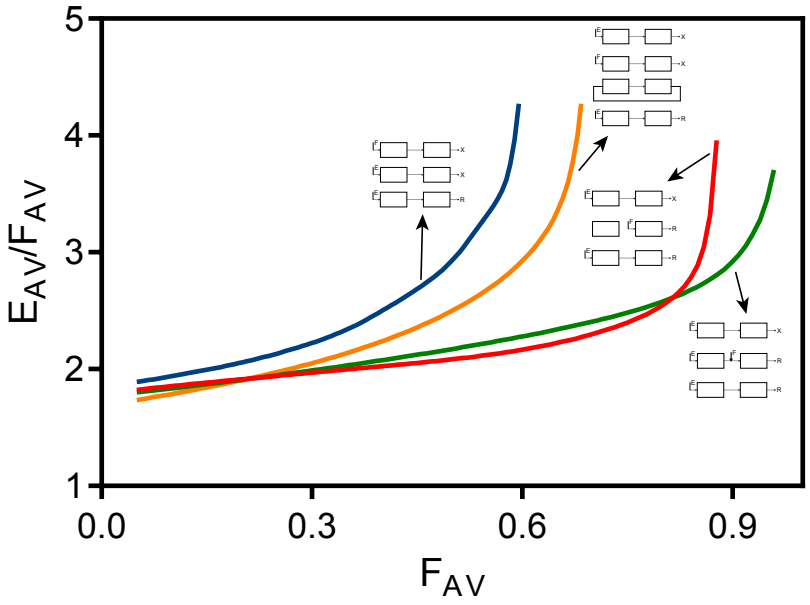

Figure 3.20: Optimal (Pareto) curves of eluent consumption (E_{av}/F_{av}) versus average feed flow rate (F_{av}), for solution of the separation problem defined in Table 3.1 with the configurations of Figs. 3.9, 3.11, 3.14 and 3.17. The blue, orange lines represent the solutions obtained for the batch and steady state recycling respectively, whereas the green and red lines represents the two-column open-loop configuration with continuous and discontinuous elution, respectively. The parameter values of the NLP design problem ($f_{obj} = maxf$) are: n_Q=3, $Q_{max} = Q'_{max}$=10 mL/min, Q_{min}=0.1 mL/min $Pur_R^{min} = Pur_X^{min}$=0.99

3.7 Concluding Remarks

In the present work, two-column, semi-continuous chromatographic processes for binary separation, with continuous and discontinuous elution strategies have been presented and were experimentally validated on a nonlinear separation . These compact systems combine a flexible node design with pulsed feeding to implement hybrid schemes between batch and simulated counter-current chromatography modes. The semi-continuous, two-column open-loop processes combine the simplicity and flexibility of the batch process and the increased productivity of multi-column chromatography.

The two-column processes reported here proved to be more efficient than single-column processes studied in this work - batch chromatography and SSR. For high-value purifications, of which many examples are found in the pharmaceutical, fine chemistry, and biotechnology industries, these processes appear to be promising alternatives to single-column batch chromatography, because of their increased performance, simplicity of implementation and operation, and easiness of scale-up.

References

[1] Giuseppe Storti, Marco Mazzotti, Massimo Morbidelli, and Sergio Carrà. Robust design of binary countercurrent adsorption separation processes. *AIChE Journal*, 39(3):471–492, 1993.

[2] Marco Mazzotti, Giuseppe Storti, and Massimo Morbidelli. Optimal operation of simulated moving bed units for nonlinear chromatographic separations. *Journal of Chromatography A*, 769(1):3–24, 1997.

[3] Douglas M Ruthven and CB Ching. Counter-current and simulated counter-current adsorption separation processes. *Chemical Engineering Science*, 44(5): 1011–1038, 1989.

[4] Jochen Strube, Sonja Haumreisser, Henner Schmidt-Traub, Michael Schulte, and Reinhard Ditz. Comparison of batch elution and continuous simulated moving bed chromatography. *Organic Process Research & Development*, 2(5): 305–319, 1998.

[5] Andreas Jupke, Achim Epping, and Henner Schmidt-Traub. Optimal design of batch and simulated moving bed chromatographic separation processes. *Journal of Chromatography A*, 944(1):93–117, 2002.

[6] Larry Miller, Charles Grill, Tony Yan, Olivier Dapremont, Elke Huthmann, and Markus Juza. Batch and simulated moving bed chromatographic resolution of a pharmaceutical racemate. *Journal of Chromatography A*, 1006(1):267–280, 2003.

[7] Charles M Grill, Larry Miller, and Tony Q Yan. Resolution of a racemic pharmaceutical intermediate: A comparison of preparative hplc, steady state recycling, and simulated moving bed. *Journal of Chromatography A*, 1026(1): 101–108, 2004.

[8] Philippe Adam, Roger Narc Nicoud, Michel Bailly, and Olivier Ludemann-Hombourger. Process and device for separation with variable-length, October 24 2000. US Patent 6,136,198.

[9] O Ludemann-Hombourger, RM Nicoud, and M Bailly. The “varicol” process: a new multicolumn continuous chromatographic process. *Separation Science and Technology*, 35(12):1829–1862, 2000.

[10] Abdelaziz Toumi, Felix Hanisch, and Sebastian Engell. Optimal operation of continuous chromatographic processes: Mathematical optimization of the varicol process. *Industrial & engineering chemistry research*, 41(17):4328–4337, 2002.

[11] Henning Schramm, Malte Kaspereit, Achim Kienle, and Andreas Seidel-Morgenstern. Improving simulated moving bed processes by cyclic modulation of the feed concentration. *Chemical engineering & technology*, 25(12): 1151–1155, 2002.

[12] H Schramm, A Kienle, M Kaspereit, and A Seidel-Morgenstern. Improved operation of simulated moving bed processes through cyclic modulation of feed flow and feed concentration. *Chemical engineering science*, 58(23): 5217–5227, 2003.

[13] Michael M Kearney and Kathleen L Hieb. Time variable simulated moving bed process, April 7 1992. US Patent 5,102,553.

[14] E Kloppenburg and ED Gilles. A new concept for operating simulated moving-bed processes. *Chemical engineering & technology*, 22(10):813–817, 1999.

[15] Ziyang Zhang, Marco Mazzotti, and Massimo Morbidelli. Powerfeed operation of simulated moving bed units: changing flow-rates during the switching interval. *Journal of Chromatography A*, 1006(1):87–99, 2003.

[16] Ziyang Zhang, Massimo Morbidelli, and Marco Mazzotti. Experimental assessment of powerfeed chromatography. *AIChE journal*, 50(3):625–632, 2004.

[17] Yifei Zang and Phillip C Wankat. Smb operation strategy-partial feed. *Industrial & engineering chemistry research*, 41(10):2504–2511, 2002.

[18] Thomas B Jensen, Tiem GP Reijns, Hugo AH Billiet, and Luuk AM van der Wielen. Novel simulated moving-bed method for reduced solvent consumption. *Journal of Chromatography A*, 873(2):149–162, 2000.

[19] Dorota Antos and Andreas Seidel-Morgenstern. Two-step solvent gradients in simulated moving bed chromatography: Numerical study for linear equilibria. *Journal of Chromatography A*, 944(1):77–91, 2002.

[20] Stefanie Abel, Marco Mazzotti, and Massimo Morbidelli. Solvent gradient operation of simulated moving beds: 2. langmuir isotherms. *Journal of Chromatography A*, 1026(1):47–55, 2004.

[21] Ricardo JS Silva, Rui CR Rodrigues, Hector Osuna-Sanchez, Michel Bailly, Eric Valéry, and José PB Mota. A new multicolumn, open-loop process for center-cut separation by solvent-gradient chromatography. *Journal of Chromatography A*, 1217(52):8257–8269, 2010.

[22] Jonathan P Meissner and Giorgio Carta. Continuous regioselective enzymatic esterification in a simulated moving bed reactor. *Industrial & engineering chemistry research*, 41(19):4722–4732, 2002.

[23] Yifei Zang and Phillip C Wankat. Three-zone simulated moving bed with partial feed and selective withdrawal. *Industrial & engineering chemistry research*, 41(21):5283–5289, 2002.

[24] Yoshiaki Kawajiri and Lorenz T Biegler. Nonlinear programming superstructure for optimal dynamic operations of simulated moving bed processes. *Industrial & engineering chemistry research*, 45(25):8503–8513, 2006.

[25] Rui CR Rodrigues, João MM Araújo, and José PB Mota. Optimal design and experimental validation of synchronous, asynchronous and flow-modulated, simulated moving-bed processes using a single-column setup. *Journal of Chromatography A*, 1162(1):14–23, 2007.

[26] José PB Mota, Isabel AAC Esteves, and Mário FJ Eusébio. Synchronous and asynchronous smb processes for gas separation. *AIChE journal*, 53(5): 1192–1203, 2007.

[27] Chim Yong Chin and Nien-Hwa Linda Wang. Simulated moving bed equipment designs. *Separation & Purification Reviews*, 33(2):77–155, 2004.

[28] Kwangnam Lee. Two-section simulated moving-bed process. *Separation Science and Technology*, 35(4):519–534, 2000.

[29] Masao Ando, Masatake Tanimura, and Masao Tamura. Method of chromatographic separation, November 13 1990. US Patent 4,970,002.

[30] Weihua Jin and Phillip C Wankat. Two-zone smb process for binary separation. *Industrial & engineering chemistry research*, 44(5):1565–1575, 2005.

[31] Weihua Jin and Phillip C Wankat. Scaling rules and increasing feed rates in two-zone and four-zone simulated moving bed systems. *Industrial & engineering chemistry research*, 45(8):2793–2807, 2006.

[32] Jin Seok Hur and Phillip C Wankat. New design of simulated moving bed (smb) for ternary separations. *Industrial & engineering chemistry research*, 44 (6):1906–1913, 2005.

[33] Jin Seok Hur and Phillip C Wankat. Two-zone smb/chromatography for center-cut separation from ternary mixtures: Linear isotherm systems. *Industrial & engineering chemistry research*, 45(4):1426–1433, 2006.

[34] Guido Ströhlein, Lars Aumann, Thomas Müller-Späth, Abhijit Tarafder, and Massimo Morbidelli. Continuous processing: The multicolumn countercurrent solvent gradient purification process. 2007.

[35] Nadia Abunasser and Phillip C Wankat. One-column chromatograph with recycle analogous to simulated moving bed adsorbers: Analysis and applications. *Industrial & engineering chemistry research*, 43(17):5291–5299, 2004.

[36] Rui CR Rodrigues, João MM Araújo, Mário FJ Eusébio, and José PB Mota. Experimental assessment of simulated moving bed and varicol processes using a single-column setup. *Journal of Chromatography A*, 1142(1):69–80, 2007.

[37] João MM Araújo, Rui CR Rodrigues, Ricardo JS Silva, and Jose PB Mota. Single-column simulated moving-bed process with recycle lag: Analysis and applications. *Adsorption Science & Technology*, 25(9):647–659, 2007.

[38] Rui CR Rodrigues, Tiago JSB Canhoto, João MM Araújo, and José PB Mota. Two-column simulated moving-bed process for binary separation. *Journal of Chromatography A*, 1180(1):42–52, 2008.

[39] Phillip C Wankat. Simulated moving bed cascades for ternary separations. *Industrial & engineering chemistry research*, 40(26):6185–6193, 2001.

[40] M.C. Ferris and J.S. Pang. *Complementarity and Variational Problems: State of the Art*. SIAM Proceedings Series. Society for Industrial and Applied Mathematics, 1997. ISBN 9780898713916. URL `http://books.google.pt/books?id=vQXA3oqLcnUC`.

[41] José PB Mota and João MM Araújo. Single-column simulated-moving-bed process with recycle lag. *AIChE journal*, 51(6):1641–1653, 2005.

[42] João MM Araújo, Rui CR Rodrigues, and José PB Mota. Use of single-column models for efficient computation of the periodic state of a simulated moving-bed process. *Industrial & engineering chemistry research*, 45(15):5314–5325, 2006.

[43] João MM Araújo, Rui CR Rodrigues, and José PB Mota. Optimal design and operation of a certain class of asynchronous simulated moving bed processes. *Journal of Chromatography A*, 1132(1):76–89, 2006.

[44] JP Barbosa Mota, E Saatdjian, D Tondeur, and AE Rodrigues. On the numerical solution of partial differential equations with two spatial scales. *Computers & chemical engineering*, 21(4):387–397, 1997.

[45] Yoshiaki Kawajiri and Lorenz T Biegler. Optimization strategies for simulated moving bed and powerfeed processes. *AIChE Journal*, 52(4):1343–1350, 2006.

[46] BT Baumrucker, JG Renfro, and Lorenz T Biegler. Mpec problem formulations and solution strategies with chemical engineering applications. *Computers & Chemical Engineering*, 32(12):2903–2913, 2008.

[47] Robert Fourer, David M Gay, and Brian W Kernighan. *AMPL: A mathematical programming language*. AT&T Bell Laboratories Murray Hill, NJ 07974, 1987.

[48] Andreas Wächter and Lorenz T Biegler. On the implementation of an interior-point filter line-search algorithm for large-scale nonlinear programming. *Mathematical programming*, 106(1):25–57, 2006.

[49] Douglas Morris Ruthven. Principles of adsorption and adsorption processes. 1984.

[50] Jörg Worlitschek, Marcello Bosco, Markus Huber, Volker Gramlich, and Marco Mazzotti. Solid-liquid equilibrium of tröger's base enantiomers in ethanol: Experiments and modelling. *Helvetica chimica acta*, 87(2):279–291, 2004.

[51] Mário FJ Eusébio. Development of an universal interface for monitoring and control of chemical and biochemical processes, 2006.

[52] João MM Araújo, Rui CR Rodrigues, and José PB Mota. Determination of competitive isotherms of enantiomers by a hybrid inverse method using overloaded band profiles and the periodic state of the simulated moving-bed process. *Journal of Chromatography A*, 1189(1):302–313, 2008.

4

Relay simulated moving bed: concept and design criteria

4.1 Introduction

Simulated moving-bed (SMB) chromatography, as a practical implementation of the true moving-bed (TMB) concept, realizes continuous and effective separation of unresolved mixtures, while achieving high throughput and low desorbent consumption [1–4].

Typically, a SMB unit consists of a train of identical chromatographic columns, as shown in the top schematic of Fig. 4.1, divided into four sections by two inlets and two outlets, in such a way that feed is continuously injected between sections 2 and 3, fresh desorbent is introduced between sections 4 and 1, the extract—enriched in the more retained solute—is withdrawn between sections 1 and 2, and the raffinate, which contains the less retained component, is collected between sections 3 and 4. In the case of the common closed-loop configuration, the outlet of section 4 is recycled to section 1, otherwise it is collected and possibly recycled off-line in the case of the open-loop configuration. The countercurrent movement of the fluid phase and of the adsorbent is simulated by periodically switching the positions of the inlet and outlet ports by one column in the same direction of the fluid flow; alternatively, the columns can be moved periodically by one position against the direction of the fluid flow. The time interval between two consecutive

switches is the switch interval, τ. Although the four-section SMB, with one or more

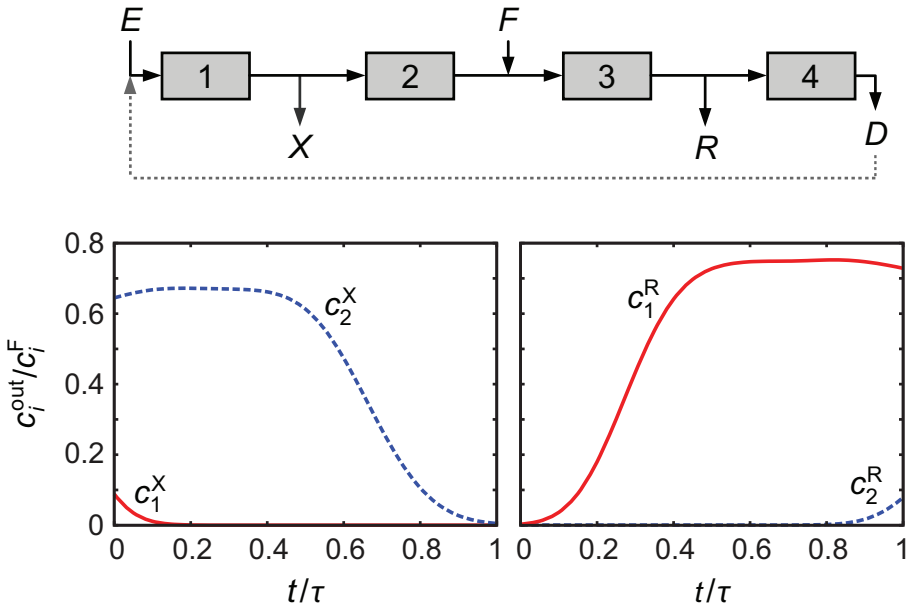

Figure 4.1: (Top) Schematic of a four-zone SMB; every τ time units, the port positions are moved one column ahead in the direction of the fluid flow or the columns move by one position against the direction of the fluid flow. The outlet D of section 4 is recycled to section 1 in the case of the closed-loop configuration (dashed line), otherwise it is collected and possibly recycled off-line in the case of the open-loop configuration. (Bottom) Steady periodic solution of the composition profiles in the extract (left) and raffinate (right) streams, during a switch interval, in a 4-column (1/1/1/1) SMB for a linear separation defined by $\alpha = 1.4$ and $Pe = 200$.

columns per section, is the most studied configuration, units with more than four sections have been developed to improve the process performance or to achieve multi-fraction separation [5, 6]. Moreover, SMB units with less than four sections, namely two [7–12] and three [1, 13, 14] sections, and even one-column SMB analogs [15–18], have also been proposed.

The increasing use of the SMB as a multipurpose unit in the pharmaceutical industry, where it can be potentially applied to different separations at all stages of the drug-development cycle, has led to the development of novel column configurations and operating schemes, some of which are substantially different from the classical four-section process. Broadly speaking, most of the new operating schemes introduce temporal modulations of selected control parameters into the operating cycle [3].

Concepts such as asynchronous port switching (alias Varicol®) [19–21], cyclic modulation of the feed concentration [22, 23], time-variable manipulation of the flow rates [24–28], and modulation of solvent strength during process operation [29–31], have been thoroughly analyzed. The extra degrees of freedom available

with the non-classical schemes improve the separation efficiency, thus allowing the units to have fewer columns. Of the recently suggested process modifications that have shown potential for improved performance, we shall briefly discuss next only those whose concepts are more closely related to the present work.

One of these modifications, termed outlet streams swing (OSS) [32, 33], varies the extract and raffinate flow rates over time, while keeping the average section flow rates over a switch interval the same as in a classic SMB. Therefore, a reduction of the extract or raffinate flow rate over an initial fraction of the switch interval is compensated by an increase of the same flow rate over the remaining part of the switch interval, or vice-versa. In one variant of the OSS technique, the extract and raffinate flow rates are both varied at the same time, with high extract and low raffinate flow rates during an initial fraction of the switch interval, followed by low extract and high raffinate flow rates, or vice-versa. In several test cases, including chiral separation, the OSS scheme was shown to improve the product purities over the classical SMB process.

Another operating concept combines non-permanent product withdrawal at one or both outlet ports with an internal recycle and re-feeding of the impure fraction in alternation to the original feed mixture [34]. Simulation studies for linear and non-linear isotherms showed [35] that this fractionation and feed-back approach (FF-SMB) is superior, in terms of process performance and product recovery, to both the conventional SMB process as well as to a previously suggested ”partial discard”-SMB strategy [36].

Yet another SMB modification is the improved or intermittent SMB (I-SMB) process developed by Nippon Rensui Corp. (Tokyo, Japan) [37], which is claimed to achieve higher productivity. In the I-SMB process the switch interval is divided in two sub-intervals, and only during the first sub-interval the product streams are collected. The potential of the I-SMB technology was demonstrated experimentally and by detailed simulations in the cases of separation of binary mixtures subject to linear and nonlinear isotherms [38–40].

For the purposes of the present discussion we are particularly interested in the open-loop configuration of a standard SMB; this is the configuration depicted in the top schematic of Fig. 4.1 but without the dashed line. We shall discuss later how to change from the open-loop to the closed-loop configuration.

The temporal profiles plotted in the two graphs of Fig. 4.1 are the composition profiles in the extract and raffinate streams, over the duration τ of a switch interval, for cyclic steady-state operation of a 4-column, SMB with linear adsorption

isotherms. The system is characterized by a selectivity $\alpha = 1.4$ and Péclet number $Pe = vL/D_{\mathrm{L}} = 200$, where v is the interstitial fluid velocity, L is the column length, and D_{L} is the axial dispersion coefficient. The selectivity is defined as

$$\alpha = \frac{\epsilon + (1-\epsilon)K_2}{\epsilon + (1-\epsilon)K_1}, \tag{4.1}$$

where K_i is the Henry constant of component i and ϵ is the bed porosity. The product purities are set at $P_{\mathrm{R}} = P_{\mathrm{X}} = 0.99$, and the flow rates in zones 1 and 4 are correctly sized to ensure that the effluent from zone 4 is clean and can be recycled back into the upstream end of the system. We shall henceforth denote the flow rate in zone j or column j by Q_j, the feed flow rate by F, the extract flow rate by X, and the raffinate flow rate by R.

During a switch interval the internal axial composition profile is displaced in the direction of the fluid flow (from left to right in the top schematic of Fig. 4.1). At the end of the switch interval the active ports or the columns are switched to implement the simulated countercurrent contact between the fluid and solid phases; the port (or column) switching repositions the composition profile with respect to the active ports as it was at the beginning of the switch interval.

Let us first analyze the extract stream (left plot in Fig. 4.1). During most of the switch interval the composition profile is 100% pure in the more retained component, but there is an initial segment of the switch interval during which the extract is contaminated with the less retained solute. This residual contamination happens because the extremity of the trailing edge of the less-retained component's axial concentration profile is initially located in zone 1 and crosses the extract port as the profile is displaced into zone 2.

As regards the raffinate stream (right plot in Fig. 4.1), during most of the switch interval the composition profile is 100% pure in the less retained component, but there is a final segment of the switch interval during which the raffinate is contaminated with the more retained component. This happens because the leading edge of the more retained component's axial concentration profile crosses the raffinate port.

The concentration profiles plotted in Fig. 4.1 illustrate what happens at the two product outlets of a classical SMB unit. At any time during a switch interval only a fraction X/Q_1 of the effluent of zone 1 is recovered as extract whereas the other fraction, Q_2/Q_1, flows through to zone 2. Similarly, only a fraction R/Q_3 of the effluent of zone 3 is collected as raffinate while the remaining fraction, Q_4/Q_3,

flows through to zone 4. This happens throughout the switch interval, even though, as it was seen above, over most of the switch interval the effluents from zones 1 and 3 are pure. It is somewhat counterintuitive why, at any time, a significant fraction of the effluents of zones 1 and 3 are allowed to flow through to the next zone and are not completely recovered as pure products. In fact, one is tempted to suggest a different way of operating the process: if the effluent from zone 1 or zone 3 is pure, it is collected as product; if the effluent is contaminated with the undesired solute, it flows through to the next downstream zone.

Of course that there is a reason for the standard operation of the SMB: the continuous splitting of the effluents of zones 1 and 3 into two streams—one providing continuous product withdrawal and the other the internal recycle—is the direct consequence of the analogy between the steady-state TMB process and the periodic SMB process. Still, the alternative way suggested above of handling the product outlets does not seem to be completely unreasonable, and was actually the motivation for the work reported here.

To be more precise, the aim of the present work is to change the way of handling the two product outlets of the SMB in order to avoid the use of flow controllers or an extra pump—the idea is to have just two- or three-way valves at the outlets—while maintaining the analogy with the SMB in terms of displaced volumes of fluid per switch interval. To achieve this, the continuous splitting of the effluents of zones 1 and 3 is replaced by two different actions applied sequentially over the switch interval: one of diverting the effluent for product collection and the other of directing the effluent to the next downstream zone. The basic idea is illustrated in the schematics of Fig. 4.2: the port configuration in the left schematic, which holds for the duration of a switch interval, is replaced by the port configurations in one of the schematics on the right, which divide the switch interval into two different sub-steps. Because of the "on-off" switching of the outlet streams, we call such process a *relay SMB* (R-SMB). We shall first derive the proper operating cycle of

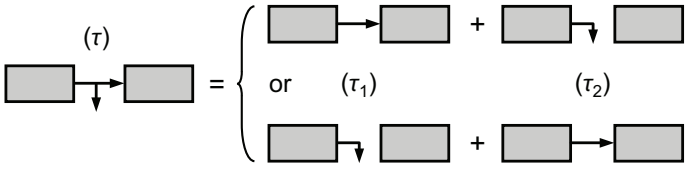

Figure 4.2: Schematic of basic idea behind the relay SMB: the continuous splitting of the effluents of zones 1 and 3 in the standard SMB (left schematic) is replaced by one of the schematics on the right, which involve diverting the effluent for product collection during a fraction of the switch interval and directing the effluent to the next downstream zone during the other fraction of the switch interval.

the R-SMB process and then demonstrate, under the framework of the equilibrium theory, that the R-SMB process has the same separation region as the classical SMB for linear adsorption systems. In addition, the results from the equilibrium theory show that the R-SMB process consists of two distinct cycles: one for selectivities smaller than a critical value and another cycle for larger values of α. Moreover, it is shown that in both instances of the R-SMB concept the flow through a zone (or column) is always in one of three states: (i) frozen, (ii) completely directed to the next zone (or column), or (iii) entirely diverted to a product line. This restricted ensemble of port configurations has been exploited before by our group to derive various classes of two- and three-column SMB processes [10–12, 41]. We then examine the R-SMB process under conditions of finite column efficiency and compare its performance to those of the classical open- and closed-loop SMBs. Finally, the work is summarized before drawing final conclusions.

4.2 Process description

Remembering the discussion of Fig. 4.1, it is apparent that the extract is contaminated during an initial stage of the switch interval, whereas the raffinate is contaminated during a final fraction of the switch interval. Thus, in the R-SMB process the raffinate should be collected first, during an initial stage of the switch interval, by means of the port configuration shown in the bottom-right schematic of Fig. 4.2, and the extract should be withdrawn last, during a final stage of the switch interval, by means of the top-right schematic of Fig. 4.2.

Let us follow this line of thought in order to complete the operating cycle of the R-SMB and to derive one way of determining the duration of its sub-steps. In a classical SMB, the amount of fluid that leaves zone 1 during a switch interval is τQ_1, the amount of collected extract is $\tau X = \tau(Q_1 - Q_2)$, and the amount of fluid that is directed to section 2 is $\tau Q_2 = \tau(Q_1 - X)$; the amount of fluid that leaves zone 3 during a switch interval is τQ_3, the amount of collected raffinate is $\tau R = \tau(Q_3 - Q_4)$, and the amount of fluid that is directed to section 4 is $\tau Q_4 = \tau(Q_3 - R)$.

To collect the same amount of raffinate per switch interval as in the SMB, the effluent of zone 3 in the R-SMB is diverted for raffinate collection during the first $\tau_1 = \tau R/Q_3$ time units of the switch interval; during the rest of the switch interval the outlet is directed to zone 4. To collect the same amount of extract per switch interval as in the SMB, the effluent of zone 1 in the R-SMB is diverted for extract withdrawal during the last $\tau_3 = \tau X/Q_1$ units of the switch interval; during the rest

of the switch interval the outlet is directed to zone 2. Using the equilibrium theory, we shall demonstrate that between these two sub-steps of the switch interval, that is, for $\tau_1 < t < \tau - \tau_3$, the internal axial concentration profile in the R-SMB should be displaced in the direction of fluid flow without any product withdrawal.

Figure 4.3 shows a schematic of the proposed three-step operating cycle, which we shall henceforward refer to as R-SMB$^-$. In the figure caption it is stated that the cycle is valid for $\alpha \leq (3+\sqrt{5})/2$; it will shortly become clear why this is so. Notice that the operating cycle of the R-SMB$^-$ has a few nonstandard features. Fresh feed and desorbent are continuously injected into the process by means of two constant-speed pumps, as in the classical SMB, but the two product streams are collected discontinuously and alternately in time (pulsed outlets). Finally, the intermediate sub-step during which there is no product withdrawal is identical to one of the sub-steps implemented in the I-SMB process [38–40]. Note that from an operational point of view, the use of constant-speed inlet pumps is desirable since it leads to the easiest-to-control and most robust configuration. We shall now

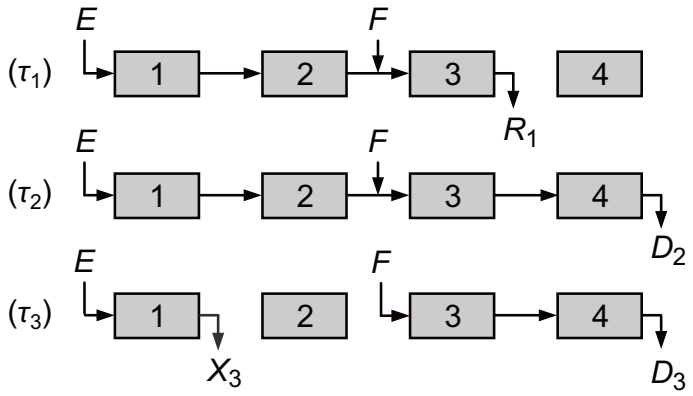

Figure 4.3: Schematic of the R-SMB's operating cycle for $\alpha \leq (3+\sqrt{5})/2$; this scheme is denoted R-SMB$^-$. As in the classical SMB, each rectangle represents a R-SMB section, with one or more columns. At the end of every switch interval the columns move by one position against the direction of the fluid flow or the port positions are moved one column ahead in the direction of the fluid flow.

demonstrate that for linear adsorption systems the R-SMB$^-$ scheme has the same performance metrics and the same separation region as the classical SMB for a specific range of selectivity values.

Using the equilibrium theory [42–44], it is possible to calculate a set of sectional elution volumes, τQ_j, that give a theoretical purity of 100% for both extract and raffinate on an SMB with ideal zones (no mass transfer and no hydrodynamic

resistances). The conditions that must be fulfilled for complete separation are

$$m_1 \geq K_2, \quad K_1 \leq m_2 < m_3 \leq K_2, \quad m_4 \leq K_1, \tag{4.2}$$

where

$$m_j = \frac{\tau Q_j - \epsilon V}{(1-\epsilon)V} \tag{4.3}$$

and V is the column volume (the N columns of the SMB are all assumed to be identical).

Note that the conditions given by Eq. (4.2) can also be expressed as

$$\tau Q_1 \geq V_2', \quad V_1' \leq \tau Q_2 < \tau Q_3 \leq V_2', \quad \tau Q_4 \leq V_1', \tag{4.4}$$

where $V_i' = [\epsilon + (1-\epsilon)K_i]V$ and τQ_j is the volume of fluid eluted through one column of zone j during a switch interval.

Alternatively, the constraints can be converted into equalities with safety margins [13], say

$$\tau Q_1 = \gamma_2 V_2', \quad \tau Q_2 = \gamma_1 V_1', \quad \tau Q_3 = V_2'/\beta_2, \quad \tau Q_4 = V_1'/\beta_1, \tag{4.5}$$

where β_1, β_2, γ_1, and γ_2 are constants ≥ 1. Note, in addition, that the selectivity, α, defined by Eq. (4.1), can also be expressed in terms of V_1' and V_2'; it is simply

$$\alpha = V_2'/V_1'. \tag{4.6}$$

If the inequalities in Eq. (4.4) are converted into equalities [or the safety margins in Eq. (4.5) are all set to 1], they define the optimum operating point of the SMB process: this operating point minimizes E' and maximizes F, where $E' = E - D$ is the flow rate of fresh desorbent introduced into the system and D is the flow rate of desorbent recycled from zone 4 back into the upstream end of the system (for the standard SMB, $E = Q_1$ and $D = Q_4$, but we shall use E and D for the R-SMB). The metrics for the optimum operating point are

$$\tau E' = \tau X = \tau F = \tau R = V_2' - V_1', \quad \tau D = V_1' \tag{4.7}$$

and, hence,

$$F/E' = 1, \quad X/E' = 1, \quad R/E' = 1. \tag{4.8}$$

It is not difficult to derive for the R-SMB$^-$ scheme the constraints, analogous to those of Eq. (4.4), which define the operating space where there is complete separation of the binary mixture. The constraints are:

(less retained component does not contaminate D)

$$\tau_2(E + F) + \tau_3 F \leq V_1', \tag{4.9}$$

(more retained component does not contaminate D)

$$(\tau_1 + \tau_2 + \tau_3)E \geq V_2', \tag{4.10}$$

(less retained component does not contaminate X)

$$(\tau_1 + \tau_2)E \geq V_1', \tag{4.11}$$

(more retained component does not contaminate R)

$$(\tau_1 + \tau_2)(E + F) + \tau_3 F \leq V_2'. \tag{4.12}$$

As was done above for the standard SMB, the inequalities defined by Eqs. (4.9)–(4.12) are converted into equalities to determine the optimal operating conditions of the R-SMB$^-$ process, i.e., those that give a theoretical purity of 100% for both extract and raffinate while minimizing E' and maximizing F. From these set of equalities, the following expressions for F, τ_1, τ_2, and τ_3, as a function of E, are obtained:

$$F = \frac{V_2' - V_1'}{V_2'}\, E, \tag{4.13}$$

$$\tau_1 = \frac{V_2'\,(V_2' - V_1')}{(2V_2' - V_1')\,E}, \quad \tau_2 = \frac{V_1'V_2' - (V_2' - V_1')^2}{(2V_2' - V_1')\,E}, \quad \tau_3 = \frac{V_2' - V_1'}{E}, \tag{4.14}$$

$$\tau = \tau_1 + \tau_2 + \tau_3 = V_2'/E. \tag{4.15}$$

Figure 4.4 shows the equilibrium solution for the optimum operating point of the R-SMB$^-$ process. For this operating point the amounts of fresh desorbent and

feedstock fluid fed into the system per switch interval are

$$\tau E' = \tau E - \tau_2 D_2 - \tau_3 D_3 = \tau E - \tau_2(E+F) - \tau_3 F = V_2' - V_1', \tag{4.16}$$

$$\tau F = V_2' - V_1', \tag{4.17}$$

and the amounts of raffinate and extract collected over the same time interval are

$$\tau_1 R = \tau_1(E+F) = V_2' - V_1', \tag{4.18}$$

$$\tau_3 X = \tau_3 E = V_2' - V_1'; \tag{4.19}$$

finally, the amount of desorbent recycled per switch interval is

$$\tau D = \tau_2 D_2 + \tau_3 D_3 = \tau_2(E+F) + \tau_3 F = V_1'. \tag{4.20}$$

From the above equations,

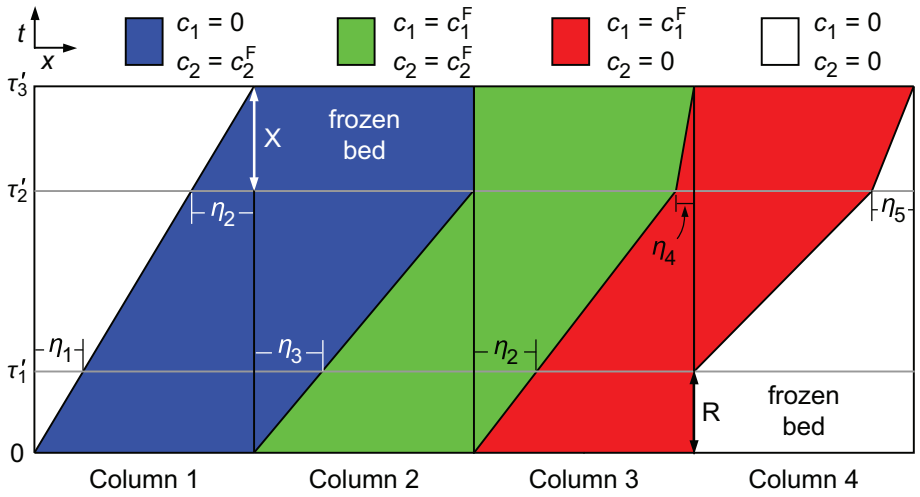

Figure 4.4: Equilibrium solution for complete separation of a linear adsorption system, for which $\alpha < (3+\sqrt{5})/2$, by the R-SMB$^-$ process under optimal operating conditions ($E'/F = 1$). The notation is as follows: $\tau_n' = \sum_1^n \tau_k$, $\eta_1 = (V_2' - V_1')/(2V_2' - V_1')$, $\eta_2 = (V_2' - V_1')/V_2'$, $\eta_3 = V_2'(V_2' - V_1')/V_1'(2V_2' - V_1')$, $\eta_4 = (\eta_2)^2$, $\eta_5 = (V_2' - V_1')^2/V_1'V_2'$. The vertical scale of the schematic matches the solution for $\alpha = 1.4$.

$$F/E' = 1, \quad X/E' = 1, \quad R/E' = 1. \tag{4.21}$$

Thus, the metrics of the optimum operating point of the R-SMB$^-$ process are exactly the same as those of the optimal operating point of the standard SMB.

If the inequalities defined by Eqs. (4.13)–(4.15) are converted into equalities, as

was done above, but this time with safety margins, say,

$$\tau_2(E+F)+\tau_3 F = V_1'/\beta_1, \tag{4.22}$$

$$(\tau_1+\tau_2+\tau_3)E = \gamma_2 V_2', \tag{4.23}$$

$$(\tau_1+\tau_2)E = \gamma_1 V_1', \tag{4.24}$$

$$(\tau_1+\tau_2)(E+F)+\tau_3 F = V_2'/\beta_2, \tag{4.25}$$

where β_1, β_2, γ_1, and γ_2 are constants ≥ 1, then it is possible to probe the operating space of the R-SMB$^-$ process that provides complete separation by changing the magnitude of the safety margins.

The solution of Eqs. (4.22)–(4.25) is

$$F = \frac{V_2'/\beta_2 - \gamma_1 V_1'}{\gamma_2 V_2'}E, \tag{4.26}$$

$$\tau_1 = \frac{\gamma_2 V_2'\,(V_2'/\beta_2 - V_1'/\beta_1)}{[(\gamma_2+1/\beta_2)V_2' - \gamma_1 V_1']\,E}, \tag{4.27}$$

$$\tau_2 = \frac{(\gamma_1\gamma_2+\gamma_1/\beta_2+\gamma_2/\beta_1)V_1'V_2' - (\gamma_1 V_1')^2 - (\gamma_2/\beta_2)(V_2')^2}{[(\gamma_2+1/\beta_2)V_2' - \gamma_1 V_1']\,E}, \tag{4.28}$$

$$\tau_3 = \frac{\gamma_2 V_2' - \gamma_1 V_1'}{E}, \tag{4.29}$$

$$\tau = \frac{\gamma_2 V_2'}{E}. \tag{4.30}$$

From the schematic of Fig. 4.3 and from Eqs. (4.22)–(4.25) it is possible to calculate the volumes of fluid displaced per switch interval in each section of the equivalent SMB process; the result is

$$\tau Q_1 = \tau E = \gamma_2 V_2', \tag{4.31}$$

$$\tau Q_2 = (\tau_1+\tau_2)E = \gamma_1 V_1', \tag{4.32}$$

$$\tau Q_3 = (\tau_1+\tau_2)(E+F)+\tau_3 F = V_2'/\beta_2, \tag{4.33}$$

$$\tau Q_4 = \tau_2(E+F)+\tau_3 F = V_1'/\beta_1. \tag{4.34}$$

But eqs. (4.31)–(4.34) are exactly the same as the equalities expressed in Eq. (4.5), which proves that the R-SMB$^-$ process has the same operating region for complete separation as the classical SMB.

There is, however, a tricky condition with the operating cycle of the R-SMB$^-$ process. Given that the three τ's must be nonnegative, Eq. (4.14) is valid for $V_1'V_2' - (V_2' - V_1')^2 \geq 0$, which is the same as $\alpha \leq \alpha_c$, where $\alpha_c = (3+\sqrt{5})/2$ is the upper limit of α for optimum operation of the R-SMB$^-$ cycle. Thus, the R-SMB$^-$ process should be applied to "difficult separations" characterized by selectivity values smaller than α_c. It is worth noting that the cycle can be employed to a certain extent above α_c by adjusting the safety margins in Eqs. (4.26–4.30). However, such operating conditions will not give the same performance metrics as the optimum operating point of the standard SMB.

For easier separations, those for which $\alpha \geq \alpha_c$, the second sub-step of the R-SMB$^-$ cycle is unnecessary—in fact it is detrimental for the separation performance—and must be replaced by the result of merging sub-steps 1 and 3. The complete cycle for $\alpha \geq \alpha_c$ is depicted in the schematic of Fig. 4.5. We shall henceforward refer to this process as R-SMB$^+$. Again, it is not difficult to derive for the R-SMB$^+$ scheme

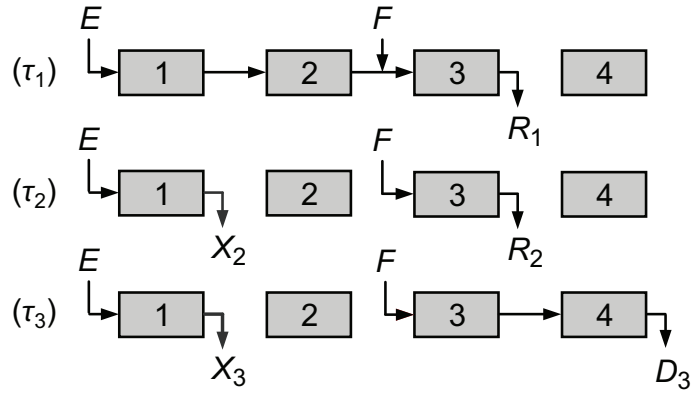

Figure 4.5: Schematic of the operating cycle for the R-SMB$^+$ process, which is applicable when $\alpha \geq (3+\sqrt{5})/2$. At the end of every switching interval the columns move by one position against the direction of the fluid flow or the port positions are moved one column ahead in the direction of the fluid flow.

the constraints that define the operating space where there is complete separation of the binary mixture. The constraints are:

(less retained component does not contaminate D)

$$\tau_3 F \leq V_1', \tag{4.35}$$

(more retained component does not contaminate D)

$$(\tau_1 + \tau_2 + \tau_3)E \geq V_2', \tag{4.36}$$

(less retained component does not contaminate X)

$$\tau_1 E \geq V_1', \tag{4.37}$$

(more retained component does not contaminate R)

$$\tau_1(E + F) + (\tau_2 + \tau_3)F \leq V_2'. \tag{4.38}$$

If these inequalities are converted into equalities, the following expressions for F, τ_1, τ_2, and τ_3, as a function of E, are obtained:

$$F = \frac{V_2' - V_1'}{V_2'}\, E, \tag{4.39}$$

$$\tau_1 = \frac{V_1'}{E}, \quad \tau_2 = \frac{(V_2' - V_1')^2 - V_1' V_2'}{(V_2' - V_1')\, E}, \quad \tau_3 = \frac{V_1' V_2'}{(V_2' - V_1')\, E}, \tag{4.40}$$

$$\tau = \tau_1 + \tau_2 + \tau_3 = V_2'/E. \tag{4.41}$$

As expected, these equations are valid for $(V_2' - V_1')^2 - V_1' V_2' \geq 0$ or $\alpha \geq (3 + \sqrt{5})/2$.

Figure 4.6 shows the equilibrium solution for the optimum operating point of the R-SMB$^+$ process. For this point the amounts of fresh eluent and feedstock fluid fed into the system per switch interval are

$$\tau E' = \tau E - \tau_3 D_3 = \tau E - \tau_3 F = V_2' - V_1', \quad \tau F = V_2' - V_1', \tag{4.42}$$

and the amounts of raffinate and extract collected over the same time interval are

$$\tau_1 R_1 + \tau_2 R_2 = \tau_1(E + F) + \tau_2 F = V_2' - V_1', \tag{4.43}$$

$$\tau_2 X_2 + \tau_3 X_3 = (\tau_2 + \tau_3)E = V_2' - V_1'; \tag{4.44}$$

finally, the amount of eluent recycle per switch interval is

$$\tau D = \tau_3 D_3 = \tau_3 F = V_1'. \tag{4.45}$$

From the above equations,

$$F/E' = 1, \quad X/E' = 1, \quad R/E' = 1. \tag{4.46}$$

Thus, the performance metrics of the optimum operating point of the R-SMB$^+$ cycle are exactly the same as those of the optimum operating point of the standard SMB. As was done above, the inequalities can also be converted into equalities with safety

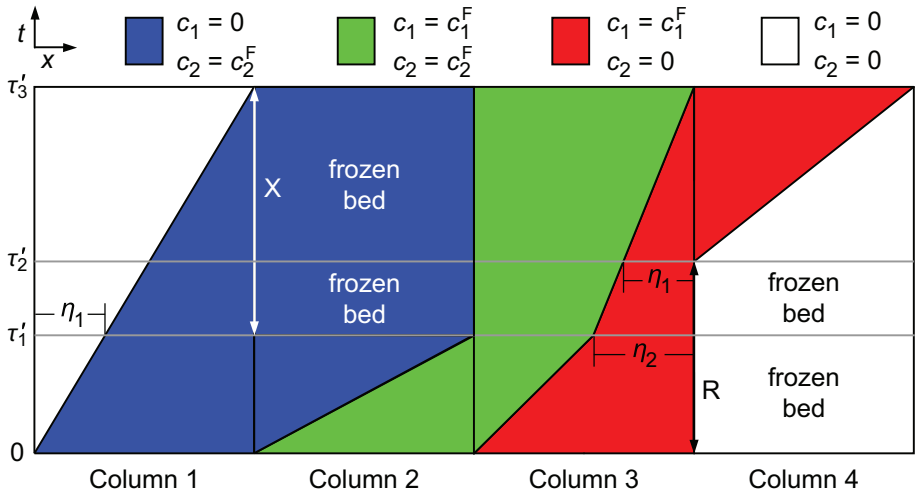

Figure 4.6: Equilibrium solution for complete separation of a linear adsorption system, for which $\alpha > (3 + \sqrt{5})/2$, by the R-SMB$^+$ process under optimal operating conditions ($E'/F = 1$). The notation is as follows: $\tau_n' = \sum_1^n \tau_k$, $\eta_1 = V_1'/V_2'$, $\eta_2 = (V_2' - V_1')^2/(V_2')^2$. The vertical scale of the schematic matches the solution for $\alpha = 3.0$.

margins,

$$\tau_3 F = V_1'/\beta_1, \tag{4.47}$$

$$(\tau_1 + \tau_2 + \tau_3)E = \gamma_2 V_2', \tag{4.48}$$

$$\tau_1 E = \gamma_1 V_1', \tag{4.49}$$

$$\tau_1(E + F) + (\tau_2 + \tau_3)F = V_2'/\beta_2, \tag{4.50}$$

where, again, β_1, β_2, γ_1, and γ_2 are constants ≥ 1. By changing the magnitude of these parameters it is possible to probe the operating space of the R-SMB$^+$ process that provides complete separation.

The solution of eqs. (4.47)–(4.50) is

$$F = \frac{V_2'/\beta_2 - \gamma_1 V_1'}{\gamma_2 V_2'}\, E, \tag{4.51}$$

$$\tau_1 = \frac{\gamma_1 V_1'}{E}, \tag{4.52}$$

$$\tau_2 = \frac{(\gamma_1 V_1')^2 + (\gamma_2/\beta_2)(V_2')^2 - (\gamma_1\gamma_2 + \gamma_1/\beta_2 + \gamma_2/\beta_1) V_1' V_2'}{(V_2'/\beta_2 - \gamma_1 V_1')\, E}, \tag{4.53}$$

$$\tau_3 = \frac{(\gamma_2/\beta_1) V_1' V_2'}{(V_2'/\beta_2 - \gamma_1 V_1')\, E}, \tag{4.54}$$

$$\tau = \frac{\gamma_2 V_2'}{E}. \tag{4.55}$$

From Fig. 4.5 and eqs. (4.51)–(4.55) it is possible to calculate the volume of fluid displaced per switch interval in each section of the equivalent SMB process; the result is

$$\tau Q_1 = \tau E = \gamma_2 V_2', \tag{4.56}$$

$$\tau Q_2 = \tau_1 E = \gamma_1 V_1', \tag{4.57}$$

$$\tau Q_3 = \tau_1 E + \tau F = V_2'/\beta_2, \tag{4.58}$$

$$\tau Q_4 = \tau_3 D_3 = \tau_3 F = V_1'/\beta_1 \tag{4.59}$$

Again, these equations are exactly the same equalities expressed in Eq. (4.5), and this proves that for $\alpha > \alpha_c$ the R-SMB$^+$ cycle has the same operating region for complete separation as the classical SMB.

Before concluding this section, we summarize in Table 4.1 the design equations for optimum operation of the two R-SMB cycles under linear adsorption conditions. Note that the design equations for F and τ are the same for both cycles. Note also that if the selectivity is small, no product stream is collected during the intermediate sub-step of the switch interval (R-SMB$^-$ cycle, Fig. 4.3); but, if the selectivity is large, both product streams are collected during the intermediate sub-step (R-SMB$^+$ cycle, Fig. 4.5) because less internal recycling of the fluid is necessary.

Table 4.1: Summary of the design equations, derived from the equilibrium theory, for the optimum operation of the two R-SMB cycles that give complete separation under linear adsorption conditions; 'eq. sol.' stands for 'equilibrium solution.'

	$\alpha \leq \alpha_c$	$\alpha \geq \alpha_c$
Cycle	R-SMB$^-$ (Fig. 4.3)	R-SMB$^+$ (Fig. 4.5)
F/E	$(V_2' - V_1')/V_2'$	$(V_2' - V_1')/V_2'$
$\tau_1 E$	$V_2'\,(V_2' - V_1')/(2V_2' - V_1')$	V_1'
$\tau_2 E$	$[V_1'V_2' - (V_2' - V_1')^2]/(2V_2' - V_1')$	$[(V_2' - V_1')^2 - V_1'V_2']/(V_2' - V_1')$
$\tau_3 E$	$V_2' - V_1'$	$V_1'V_2'/(V_2' - V_1')$
τE	V_2'	V_2'
Eq. sol.	Fig. 4.4	Fig. 4.6

4.3 Analysis under conditions of finite column efficiency

The discussion above was based on the equilibrium theory, a convenient idealization that assumes that the column efficiency is infinite. In practice this is never true because there is always some band broadening in the system. Thus, a more realistic design must take into account the limitations imposed by a finite column efficiency. We shall adopt the simple chromatographic column model given in Table 4.2 to design the processes in the presence of band broadening. In this simple model the column efficiency is measured by the value of the Péclet number, $Pe = vL/D_L$. If each column has an efficiency equivalent to N_{TP} theoretical plates, then the Péclet number is $Pe = 2N_{\mathrm{TP}}$ [45]. To determine the optimal SMB operating parameters

Table 4.2: Linear adsorption column model.

$$\frac{\partial c_i}{\partial \theta} = \frac{\tau Q}{V_i'}\left(\frac{1}{Pe}\frac{\partial^2 c_i}{\partial x^2} - \frac{\partial c_i}{\partial x}\right), \quad \forall x \in]0,1[$$

$$c_i - \frac{1}{Pe}\frac{\partial c_i}{\partial x} = c_i^{\mathrm{in}} \text{ for } x = 0, \quad \frac{\partial c_i}{\partial x} = 0 \text{ for } x = 1$$

$$\theta = t/\tau, \quad x = z/L, \quad c_i^{\mathrm{out}} \equiv (c_i)_{x=1}$$

for a finite column efficiency (i.e., for a given finite value of Pe), we can restrict the flow rate in zone 1 to a maximum operating value, say $Q_1 \leq Q_{\max}$, because zone 1 is where the flow rate is highest, and then calculate by mathematical programming

the optimal values of the four Q_j's and of τ that maximize the feed flow rate, F, under cyclic steady state (CSS) conditions.

To do this, we solve the following optimization problem:

$$\begin{aligned} \text{maximize} \quad & F(\tau, Q_j) \\ \text{s.t.} \quad & \text{SMB model under CSS conditions} \\ & Q_1 \le Q_{\max}, \quad P_{\mathrm{R}} \ge P_{\mathrm{R}}^{\min}, \quad P_{\mathrm{X}} \ge P_{\mathrm{X}}^{\min}, \end{aligned} \tag{4.60}$$

where $P_{\mathrm{R}}^{\min}$ and $P_{\mathrm{X}}^{\min}$ are the target raffinate and extract purities, respectively. The product purities are defined as follows:

$$P_{\mathrm{R}} = \langle c_1^{\mathrm{R}} \rangle / \langle c_1^{\mathrm{R}} + c_2^{\mathrm{R}} \rangle, \quad P_{\mathrm{X}} = \langle c_2^{\mathrm{X}} \rangle / \langle c_1^{\mathrm{X}} + c_2^{\mathrm{X}} \rangle, \tag{4.61}$$

where c_i^{s} is the concentration of solute i in product stream 's' ('R' stands for raffinate, 'X' for extract) and $\langle y \rangle$ denotes the average of $y(t)$ over a switch interval: it is the value of y in the volume of liquid collected into a perfectly mixed cup during a switching interval. For example, the average concentration of solute i in the extract collected over a switch interval is

$$\langle c_i^{\mathrm{X}} \rangle = \langle c_i^{\mathrm{out}} \rangle_1 = \int_\tau (c_i^{\mathrm{out}})_1 X \, \mathrm{d}t \Big/ \int_\tau X \, \mathrm{d}t \tag{4.62}$$

$$= \tau^{-1} \int_\tau (c_i^{\mathrm{out}})_1 \, \mathrm{d}t \qquad (X = \text{const}). \tag{4.63}$$

(Hereafter we shall employ the superscripts 'in' and 'out' to denote, respectively, the inlet and outlet conditions for a zone or column.) For a standard SMB the flow rate can be taken out of the integrals in Eq. (4.62) and give Eq. (4.63), because the process is operated with constant-speed pumps. Note that under CSS conditions, $\langle y \rangle$ is independent of the number of elapsed switch intervals or cycles (one cycle is equal to N switch intervals, where N is the number of columns).

The design problem can also include the raffinate and/or extract recoveries, R_{R} and R_{X}, as constraints; these are defined as

$$R_{\mathrm{R}} = \langle c_1^{\mathrm{R}} \rangle R / (c_1^{\mathrm{F}} F), \quad P_{\mathrm{X}} = \langle c_2^{\mathrm{X}} \rangle X / (c_2^{\mathrm{F}} F), \tag{4.64}$$

where c_i^{F} represents the concentration of component i in the feed.

Consider, for example, a 4-column SMB unit where each column has an efficiency equivalent to 100 theoretical plates; the Péclet number in this case is $Pe = 2 \times 100 =$

200. Also, consider the case where $\alpha = 1.4$. If we choose $P_{\mathrm{R}}^{\min} = P_{\mathrm{X}}^{\min} = 0.99$, which are realistic values close to a theoretical 100% purity, and set $Q_{\max}/V_1' = 1$ min^{-1}, then the optimal SMB operating parameters are $\tau = 1.514$ min, $Q_1/V_1' = 1$ min^{-1}, $Q_2/V_1' = 0.701$ min^{-1}, $Q_3/V_1' = 0.860$ min^{-1}, and $Q_4 = 0.607$ min^{-1}; this gives, $E/V_1' = 0.393$ min^{-1}, $X/V_1' = 0.299$ min^{-1}, $F/V_1' = 0.159$ min^{-1}, $R/V_1' = 0.253$ min^{-1}, and $E/F = 2.47$. The corresponding volumes of fluid eluted through each zone during a switch interval are $\tau Q_1/V_1' = 1.514 = (1 + 8.1\%) \times \alpha$, $\tau Q_2/V_1' = 1.061 = (1 + 6.1\%) \times 1$, $\tau Q_3/V_1' = 1.302 = (1 - 7.0\%) \times \alpha$, and $\tau Q_4/V_1' = 0.919 = (1 - 8.1\%) \times 1$ [cf. Eq. (4.4) with all terms divided by V_1']. Actually, this set of operating parameters gave rise to the composition profiles plotted in Fig. 4.1. Because of the finite number of theoretical plates, the system is operated with conservative m_j (or $\tau Q_j/V_1'$) values that deviate from the theoretical ones by roughly 7.3%.

These operating parameters are for a closed-loop SMB. In this configuration the effluent from zone 4 is recycled back to the inlet of zone 1. For a closed-loop SMB the material balance at the inlet of zone 1, that is, the equation that governs the desorbent recycle strategy, is

$$(Qc_i^{\mathrm{in}})_1 = (Qc_i^{\mathrm{out}})_4 \quad \text{or} \quad (c_i^{\mathrm{in}})_1 = (Q_4/Q_1)(c_i^{\mathrm{out}})_4. \tag{4.65}$$

For the example considered above the average solute concentrations in the effluent from zone 4 (which is recycled desorbent) over a switch interval are $\langle c_1^{\mathrm{out}} \rangle_4 = 1.66 \times 10^{-3} c_1^{\mathrm{F}}$ and $\langle c_2^{\mathrm{out}} \rangle_4 = 3.69 \times 10^{-3} c_2^{\mathrm{F}}$. This effluent is continuously mixed with fresh desorbent before being introduced into the upstream end of zone 1; at that point the average residual solute concentrations drop to $\langle c_1^{\mathrm{in}} \rangle_1 = 1.01 \times 10^{-3} c_1^{\mathrm{F}}$ and $\langle c_2^{\mathrm{in}} \rangle_1 = 2.24 \times 10^{-3} c_2^{\mathrm{F}}$ because of the dilution with fresh desorbent.

Because of the way the R-SMB was designed (Figs. 4.3 and 4.5), we are more interested in employing an open-loop configuration to mimic the in-line desorbent recycling of the closed-loop SMB. There are two straightforward ways of doing this. As long as the exit stream of zone 4 is sufficiently clean, it can be sent back to the desorbent storage tank or to an auxiliary storage tank. In the former case the process does not require a separate recycle pump, but the inlet pump for the desorbent must deliver a flow rate equal to $Q_1 = Q_4 + E'$; in the latter case, the recycle pump is fed from the auxiliary tank instead of being fed from the downstream end of zone 4.

To ensure that the exit stream of zone 4 is clean, we can impose explicit limits on the maximum values of $(c_1^{\mathrm{out}})_4$ and $(c_2^{\mathrm{out}})_4$; the former concentration (that of the

less retained component) reaches a maximum at the end of the switch interval, whereas the latter (that of the more retained component) attains a maximum at the beginning of the switch interval. Alternatively, limits on the averages $\langle c_1^{\mathrm{out}} \rangle_4$ and $\langle c_2^{\mathrm{out}} \rangle_4$ can be imposed. The specification of maximum limits for $(c_1^{\mathrm{out}})_4$ and $(c_2^{\mathrm{out}})_4$ is equivalent to manipulating the safety margins β_1 and γ_2 in Eq. (4.5), Eqs. (4.26–4.30), or Eqs. (4.51–4.55), derived from the equilibrium theory.

We are, however, more interested in solving the design problem using a formulation similar to that given by Eq. (4.60). In this case, we must formulate mathematically how clean the exit stream of zone 4 should be to make sure it can be recycled by the process. The exact answer depends on how the recycled desorbent is reintroduced into the system, namely whether the exit stream of zone 4 is sent to the main desorbent tank or to a smaller, auxiliary storage tank.

We shall tackle this issue in a generic way that hides the specific details of the desorbent recycle strategy; this issue is of secondary importance here given that the focus of the present work is the presentation of the R-SMB concept.

Firstly, note that under CSS conditions the inlets and outlets of a closed-loop SMB are related by the following global solute material balances:

$$\langle c_i^{\mathrm{X}} \rangle X + \langle c_i^{\mathrm{R}} \rangle R = c_i^{\mathrm{F}} F \quad (i = 1, 2; \text{ CSS conditions}). \tag{4.66}$$

This means that, under CSS conditions, the amount of each solute injected into the system over a switch interval comes out in the ensemble of the two product streams collected over the same amount of time. Because of this, Eq. (4.60), which defines the design problem of a closed-loop SMB, does not include any specification about the cleanliness level of the exit stream of zone 4; this is implicitly determined by the design procedure.

It would be convenient if Eq. (4.66) was also valid for the open-loop SMB configuration, since this would facilitate the design procedure. Let us determine under which circumstances this is true. Consider again the material balance at the inlet of zone 1 (the desorbent recycle equation), as expressed by Eq. (4.65), and integrate it over a switch interval; the result is

$$\langle Q c_i^{\mathrm{in}} \rangle_1 = \langle Q c_i^{\mathrm{out}} \rangle_4 \qquad (i = 1, 2). \tag{4.67}$$

Note that Eq. (4.66) is valid under CSS conditions because Eq. (4.67) holds true; that is, Eq. (4.66) is valid under CSS conditions as along as the amount of solute that leaves the system through zone 4 over a switch interval is put back into the

system over the same time interval.

But this means that any SMB configuration that satisfies Eq. (4.67) also satisfies Eq. (4.66) under CSS conditions. For example, an SMB process whose material balance at the inlet of zone 1 is given by

$$(Qc_i^{\mathrm{in}})_1 = \langle Qc_i^{\mathrm{out}} \rangle_4 \qquad (i = 1, 2), \tag{4.68}$$

(notice the notation: round brackets on the l.h.s. and angle brackets on the r.h.s.) satisfies Eq. (4.67), because the average of a constant is the constant itself, and thus also satisfies Eq. (4.66) under CSS conditions. It is important to understand the practical meaning of Eq. (4.68): zone I is continuously fed with the admixture of fresh eluent and the average over a switch interval of the effluent from zone 4. In our opinion this is the easiest way to tackle the problem of recycling the exit stream of zone 4 in an open-loop configuration since it avoids addressing technical details such as the size of the auxiliary storage tank, or the time-dependent variation of the desorbent composition if the recycled eluent is sent back to the original desorbent storage tank.

We thus replace Eq. (4.65) by Eq. (4.68) in the SMB model to convert the closed-loop SMB into a pseudo closed-loop SMB that uses recycled desorbent with solute concentrations equal to the time-average concentrations in the exit stream of zone 4 under CSS conditions. If this process is operated with the parameters determined above for the classical closed-loop SMB, the obtained product purities are $P_{\mathrm{R}} = 98.75\%$ and $P_{\mathrm{X}} = 98.84\%$. These values are nearly as good, but not the same, as those of the classical closed-loop SMB.

To get exactly the same product purities and recoveries we solve the optimization problem given by Eq. (4.60) for the pseudo closed-loop SMB. The optimal operating parameters are $\tau = 1.549$ min, $Q_1/V_1' = 1$ min^{-1}, $Q_2/V_1' = 0.686$ min^{-1}, $Q_3/V_1' = 0.838$ min^{-1}, and $Q_4/V_1' = 0.577$ min^{-1}; this gives, $E/V_1' = 0.423$ min^{-1}, $X/V_1' = 0.314$ min^{-1}, $F/V_1' = 0.152$ min^{-1}, $R/V_1' = 0.262$ min^{-1}, and $E/F = 2.78$. The corresponding volumes of fluid eluted through each zone during a switch interval are $\tau Q_1/V_1' = 1.549 = (1 + 10.6\%)\alpha$, $\tau Q_2/V_1' = 1.062 = (1 + 6.2\%) \times 1$, $\tau Q_3/V_1' = 1.299 = (1 - 7.2\%)\alpha$, and $\tau Q_4/V_1' = 0.893 = (1 - 10.7\%) \times 1$. The values of $\tau Q_1/V_1'$ and $\tau Q_4/V_1'$ changed (and τ), but those of $\tau Q_2/V_1'$ and $\tau Q_3/V_1'$ remained equal to those of the closed-loop SMB. The point to note is that this desorbent recycle strategy incurs a small penalty in performance with respect to that of the standard closed-loop SMB: the productivity is reduced by 4.2% and the desorbent consumption is increased by 7.7%.

We can also reason the other way around: what product purities are obtained by a closed-loop SMB with the optimal operating parameters of the pseudo closed-loop SMB? As expected, the obtained purities, $P_{\mathrm{R}} = 99.08\%$, $P_{\mathrm{X}} = 99.03\%$, are above the specifications of 99%. Thus, the optimal parameters for the pseudo closed-loop SMB are a conservative set of operating parameters for the classical closed-loop SMB. Moreover, by adopting Eq. (4.68) the open-loop configuration is not favored over the closed-loop system.

We shall now proceed to compare the performance of the R-SMB process against those of the closed- and open-loop SMB processes under conditions of finite column efficiency. This comparison is first done for a fixed value $\alpha = 1.4$, which falls under the scope of the R-SMB$^-$ configuration (Fig. 4.3); the product purity specifications are kept at $P_{\mathrm{R}} = P_{\mathrm{X}} = 0.99$. The results are shown in Fig. 4.7, where the maximum specific productivity (F/V_1') achieved by each process configuration and the required desorbent consumption (E'/F) are plotted against the Péclet number, Pe.

The curves for all process configurations were obtained by solving the optimization problem, given by Eq. (4.60), with $Q_{\max}/V_1' = 1$ min^{-1}. The optimization variables for the closed- and open-loop SMB are the four zone flow rates, $Q_1, \ldots, Q_4$, and the switch interval, τ; those for the R-SMB are E, F, and the three sub-step durations τ_1, τ_2, and τ_3. Since the objective function of the design problem is the maximization of F, the optimum solution gives $E = Q_{\max}$; thus, E (or Q_1) can be fixed at $Q_{\max}$ to eliminate it from the set of optimization variables. The node balance at the inlet of zone 1 for the closed-loop SMB is given by Eq. (4.65) and by Eq. (4.68) for the open-loop SMB and R-SMB processes.

Figure 4.7 shows that for a given Péclet number the R-SMB$^-$ process requires less desorbent and is more productive than the standard SMB process under conditions of finite column efficiency. Moreover, the R-SMB$^-$ process compares more favorably as the column efficiency decreases. Obviously, the three processes should converge to the same asymptotic solution at large Péclet number, i.e., to the solution obtained under the framework of the equilibrium theory. Although this is clearly shown by the curves of E'/F vs Pe, it is necessary to go higher in Péclet number to superimpose the SMB's productivity curve over that of the R-SMB$^-$ process.

The adoption of Eq. (4.68) to model the desorbent recycling in the open-loop SMB and R-SMB$^-$ seems reasonable: the performance curves for the open- and closed-loop SMB configurations are close to each other and the use of Eq. (4.68) does not favor the open-loop configuration over the classical closed-loop system; on the contrary, it gives rise to a slightly more conservative design.

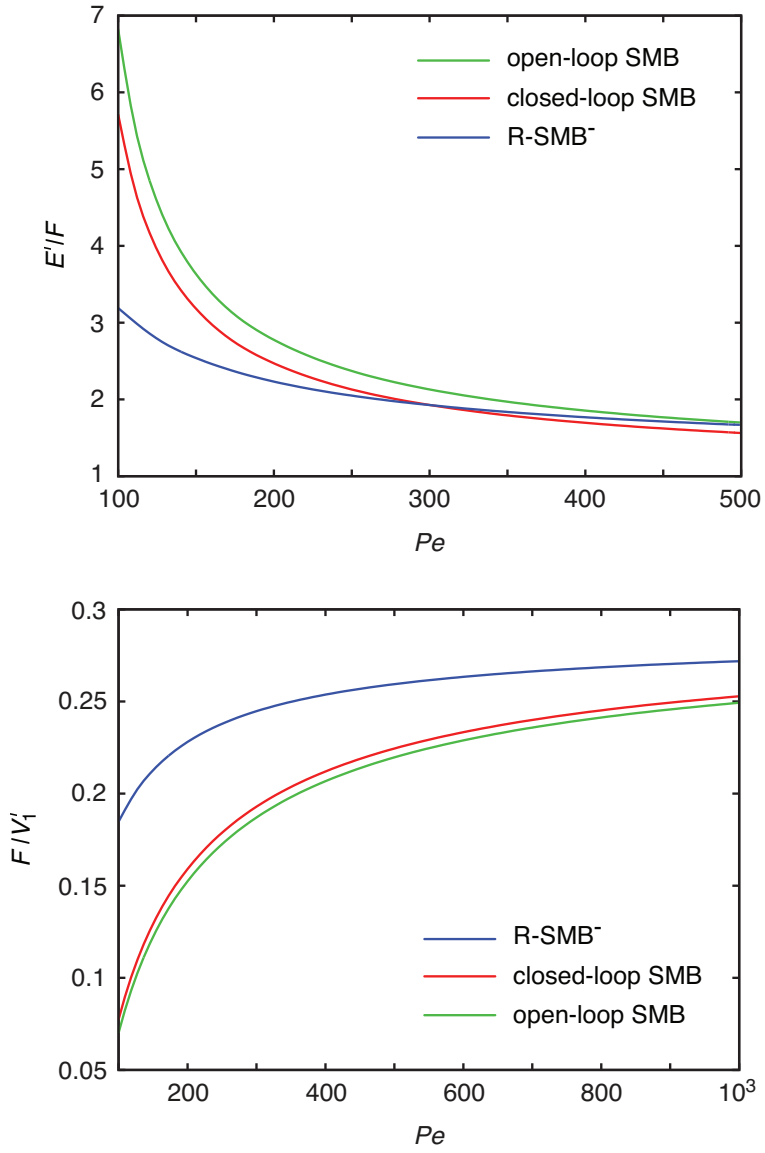

Figure 4.7: Desorbent consumption (E'/F) and specific productivity (F/V_1') as a function of Péclet number per column (Pe) for complete separation ($P_{\mathrm{R}} = P_{\mathrm{X}} = 0.99$) of a linear adsorption system ($\alpha = 1.4$) with different four-column configurations: closed-loop SMB (top schematic in Fig. 4.1 including the dashed line), open-loop SMB (top schematic in Fig. 4.1 without the dashed line), and R-SMB$^-$ (Fig. 4.3); in the latter two cases, the desorbent recycling is given by Eq. (4.68)

Fig. 4.8 gives some insight into why the productivity of the R-SMB$^-$ is much higher than that of the classical SMB process under conditions of small column efficiency. This figure shows a snapshot of the axial concentration profile along the train of columns, taken at the middle of the switch interval, for the R-SMB$^-$ (solid lines) and closed-loop SMB (dashed lines) for $Pe = 200$; the profiles for the closed-loop SMB at $Pe = 1000$ are also included for comparison. Because the R-SMB$^-$ system can withstand a much higher feed flow rate than the SMB for $Pe = 200$, the R-SMB$^-$

is loaded with substantially more solute than the SMB system. More interesting, however, is that the concentration profile of the more retained solute, c_2, in sections 1 and 2 of the R-SMB$^-$ system for $Pe = 200$ is close to that of the SMB process in the same two zones but for $Pe = 1000$. The same observation applies to the concentration profile of the less retained solute, c_1, but in sections 3 and 4. Hence, for small Péclet numbers, such as $Pe = 200$, the concentration profiles in the R-SMB$^-$ process are much closer to those given by the equilibrium solution (infinite column efficiency) than the concentration profiles in the closed-loop SMB. Thus, the influence of column efficiency on process performance is much less detrimental on the R-SMB$^-$ than on the classical SMB.

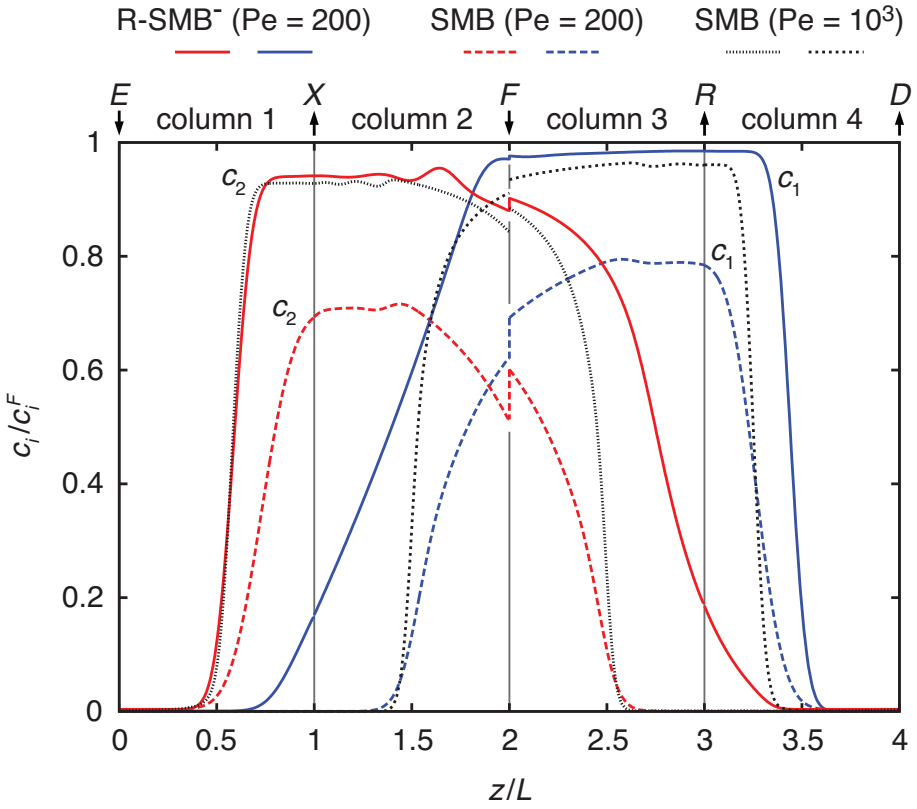

Figure 4.8: Axial concentration profiles, taken at the middle of the switch interval ($\tau/2$) under CSS conditions, for the 4-column R-SMB$^-$ (solid lines) and 4-column closed-loop SMB (dashed lines). The operating parameters are: $\alpha = 1.4$, $Pe = 200$, and $P_{\mathrm{R}} = P_{\mathrm{X}} = 0.99$. The concentration profiles for the closed-loop SMB at $Pe = 1000$ are included for comparison.

Figure 4.9 shows graphs of F/V_1' and E'/F plotted against Pe for a fixed value $\alpha = 3.0$, which falls under the scope of the R-SMB$^+$ configuration (Fig. 4.5); the design problem and purity constraints are the same as before. Again, it is observed that for a given Péclet number the R-SMB$^+$ process is more productive and requires less desorbent than the standard SMB process under conditions of small column

efficiency, and that the comparison increasingly favors the R-SMB$^+$ configuration as the column efficiency decreases. Although for $\alpha = 1.4$ the superimposition of the E'/F-vs-Pe curves of the three processes is observed for ca. $Pe > 300$, for $\alpha = 3.0$ the superimposition is shifted to higher Pe values, well above $Pe = 500$.

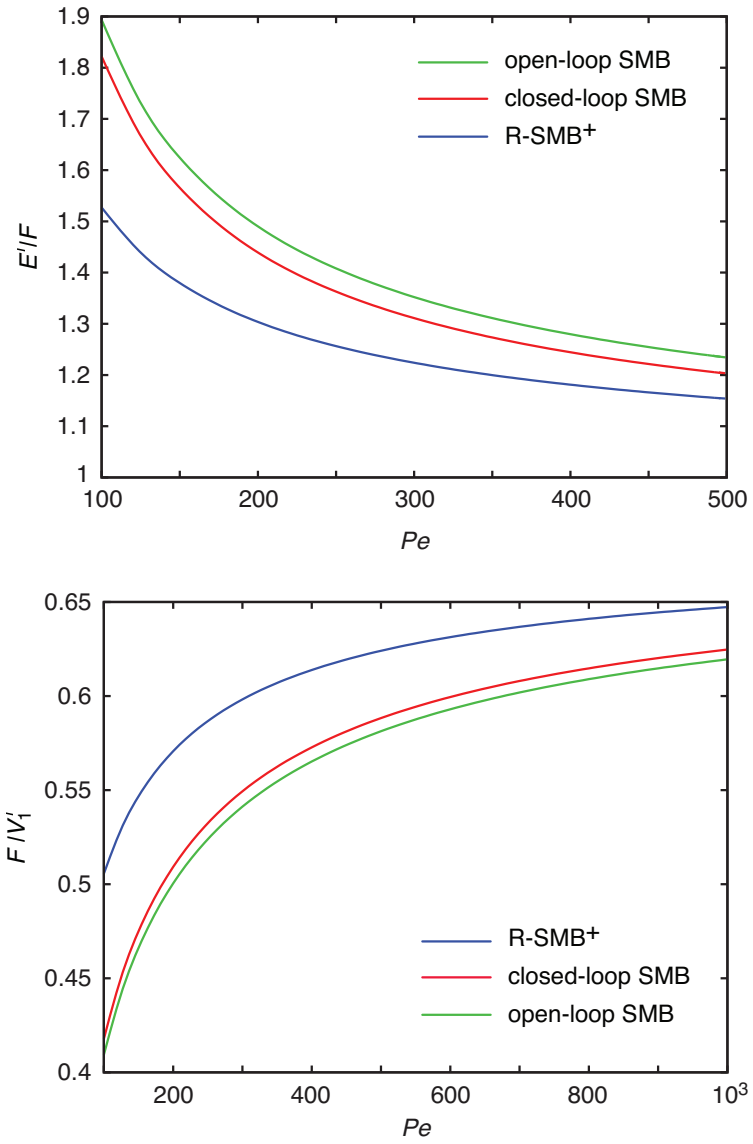

Figure 4.9: Desorbent consumption (E'/F) and specific productivity (F/V_1') as a function of Péclet number per column (Pe) for complete separation ($P_\mathrm{R} = P_\mathrm{X} = 0.99$) of a linear adsorption system ($\alpha = 3.0$) with different four-column configurations: closed-loop SMB (top schematic in Fig. 4.1 including dashed line), open-loop SMB (top schematic in Fig. 4.1 without dashed line), and R-SMB$^+$ (Fig. 4.5); in the latter two cases, the desorbent recycling is governed by Eq. (4.68).

In Figs. 4.7 and 4.9 we examined the performance of the various process configurations for a fixed value of α and variable Péclet number. It is also instructive to examine how the R-SMB process compares against the classical SMB configurations

as a function of α at a fixed value of Pe. This is shown in Fig. 4.10 for $Pe = 200$ and in Fig. 4.11 for $Pe = 1000$. As in Figs. 4.7 and 4.9, the performance indicators are the specific productivity (F/V_1') and the desorbent consumption (E'/F).

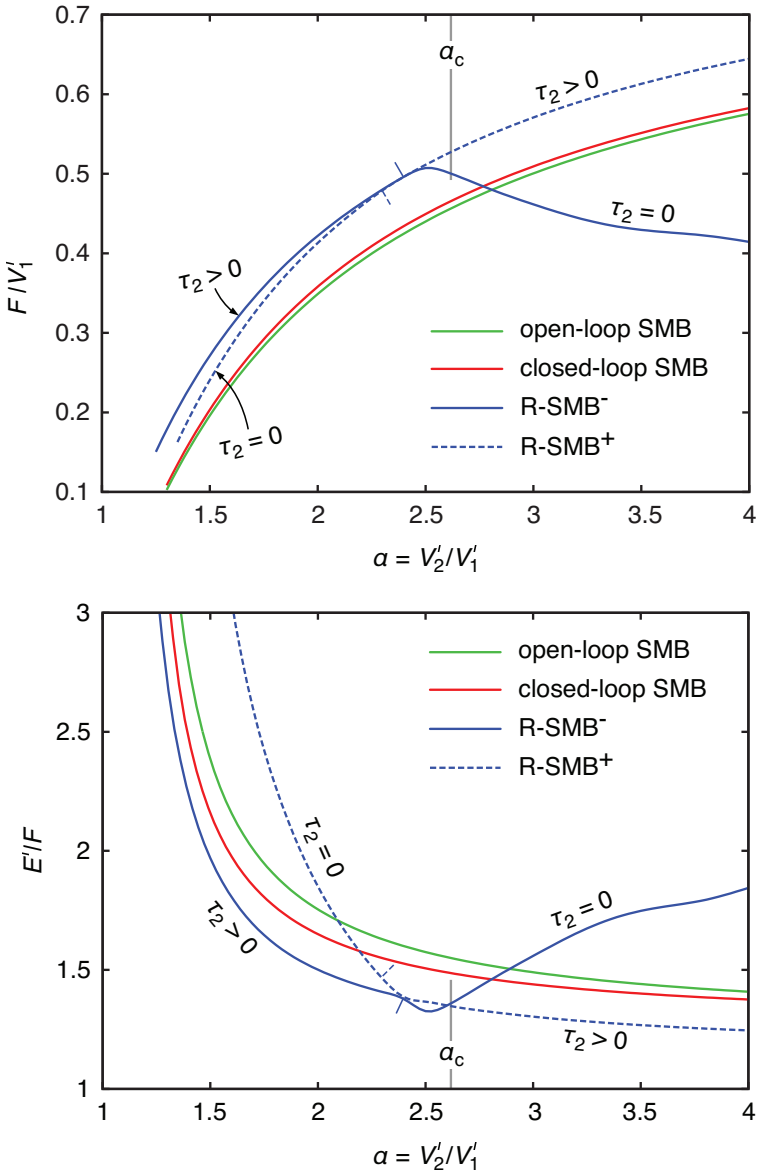

Figure 4.10: Specific productivity (F/V_1') and desorbent consumption (E'/F) as a function of selectivity (α) for complete separation ($P_R = P_X = 0.99$) of a linear adsorption system at a Péclet number per column $Pe = 200$ with different four-column configurations: closed-loop SMB, open-loop SMB, and the two R-SMB schemes; Eq. (4.68) governs the desorbent recycling policy of all open-loop schemes. $\alpha_c = (3+\sqrt{5})/2$; the two small straight lines split each R-SMB curve into a segment over which τ_2 (second sub-step of the switch interval) is zero and another segment over which $\tau_2 > 0$.

In each graph of Figs. 4.10 and 4.11 there are two curves for the R-SMB process: one curve for the R-SMB$^-$ configuration (solid blue line) and another curve for the R-SMB$^+$ configuration (dashed blue line). Consider what happens when one

moves along the x-axis of the graphs, that is, from small towards large values of α or vice versa, and take Fig. 4.10 as an example. As expected, for values of $\alpha < \alpha_c = (3+\sqrt{5})/2$, the R-SMB$^-$ configuration is better than the R-SMB$^+$ configuration: the specific productivity is higher and the desorbent consumption is lower; but the reverse trend is observed for $\alpha > \alpha_c$. This is because the R-SMB$^-$ was designed for $\alpha < \alpha_c$, whereas the R-SMB$^+$ is well suited for $\alpha > \alpha_c$.

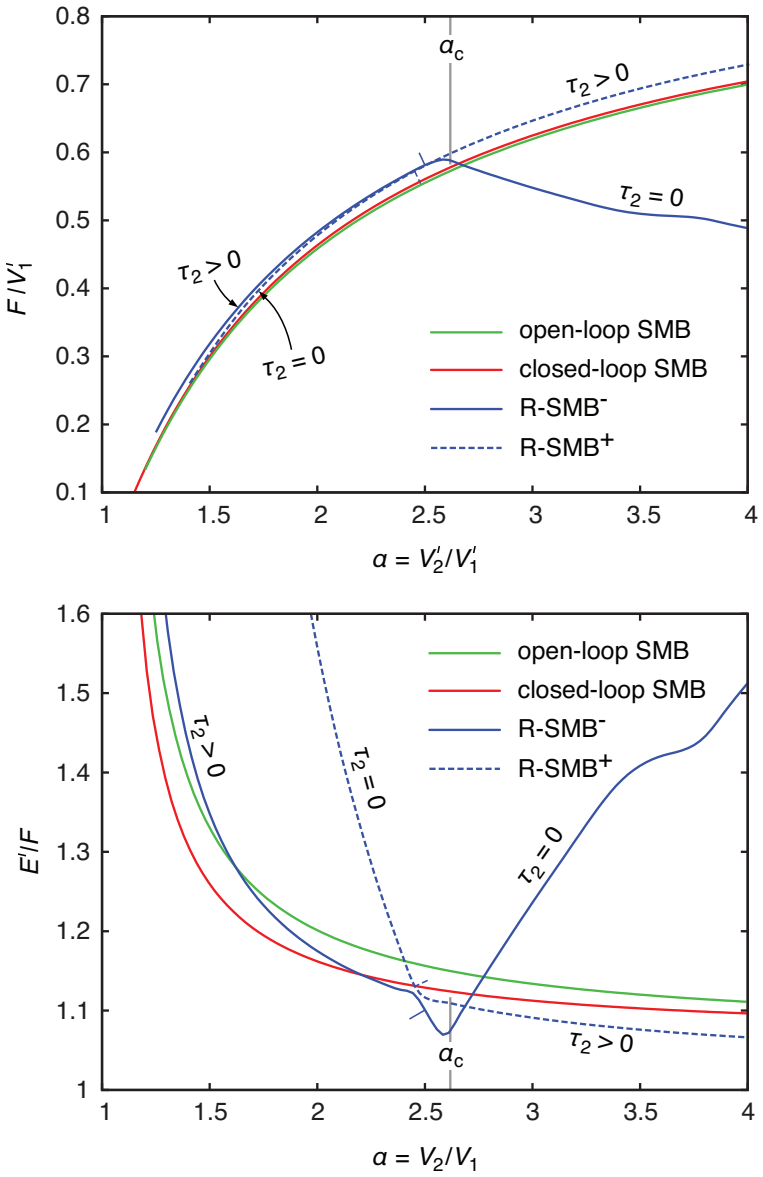

Figure 4.11: Specific productivity (F/V_1') and desorbent consumption (E'/F) as a function of selectivity (α) for complete separation ($P_R = P_X = 0.99$) of a linear adsorption system at a Péclet number per column $Pe = 1000$ with different four-column configurations: closed-loop SMB, open-loop SMB, and the two R-SMB schemes; Eq. (4.68) governs the desorbent recycling policy of all open-loop configurations. $\alpha_c = (3+\sqrt{5})/2$; the two small straight lines split each R-SMB curve into a segment over which τ_2 (second sub-step of the switch interval) is zero and another segment over which $\tau_2 > 0$.

The optimum duration τ_2 of the intermediate sub-step of the R-SMB$^-$ process, the one during which the axial concentration profile is displaced in the direction of fluid flow without any product withdrawal, decreases as the value of α increases from a small value below α_c until it shrinks to zero at a value of α slightly smaller than α_c. For larger values of α and if we stick to the R-SMB$^-$ configuration, it is best to operate the process with only sub-steps 1 and 3, because $\tau_2 = 0$ will always give better results than $\tau_2 > 0$, but at the cost of a high penalty in performance: a sharp decrease in productivity and increase in desorbent consumption are observed.

Now consider the behavior of the R-SMB$^+$ process as α decreases from values well above α_c down to a small value. The optimum duration τ_2 of the intermediate sub-step of the R-SMB$^+$ process, the one during which there is simultaneous extract and raffinate withdrawals, decreases as the value of α decreases until it shrinks to zero at a value of α slightly smaller than α_c. Below that value it is preferable to operate the R-SMB$^+$ process without the intermediate sub-step, but at the cost of a large performance penalty, especially a significant increase in desorbent consumption.

Notice that if the intermediate step is removed from both the R-SMB$^-$ and R-SMB$^+$ processes, we end up with the same two-step process configuration (cf. Figs. 4.3 and Fig. 4.5 without step 2). Actually, there is a small region around α_c where the optimum value of τ_2 is impracticably small; over this region it is best to operate the R-SMB process using the 2-step cycle with negligible loss in performance.

An interesting observation drawn from the graphs in Figs. 4.10 and 4.11 is that when the line segment of the R-SMB$^-$ for which $\tau_2 > 0$ is connected to the line segment of the R-SMB$^+$ for which $\tau_2 > 0$, a smooth curve is obtained without any discontinuous transition in the slope around α_c. This observation strengths our belief that the R-SMB$^-$ and R-SMB$^+$ are indeed the correct SMB analogs for intermittent operation of the product outlets. Lastly, it is shown that for $Pe = 200$ the R-SMB process performs significantly better than the classical SMB process over the whole range of α values studied, but less so for $Pe = 1000$ because both processes should have the same performance under conditions of infinite column efficiency.

4.4 Conclusions

The present work gives the first account of the R-SMB concept and its realization under the form of the analog of the classical four-section SMB process. R-SMB

schemes are based on a restricted set of port configurations that reduce the capital cost of a SMB unit and are expected to be easier to operate and control. A R-SMB unit does not require pumps or flow controllers to regulate the flow rates of the product lines. Additionally, there is no need for one of the inlet or outlet pumps to be controlled by the system pressure to accommodate pump flow rate fluctuations. Despite the simplified manipulation of the zone flow rates, the R-SMB process maintains the analogy with the SMB in terms of displaced volumes of fluid per switch interval.

For simplicity and conciseness, the analysis given here of the R-SMB was restricted to linear adsorption isotherms and four-column configurations. Nevertheless, it is clear that the R-SMB$^-$ and R-SMB$^+$ cycles remain valid for nonlinear adsorption isotherms and that the qualitative trends drawn from the performance comparison between the R-SMB and SMB for linear systems should also hold for nonlinear separations. However, it is expected that the R-SMB and SMB processes will have slightly different separation regions under nonlinear adsorption conditions.

Another issue that was not addressed in the present work is the impact of the section discretization, that is, the number of columns per section, on the separation efficiency of the R-SMB. It is well known that increasing the number of columns per section brings the SMB concentration profiles closer to those of the TMB [46, 47]. It is also apparent that, as the number of columns per section is increased, the performance gain obtained over the SMB with most of the non-classical schemes becomes increasingly smaller [48, 49]. A similar trend is expected to apply to the R-SMB when it is compared against the SMB under conditions of low column efficiency. On the other hand, in the pharmaceutical, fine chemistry, and biotechnological industries, SMB chromatography is now realized mostly with five or six columns, and the trend is to reduce the number of columns not the other way around. Thus, the problem of section discretization, although theoretically very interesting, may not be as important in practice.

Finally, it is worth noting that the R-SMB concept can also be generalized to other SMB configurations. For example, it can be shown that the R-SMB equivalent to the three-zone SMB configuration, which takes the four-zone open-loop SMB and removes zone 4, consists of a two-step scheme per switch interval. This scheme consists of steps 1 and 3 of the R-SMB$^-$ process, but without section 4, and with the outlet stream from zone 3 collected as raffinate during both sub-steps.These issues, as well as an experimental proof of concept of the R-SMB, will be addressed in future work.

References

[1] Chim Yong Chin and Nien-Hwa Linda Wang. Simulated moving bed equipment designs. *Separation & Purification Reviews*, 33(2):77–155, 2004.

[2] Pedro Sá Gomes, Mirjana Minceva, and Alírio E. Rodrigues. Simulated moving bed technology: old and new. *Adsorption*, 12(5-6):375–392, 2006.

[3] A. Seidel-Morgenstern, L. C. Keßler, and M. Kaspereit. New developments in simulated moving bed chromatography. *Chemical Engineering & Technology*, 31(6):826–837, 2008.

[4] Arvind Rajendran, Galatea Paredes, and Marco Mazzotti. Simulated moving bed chromatography for the separation of enantiomers. *Journal of Chromatography A*, 1216(4):709 – 738, 2009.

[5] Alexandre Nicolaos, Laurence Muhr, Patrice Gotteland, Roger-Marc Nicoud, and Michel Bailly. Application of equilibrium theory to ternary moving bed configurations (four+ four, five+ four, eight and nine zones): I. linear case. *Journal of Chromatography A*, 908(1):71–86, 2001.

[6] Alexandre Nicolaos, Laurence Muhr, Patrice Gotteland, Roger-Marc Nicoud, and Michel Bailly. Application of the equilibrium theory to ternary moving bed configurations (4+ 4, 5+ 4, 8 and 9 zones): Ii. langmuir case. *Journal of Chromatography A*, 908(1):87–109, 2001.

[7] Kwangnam Lee. Two-section simulated moving-bed process. *Separation Science and Technology*, 35(4):519–534, 2000.

[8] Weihua Jin and Phillip C. Wankat. Two-zone smb process for binary separation. *Industrial & Engineering Chemistry Research*, 44(5):1565–1575, 2005.

[9] Weihua Jin and Phillip C. Wankat. Scaling rules and increasing feed rates in two-zone and four-zone simulated moving bed systems. *Industrial & Engineering Chemistry Research*, 45(8):2793–2807, 2006.

[10] Rui C.R. Rodrigues, Tiago J.S.B. Canhoto, João M.M. Araújo, and José P.B. Mota. Two-column simulated moving-bed process for binary separation. *Journal of Chromatography A*, 1180(1–2):42 – 52, 2008.

[11] Rui CR Rodrigues, Ricardo JS Silva, and José PB Mota. Streamlined, two-column, simulated countercurrent chromatography for binary separation. *Journal of Chromatography A*, 1217(20):3382–3391, 2010.

[12] João M.M. Araújo, Rui C.R. Rodrigues, Mário F.J. Eusébio, and José P.B. Mota. Chiral separation by two-column, semi-continuous, open-loop simulated moving-bed chromatography. *Journal of Chromatography A*, 1217(33): 5407 – 5419, 2010.

[13] Douglas M. Ruthven and C.B. Ching. Counter-current and simulated counter-current adsorption separation processes. *Chemical Engineering Science*, 44(5): 1011 – 1038, 1989.

[14] Yifei Zang and Phillip C. Wankat. Three-zone simulated moving bed with partial feed and selective withdrawal. *Industrial & Engineering Chemistry Research*, 41(21):5283–5289, 2002.

[15] Nadia Abunasser, Phillip C. Wankat, Y.-S. Kim, and Yoon Mo Koo. One-column chromatograph with recycle analogous to a four-zone simulated moving bed. *Industrial & Engineering Chemistry Research*, 42(21):5268–5279, 2003.

[16] Nadia Abunasser and Phillip C. Wankat. One-column chromatograph with recycle analogous to simulated moving bed adsorbers: Analysis and applications. *Industrial & Engineering Chemistry Research*, 43(17):5291–5299, 2004.

[17] José PB Mota and João MM Araújo. Single-column simulated-moving-bed process with recycle lag. *AIChE journal*, 51(6):1641–1653, 2005.

[18] João M. M. Araújo, Rui C. R. Rodrigues, Ricardo J. S. Silva, and José P. B. Mota. Single-column simulated moving-bed process with recycle lag: Analysis and applications. *Adsorption Science & Technology*, 25(9):647 – 660, 2007.

[19] Philippe Adam, Roger Narc Nicoud, Michel Bailly, and Olivier Ludemann-Hombourger. Process and device for separation with variable-length, October 24 2000. US Patent 6,136,198.

[20] O. Ludemann-Hombourger, R. M. Nicoud, and M. Bailly. The varicol process: A new multicolumn continuous chromatographic process. *Separation Science and Technology*, 35(12):1829–1862, 2000.

[21] Abdelaziz Toumi, Felix Hanisch, and Sebastian Engell. Optimal operation of continuous chromatographic processes: Mathematical optimization of the varicol process. *Industrial & Engineering Chemistry Research*, 41(17): 4328–4337, 2002.

[22] H. Schramm, M. Kaspereit, A. Kienle, and A. Seidel-Morgenstern. Improving simulated moving bed processes by cyclic modulation of the feed concentration. *Chemical Engineering & Technology*, 25(12):1151–1155, 2002. ISSN 1521-4125.

[23] H Schramm, A Kienle, M Kaspereit, and A Seidel-Morgenstern. Improved operation of simulated moving bed processes through cyclic modulation of feed flow and feed concentration. *Chemical engineering science*, 58(23): 5217–5227, 2003.

[24] Michael M Kearney and Kathleen L Hieb. Time variable simulated moving bed process, April 7 1992. US Patent 5,102,553.

[25] E. Kloppenburg and E. D. Gilles. A new concept for operating simulated moving-bed processes. *Chemical Engineering & Technology*, 22(10):813–817, 1999. ISSN 1521-4125.

[26] Ziyang Zhang, Marco Mazzotti, and Massimo Morbidelli. Powerfeed operation of simulated moving bed units: changing flow-rates during the switching interval. *Journal of Chromatography A*, 1006(1):87–99, 2003.

[27] Ziyang Zhang, Marco Mazzotti, and Massimo Morbidelli. Multiobjective optimization of simulated moving bed and varicol processes using a genetic algorithm. *Journal of Chromatography A*, 989(1):95–108, 2003.

[28] Yifei Zang and Phillip C. Wankat. Smb operation strategyâˆ’partial feed. *Industrial & Engineering Chemistry Research*, 41(10):2504–2511, 2002.

[29] Thomas B. Jensen, Tiem G.P. Reijns, Hugo A.H. Billiet, and Luuk A.M. van der Wielen. Novel simulated moving-bed method for reduced solvent consumption. *Journal of Chromatography A*, 873(2):149 – 162, 2000.

[30] Dorota Antos and Andreas Seidel-Morgenstern. Two-step solvent gradients in simulated moving bed chromatography: Numerical study for linear equilibria. *Journal of Chromatography A*, 944(1):77–91, 2002.

[31] Stefanie Abel, Marco Mazzotti, and Massimo Morbidelli. Solvent gradient operation of simulated moving beds: I. linear isotherms. *Journal of chromatography A*, 944(1):23–39, 2002.

[32] Pedro Sá Gomes and Alírio E Rodrigues. Outlet streams swing (oss) and multifeed operation of simulated moving beds. *Separation Science and Technology*, 42(2):223–252, 2007.

[33] Pedro Sa Gomes and Alírio E Rodrigues. Outlet stream swing simulated moving bed: Separation and regeneration regions analysis. *Separation Science and Technology*, 45(16):2259–2272, 2010.

[34] Lars Christian Keßler and Andreas Seidel-Morgenstern. Improving performance of simulated moving bed chromatography by fractionation and feedback of outlet streams. *Journal of Chromatography A*, 1207(1–2):55 – 71, 2008.

[35] Suzhou Li, Yoshiaki Kawajiri, Jörg Raisch, and Andreas Seidel-Morgenstern. Optimization of simulated moving bed chromatography with fractionation and feedback: Part ii. fractionation of both outlets. *Journal of Chromatography A*, 1217(33):5349–5357, 2010.

[36] Youn-Sang Bae and Chang-Ha Lee. Partial-discard strategy for obtaining high purity products using simulated moving bed chromatography. *Journal of Chromatography A*, 1122(1):161–173, 2006.

[37] T. Teshima M. Tanimura, M. Tamura, 1995. Japanese Patent JP-B-H07-046097.

[38] Shigeharu Katsuo and Marco Mazzotti. Intermittent simulated moving bed chromatography: 1. design criteria and cyclic steady-state. *Journal of Chromatography A*, 1217(8):1354–1361, 2010.

[39] Shigeharu Katsuo and Marco Mazzotti. Intermittent simulated moving bed chromatography: 2. separation of tröger's base enantiomers. *Journal of Chromatography A*, 1217(18):3067–3075, 2010.

[40] Shigeharu Katsuo, Christian Langel, Anne-Laure Sandré, and Marco Mazzotti. Intermittent simulated moving bed chromatography: 3. separation of tröger's base enantiomers under nonlinear conditions. *Journal of Chromatography A*, 1218(52):9345–9352, 2011.

[41] Ricardo JS Silva, Rui CR Rodrigues, Hector Osuna-Sanchez, Michel Bailly, Eric Valéry, and José PB Mota. A new multicolumn, open-loop process for center-cut separation by solvent-gradient chromatography. *Journal of Chromatography A*, 1217(52):8257–8269, 2010.

[42] Giuseppe Storti, Marco Mazzotti, Massimo Morbidelli, and Sergio Carrà. Robust design of binary countercurrent adsorption separation processes. *AIChE Journal*, 39(3):471–492, 1993.

[43] Marco Mazzotti, Giuseppe Storti, and Massimo Morbidelli. Optimal operation of simulated moving bed units for nonlinear chromatographic separations. *Journal of Chromatography A*, 769(1):3 – 24, 1997.

[44] Marco Mazzotti. Equilibrium theory based design of simulated moving bed processes for a generalized langmuir isotherm. *Journal of Chromatography A*, 1126(1):311–322, 2006.

[45] Georges Guiochon, Dean G Shirazi, Attila Felinger, and Anita M Katti. *Fundamentals of preparative and nonlinear chromatography*. Academic Press, 2006.

[46] Luís S. Pais, José M. Loureiro, and Alírio E. Rodrigues. Modeling strategies for enantiomers separation by smb chromatography. *AIChE Journal*, 44(3): 561–569, 1998.

[47] João MM Araújo, Rui CR Rodrigues, and José PB Mota. Use of single-column models for efficient computation of the periodic state of a simulated moving-bed process. *Industrial & engineering chemistry research*, 45(15):5314–5325, 2006.

[48] Rui CR Rodrigues, João MM Araújo, Mário FJ Eusébio, and José PB Mota. Experimental assessment of simulated moving bed and varicol processes using a single-column setup. *Journal of Chromatography A*, 1142(1):69–80, 2007.

[49] Rui CR Rodrigues, João MM Araújo, and José PB Mota. Optimal design and experimental validation of synchronous, asynchronous and flow-modulated,

simulated moving-bed processes using a single-column setup. *Journal of Chromatography A*, 1162(1):14–23, 2007.

5

Relay simulated moving bed: experimental validation

5.1 Introduction

In chapter 2, we have already discussed the standard operation of a SMB unit, and the variations to this operation that extend the application and enhance this process. Also, in chapter 3 we have introduced a new type of node operation that can be used as an alternative to the implicitly discarding the flow splitting at an active outlet, i.e., by obtaining the product, waste or recycling fractions by completely directing the effluent over a certain period of the cycle to the appropriate destination. In this sense, the previous chapter (Ch. 4), aims to apply the same technique of outlet handling to the two product outlets of the SMB in order to avoid the use of flow controllers or an extra pump. As before, the idea is to have just two- or three-way valves at the outlets—while maintaining the analogy with the SMB in terms of displaced volumes of fluid per switch interval. To achieve this, the continuous splitting of the effluents of zones I and III is replaced by two different actions applied sequentially over the switch interval: one of diverting the effluent for product collection and the other of directing the effluent to the next downstream zone.

In the present chapter, we intend to validate experimentally the concept developed before. In order to do it, we need two different separation systems with

selectivities (α) that fall in the two regions defined in the previous chapter, i.e., $\alpha_C \leq (3+\sqrt{5})/2$ and $\alpha_C \geq (3+\sqrt{5})/2$. The separation of some pairs of nucleosides, uridine/guanosine and uridine/adenosine, in Source 30 RPC with a desorbent composed of 5%(v/v) ethanol/water, provides the separation problem needed for these experiments.

We defined the selectivity of a separation in the previous chapter as:

$$\alpha = \frac{\epsilon + (1-\epsilon)K_2}{\epsilon + (1-\epsilon)K_1} \tag{5.1}$$

The selectivity of the pairs uridine/guanosine (U/G) and uridine/adenosine (U/A) is distributed with the order: $\alpha_{U/G} < \alpha_C < \alpha_{U/A}$. In this chapter, we will assess the performance of the two variants of the R-SMB process, comparing it to a open-loop SMB process with recycle for each separation problem.

5.2 Chromatographic Column Model

The operation of a chromatographic column in isothermal conditions is adequately described by a dispersed-plug-flow model, with linear driving-force (LDF) approximation for mass transfer under the form of a lumped solid-diffusion model. These assumptions are standard practice in preparative chromatography and SMB modeling [1], and can be reasonably well approximated by an equilibrium-dispersed model with dispersion coefficients dependent on the local slopes of the adsorption isotherms [2].

For a linear adsorption system the equilibrium-dispersed model is given by the following equations:

$$\frac{\partial c_i}{\partial \theta} = \frac{\tau Q_j}{(1+\beta K_i)V_C}\left(\frac{1}{Pe}\frac{\partial^2 c_i}{\partial x^2} - \frac{\partial c_i}{\partial x}\right) \qquad \text{for} \quad 0 < x < 1 \tag{5.2}$$

with boundary conditions

$$c_i - \frac{1}{Pe}\frac{\partial c_i}{\partial x} = c_i^{in} \qquad \text{for} \quad x = 0, \tag{5.3}$$

$$\frac{\partial c_i}{\partial x} = 0 \qquad \text{for} \quad x = 1. \tag{5.4}$$

where subscript i is the solute index, $\theta = t/\tau$ and $x = z/L$, the dimensionless temporal and axial coordinates, respectively; c_i, the liquid phase concentration;

K_i, the Henry constant for component i, i.e., $q_i^* = K_i c_i$ where q_i^* is the equilibrium concentration in the adsorbed phase; $\beta = (1-\epsilon)/\epsilon$ the phase ratio; V_C, the geometrical column volume; Q_j, the flow-rate of the fluid phase; τ, a reference time; Pe, the Péclet number $Pe = vL/D_L$; c_i^{in}, the solute concentration in the inlet effluent.

The dimensionless plate height, h_i, governing band broadening for the i^{th} component, can be expressed as follows in eq.5.5, [2], where k_i is the LDF coefficient for lumped solid-diffusion mass transfer. The variation of h_i with the volumetric flow-rate calculated from a simplified van Deemter plot [1]

$$\frac{h_i}{2} = \frac{1}{Pe} + \alpha_i \frac{Q}{V_C}, \qquad \alpha_i = \frac{\beta K_i}{k_i(1+\beta K_i)^2} \tag{5.5}$$

5.3 Experimental

The performances of the chromatographic processes reported in the present work have been verified with preparative-scale experiments on the nucleosides linear binary separation of uridine/guanosine and uridine/adenosine, on reversed-phase Source 30 RPC (GE Healthcare Amersham Biosciences, Uppsala, Sweden). The mobile phase was fixed at 5% (v/v) ethanol in water, which was previously found to give adequate retention and separation factors [3, 4]. All experiments were performed isothermally at 30°C, and the feed concentration was fixed at 0.05 g/L for each solute. Uridine (99%), guanosine (98%) and adenosine (98%) were purchased from Sigma–Aldrich (Steinheim, Germany), and HPLC-grade ethanol from Panreac (Spain). The solvents were mixed in the appropriate volumetric proportions after filtration. The chromatographic columns are Superformance 26 mm i.d. thermojacketed glass columns (Götec Labortechnik, Germany). The stationary phase was slurry packed into each column to a bed height L = 6.0 cm, with mobile phase at 25 ml/min, back-pressure of 30 bar, and 30 min packing time. The experimental set-ups follow the schematics depicted in Fig. 5.1. The distributed valve design is based on normally closed two-way valves, since they allow independent port switching and are quite versatile. Two-way valves can let the flow pass when actuated or stop the flow in its default position. The two-way valves are model SFVO from Valco International (Schenkon, Switzerland) with pneumatic actuation. Each valve is automated by means of a single computer-controlled three-way solenoid: application of 50 psi opens the valve; venting the air allows the spring to return the valve to the default position.

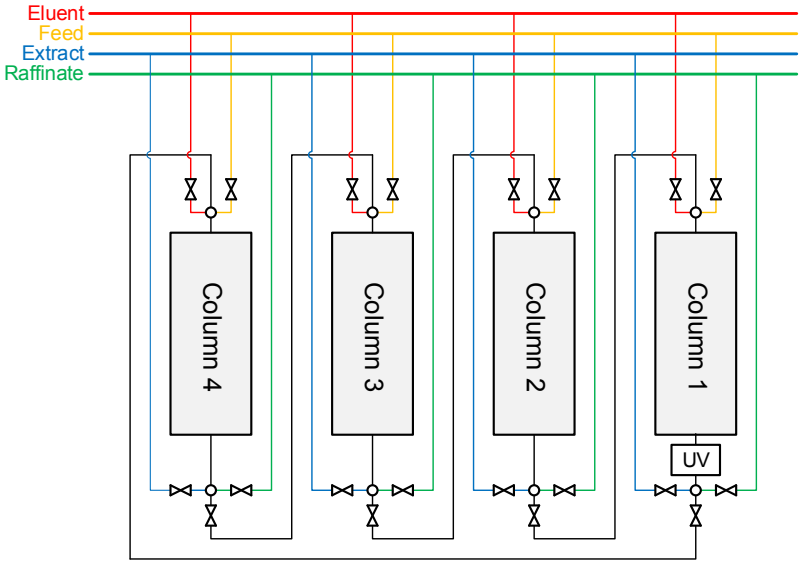

Figure 5.1: Schematic of the four-column SMB unit used in the experimental runs.

The HPLC pumps are model K-501 from Knauer (Berlin, Germany) with 10 mL heads, controlled via RS232 communication protocol. The experimental set-up is fully automated and driven by an in-house developed automation system using LabView [5] software (National Instruments).

A multi-wavelength UV detector (USB2000 from Ocean Optics, USA) equipped with a DH-2000-S-DUV light source (Micropack, Ostfildern, Germany), and attenuator, was employed to continuously monitor the composition of the outlet effluent.

The porosity of each column (interparticle void fraction, ϵ) was determined from the retention times of diluted pulses of blue dextran. Packing reproducibility was assessed by comparing the peak shapes and retention times of the chromatograms; both columns were found to be identically, and reasonably well, packed. The extra volume per column, V_e, in each experimental set-up was estimated from blue-dextran pulse experiments with and without the chromatographic columns. The experimentally obtained value for V_e in each node is less than 0.3% of the column volume and therefore included in the Henry constant [4].

The intercept and slope of the linearized van Deemter plot (given by equation 5.5) for each nucleoside were determined by fitting the experimental dependence of the plate height on flow rate for diluted pulses of the solutes; the Henry constants were determined from the retention times of the same chromatograms, and averaged based on all column results. Table 5.1 summarizes the obtained parameters.

Table 5.1: Column characterization and adsorption parameters for the linear separation of uridine/guanosine and uridine/adenosine on Source 30 RPC (reversed phase) and 5% (v/v) ethanol in water at 30°C; ϵ is the packing porosity, all values are averages of measurements based on all columns used.

$\epsilon = 0.325$	K	Pe	$\alpha L(s)$	$k(s^{-1})$
Uridine $(i = 1)$	1.240	744	0.108	1.851
Guanosine $(i = 2)$	1.893	640	0.163	0.930
Adenosine $(i = 3)$	5.593	460	0.316	0.231

5.4 Results and discussion

The optimal cycle was determined by solving the NLP design problem with the chromatographic parameters listed in Table 5.1, subject to a minimal product purity $Pur^X_{min} = Pur^R_{min} = 99\%$ and to a maximum flow rate, corresponding to the highest flow rate attainable by the pumps used in the experimental unit (10.00 mL/min). Fig. 5.2 depict the operating cycles for the R-SMB process for selectivity region of $\alpha < \alpha_C$ and $\alpha > \alpha_C$ respectively. The optimal cycle parameters for each process are represented in Table 5.2. The cycles for the R-SMB processes were reproduced

Table 5.2: Optimal cycle parameters for the R-SMB processes. The time of each step is given in minutes and the flow rates in mL/min. E, F, X, R and D represent the desorbent, feed, extract, raffinate and desorbent flow rates, respectively.

	t_i	E	F	X	R	D
$R-SMB^-$	1.405	10.000	2.249	0.000	12.249	0.000
	2.322	10.000	2.249	0.000	0.000	12.249
	2.066	10.000	2.249	10.000	0.000	2.249
$R-SMB^+$	3.665	10.000	6.298	0.000	16.298	0.000
	4.915	10.000	6.298	10.000	6.298	0.000
	5.648	10.000	6.298	10.000	0.000	6.298

experimentally in a prototype apparatus with a schematic identical to that shown in Fig. 5.1. The temporal concentration profiles, measured at the outlet of column 1 in the cyclic steady state, are shown and compared with the simulated profiles in Figs. 5.3 and 5.4. The purity of the products for each process is presented in Table 5.3

Table 5.3: Purities of the experimental runs for the R-SMB processes

	10^{th} cycle	11^{th} cycle	12^{th} cycle	average purity
R-SMB$^-$ (X/R)	98.99/99.19	99.12/99.12	99.09/99.15	99.1/99.2
R-SMB$^+$ (X/R)	99.19/90.09	99.17/99.07	99.18/99.28	99.2/99.2

The performance of the R-SMB process was compared against the open-loop SMB

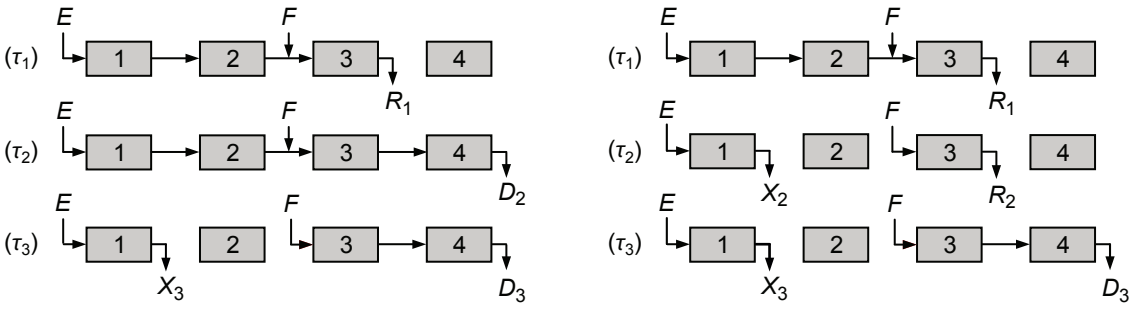

(a) R-SMB$^-$ $(\alpha < \alpha_C)$ **(b)** R-SMB$^+$ $(\alpha > \alpha_C)$

Figure 5.2: Schematic of the R-SMB process for the two selectivity regions. E, F, X, R and D represent the desorbent, feed, extract, raffinate and desorbent flow rates, respectively.

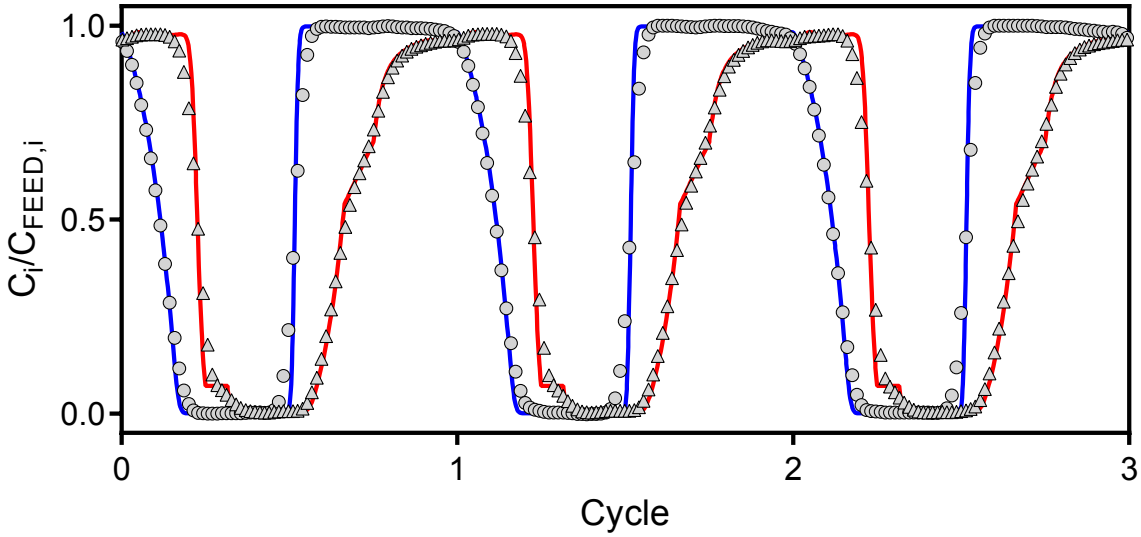

Figure 5.3: Solute concentration profiles at the outlet of column 1 for the chromatographic parameters given in Table 5.2 for the R-SMB process with $\alpha < \alpha_C$. Symbols denote experimental data, whereas lines represent the solution of the dynamic process model (blue for uridine and red for guanosine). For visual clarity, only the last 3 cycles of the CSS are plotted.

process with recycle, as seen in Fig. 5.5. In order to establish such comparison, we have performed a series of optimizations conducting to the construction of Pareto curves in terms of average eluent consumption versus productivity: $(E_{AV}/F_{AV} \times F_{AV})$ plane. Each curve represents a set of optimal solutions for a given process and a fixed set of product specifications (e.g., purity and yield). Special care is taken to subject all the Pareto curves to the same product constraints and same amount of stationary phase so that curves for different column configurations can be directly compared. In the present work, the objective function, f_{obj}, is

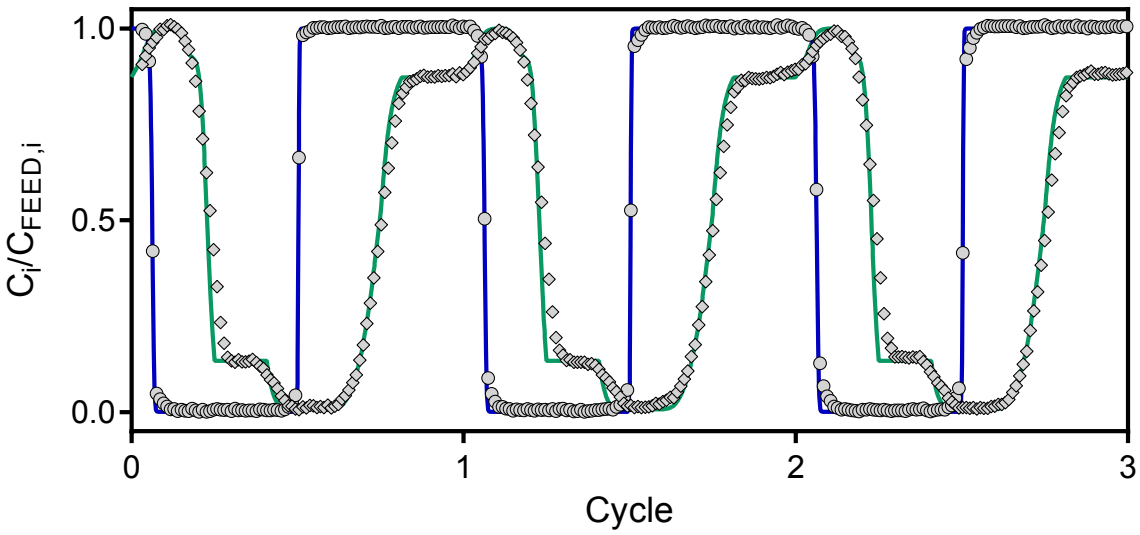

Figure 5.4: Solute concentration profiles at the outlet of column 1 for the chromatographic parameters given in Table 5.2 for the R-SMB process with $\alpha > \alpha_C$. Symbols denote experimental data, whereas lines represent the solution of the dynamic process model (blue for uridine and green for adenosine). For visual clarity, only the last 3 cycles of the CSS are plotted.

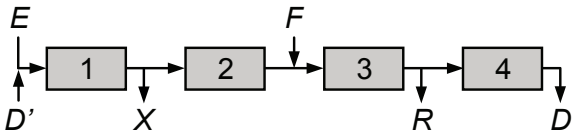

Figure 5.5: Shematic of the open-loop smb with recycle process. E, X, F and R denote the desorbent, extract, feed and raffinate flow rates respectively. D and D' denote the regenerated and recycled desorbent flow rates.

chosen to be the maximization of productivity, or feed throughput:

$$F_{AV} = \frac{1}{\tau}\int_{t}^{t+\tau} F dt \tag{5.6}$$

In the open-loop process, the recycled desorbent D', should be interpreted as an off-line recycle of D, which was for simplicity was set as $D' = D$. In the R-SMB process the regenerated solvent D is not recycled as before, in order to define a comparison on the same basis in terms of desorbent consumption we need to account for this fact. We define E_{AV} for the R-SMB process as:

$$E_{AV} = \frac{1}{\tau}\int_{t}^{t+\tau} (E - D)\, dt \tag{5.7}$$

and for the open-loop process:

$$E_{av} = \frac{1}{\tau}\int_{t}^{t+\tau} E dt \tag{5.8}$$

To construct a Pareto curve on this plane, we constraint the average desorbent consumption to a constant value of desorbent flow rate, E_{max}, and carry out a series of single-objective optimizations that maximize F_{av} for progressively larger values of E_{max}. Hence we solve:

$$f_{obj} = max\ F_{av}, \quad s.t. \quad E \leq E_{max}. \tag{5.9}$$

for increasing values of the parameter E_{max}. The set of points thus generated gives the desired Pareto curve. Each NLP problem defined by Eq. 5.9 is solved directly for steady periodic operation of the process, i.e., for cyclic steady state (CSS) conditions.

Figure 5.6: The full and traced curves correspond to the R-SMB and open-loop SMB processes, respectively. The dotted curve in b) corresponds to the extension in productivity in the R-SMB process, when the constrain due to the maximum flow rate of the pumps is dropped.

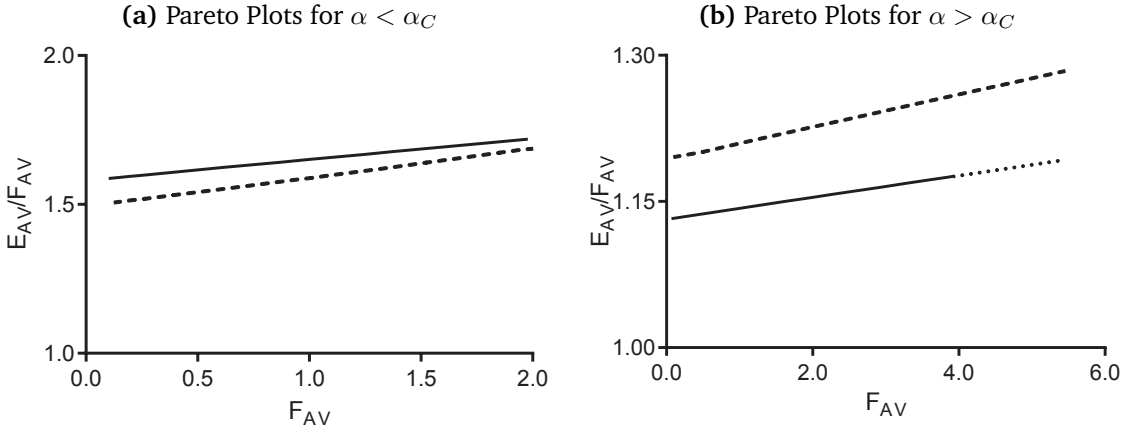

5.5 Concluding Remarks

In the present work, we have validated experimentally the concept of the R-SMB process, using a linear separation problem for each region of selectivity described in chapter 4, using the separations of nucleosides pairs uridine/guanosine and uridine/adenosine in a reversed phase system.

The R-SMB, when compared to a open-loop SMB with recycle process performed reasonably well, this demonstrates that the R-SMB process is an attractive alternative to the open and closed-loop versions of the SMB process.

Due to the simplification of the product lines, the R-SMB process permits to reduce the capital costs of a SMB unit, maintaining the analogy with standard process in terms of yield, and product quality specifications with the additional benefits of simplicity of implementation and operation.

References

[1] Georges Guiochon, Dean G Shirazi, Attila Felinger, and Anita M Katti. *Fundamentals of preparative and nonlinear chromatography*. Academic Press, 2006.

[2] Douglas Morris Ruthven. Principles of adsorption and adsorption processes. 1984.

[3] Stefanie Abel, Gültekin Erdem, Mohammad Amanullah, Manfred Morari, Marco Mazzotti, and Massimo Morbidelli. Optimizing control of simulated moving beds - experimental implementation. *Journal of Chromatography A*, 1092(1):2–16, 2005.

[4] Rui CR Rodrigues, Ricardo JS Silva, and José PB Mota. Streamlined, two-column, simulated countercurrent chromatography for binary separation. *Journal of Chromatography A*, 1217(20):3382–3391, 2010.

[5] Mário FJ Eusébio. Development of an universal interface for monitoring and control of chemical and biochemical processes, Ph.D. Thesis, Universidade Nova de Lisboa, 2006.

6

Gradient with Steady State Recycle process: rationalization and pilot unit validation

6.1 Introduction

The advances in biotechnology and developments in genetic engineering have resulted in the scale up and manufacturing of biopharmaceutical products [1]. Today, downstream processing is facing the challenge of manufacturing products with the highest degrees of purity and integrity, and overall process economy, while keeping pace with the rapidly increasing upstream yields in biotechnology. The fulfillment of the strict requirements by downstream purification is the major cost factor in biotechnological production with 50-80% of the total manufacturing cost [2].

A major part of the purification costs is related to chromatographic processes, which, at present, are still largely operated in batch mode. This is not because chromatography is inherently expensive, but because it is heavily used: chromatography plays a central role in fast and efficient separation of biochemical and pharmaceutical compounds; in fact, it still remains the work horse method in biopurification.

For most biopurification problems, the desired product is intermediate between

weakly and strongly adsorbing impurities, and a central cut is thus required to get the desired product. Conventionally, the generic three-fraction biopurification problem is solved using batch column chromatography, often incorporating solvent gradients. Typically, the target product is separated from process-related impurities through a series of steps wherein a selected cut or fraction of the effluent from the previous step is selectively adsorbed and desorbed onto a given stationary phase using time and elution conditions as manipulated variables, until, ultimately, yielding the product purified to the desired level. Solvent gradients are easy to apply in sequential batch chromatography, but this operating mode suffers from high product dilution, low efficiency and productivity, and high solvent consumption.

As a general rule, multicolumn processes combining freely adjustable, smooth gradients and simulated countercurrent (SCC) adsorption can achieve better performance than sequential batch chromatography. Early studies [3–6] on ternary separation by isocratic SCC chromatography were focused on continuous processes (i.e., with continuous feeding and product withdrawal) and showed that this restrictive design criterium can only be achieved with column configurations comprising several fluid zones (here, a zone refers to the columns between two active ports). The most commonly explored column configurations have been simulated moving-bed (SMB) cascades [4, 7] and five-zone systems with side streams [8–11].

Bioseparation, on the other hand, does not require that the separation scheme be continuous; this allows several possibilities and a multitude of operating modes to be considered in the design of the process, which otherwise would have to be excluded. In principle, a semi-continuous, multicolumn process can make use of various techniques to achieve the desired separation; for example, some columns can be dynamically interconnected, so that non-pure product cuts are internally and countercurrently recycled, while other columns can be short circuited to operate in pure batch mode, and others frozen to introduce time lags between the positions of the various concentration fronts. This way some fractions can be separated by a SCC approach (the mass-transfer zone is kept inside the system by means of the port switching and the remixing with the feed), whereas the separation of other fractions can be chromatographic (the mass-transfer zone is taken out of the system). By freezing one or more columns (i.e., stopping the flow through them) for some steps of the cycle, it is possible to decouple the migrating velocities of the various solutes.

The schemes developed by Jin and Wankat [12, 13] and by our group [14–16] are examples of existing processes for isocratic binary separation that combine some

of the techniques above into a single hybrid scheme. The case of isocratic ternary separation is clearly more complicated. The idea of operating only partially in a countercurrent fashion was exploited by Masuda et al. [17] in a single cascade process for fractional separation that is commercialized by Organo Corp., Tokyo, Japan; the performance of this process has been analyzed by other authors [18–20]. Hur and Wankat [21] developed a two-zone SMB/chromatography hybrid system for ternary separations, and compared its performance to those of cascades of two-zone and four-zone SMBs. Subsequently, the same authors [22] designed a semi-continuous, center-cut, two-zone SMB/chromatography system and a recycled cascade with two four-zone SMBs to separate the intermediate component from ternary mixtures.

Recently, Morbidelli and co-workers [23–28] developed a chromatographic process for ternary separation (MCSGP-process) that exploits the power of gradient chromatography and hybrid SMB/chromatography modes. In this process some columns operate in counter-current mode during a fraction of the cycle while others are short-circuited and operate in batch mode. Continuous operation of the MCSGP requires six columns [24, 26], but the process can be reduced to a fully equivalent semi-continuous configuration with only three chromatographic columns and three gradient pump modules [27, 28]. Using a series of working examples, these authors have demonstrated the superiority of MCSGP over batch chromatography.

In the present work, we describe a new multicolumn, open-loop process for center-cut separation by solvent-gradient chromatography. The key idea is to extend solvent-gradient batch chromatography to a train of columns and to exploit the fractionation of the stationary phase. In single-column batch chromatography the product and waste cuts are obtained at the same point in the system—at the downstream end of the column—but at different times. Therefore, time (or elution volume) is the only variable for defining the fractional cuts. If a solvent gradient is used, it is introduced into the system at a single point—the upstream end of the column. This, of course, does not give much freedom for dynamically adjusting the solvent composition profile inside the column.

Although packing the stationary phase into a single column works fine for many binary separations, this seems to be overly restrictive for center-cut separations. The introduction of space as an additional variable (although being a discrete one), by dividing the stationary phase into a train of columns, adds more flexibility for manipulating the cuts and for generating the solvent gradient; furthermore, with such a column arrangement it is possible to recycle some of the cuts from the

downstream end of the system to its upstream end.

In this work we show that this can be done while working in a simple, open-loop system that resembles the batch system. Although our process implements a solvent-gradient moving around a ring of columns, it is similar to a batch process in terms of feeding and product collecting. We provide experimental validation in a pilot unit, using the purification of a crude peptide mixture by reversed phase as a working example; this proof of concept serves to highlight the versatility, flexibility, and ease of operation of the process.

6.2 Process description

The new process, nicknamed GSSR (gradient with steady state recycle), comprises a multi-column, open-loop system, with cyclic steady-state operation, that simulates a solvent gradient moving countercurrently with respect to the solid phase. It is particularly suited for ternary separations: it provides three main fractions or products, with a target product contained in the intermediate fraction. The process can be pictured as the superposition of three steady periodic events applied to a ring of columns with an open-loop configuration: a moving solvent gradient, a feeding step, and a step of product collection. A comprehensive description of the GSSR process is provided next.

First, consider how a moving solvent gradient is implemented by means of a plurality of solvent lines. For this purpose, consider the schematic of Fig. 6.1, which is an example of the simplest GSSR sequence applied to a three-column train. Note, however, that the process can operate with more columns. The three-column train of Fig. 6.1 is supplied with three different solvents: solvent A, which has a linear-gradient composition, and two isocratic solvents, B and C, with elution strengths different from A.

The inlet positions and flow rates of the solvent lines are defined for a single switching interval as a set of steps over that period of time. The sequence is then repeated a number of times equal to the number of columns, the only difference between a switching interval and the next being the shift of the solvent inlets by one column in the direction of the fluid flow. A complete cycle is defined by the sequence of steps for the set of switching intervals.

From this description, it follows that the inlet positions and flow rates of the solvent lines are periodic in time, with period τ, where τ is the duration of a switching

interval. There is always an open outlet, which is taken as a waste fraction, in order to keep the system in open loop. The net effect of this cyclic scheme is the simulation of the counter-current movement of the solid phase relative to an open-loop solvent gradient that is τ-periodic in time.

If the system is operated for a large number of cycles, the solvent will develop a steady, τ-periodic, axial composition profile extending over the columns. Note that the solvent composition profile will not be spatially periodic (i.e., it will not be periodic along a coordinate extending from the upstream end of the first column to the downstream end of the last column), but only time periodic; for the profile to be spatially periodic, all columns would have to the supplied with the same solvent gradient.

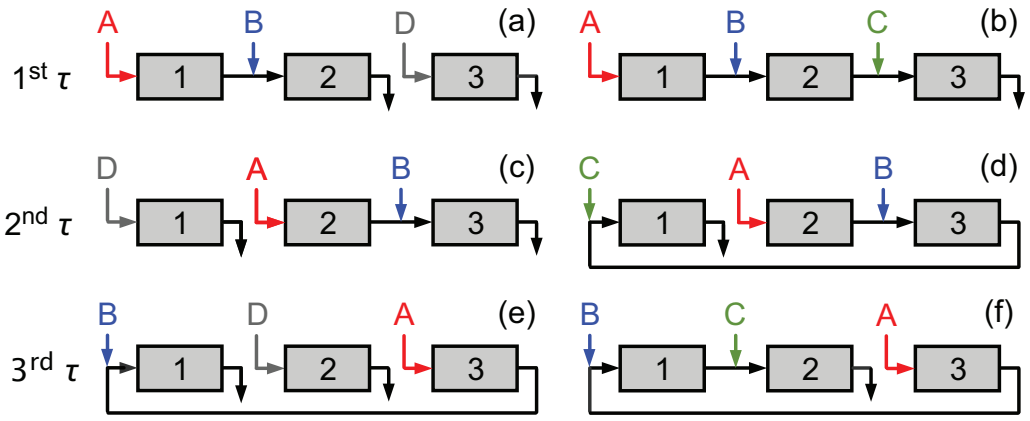

Figure 6.1: Basic sequencing of the solvent lines for a three-column GSSR process. The righthand sequence—steps b, d, and f—is for operation without on-line regeneration or cleaning in place. A sequence with desorption zone consists of performing the lefthand step for an initial fraction, say α, of the corresponding switching interval, followed by its righthand counterpart for the remaining $(1 - \alpha)$. All active outlets are diverted to waste.

In biochromatography a suitable regeneration method is essential for maximizing column performance and obtaining reproducible results. The regeneration usually entails the use of a strong solvent to remove highly adsorbed impurities, and may require post-equilibration of the column with regular buffer. For this purpose, the GSSR process provides the possibility for in-line regeneration or cleaning in place (CIP) by dividing the switching interval into two sub-steps and replacing solvent C by a stronger solvent D over the first sub-step. Thus, during an initial fraction, say α, of each switching interval, the column whose upstream end is attached to the active inlet line of solvent C is partially or totally flushed with solvent D; during this time, the addition of solvent C is halted. Moreover, while the column is desorbed with solvent D, the outlet effluent of the upstream column is diverted to waste. Once the initial sub-step of the switching interval is completed, the two columns

resume their normal operation. It is worth noting that nothing has yet been said about feeding and product collecting; thus, for the moment all active outlets (e.g., those depicted in Fig. 6.1) should be interpreted as waste outlets.

In order to establish a GSSR cycle, two additional steps must be defined: (i) the time interval during which fresh feed is supplied into the system; and (ii) the time interval during which the target product is collected. These two steps are cyclic, but take place only once per cycle, i.e., they are both $N\tau$-periodic, where N is the number of columns. Moreover, they can be applied anywhere within the cycle and can cross or extend over consecutive switching intervals; depending on the difficulty of separation, the feed injection and product withdrawal can be performed over different intervals of the cycle, or they can take place at the same time, or they can partially overlap. However, the feed is always injected into the same column as a rectangular pulse and the product is always collected from the same column.

In order to explain how the feed and production steps work in a GSSR process, let us consider again a three-column ring, such as the one shown in Fig. 6.1. For difficult separations—those in which the target product is surrounded by closely eluting impurities—the feeding and product collecting should occur at opposite ends of the ring to establish the longest path between the feed inlet and the product outlet, and thus help to separate the impurities nearest to the target component. Without loss of generality, it will be assumed that the feed line is connected to the inlet of column 1 and the product line connected to the outlet of column 3.

Since in many cases the target solute will not be completely separated from its two nearest neighbor impurities when it reaches the collection point at the downstream end of the ring, the two impure cuts surrounding the purified product—one containing the leading edge of the target component and the other the trailing edge—must be recycled to the feed point at the upstream end of the system in order to maximize the recovery rate. For optimal performance, the two mixed cuts must be recycled in a such a way as to surround the feed pulse loaded into the feed column. Therefore, for difficult separations that require this recycling strategy the feed and product withdrawal steps must necessarily overlap. Moreover, to get the most efficient separation the feed pulse should be moved through the system by the moving solvent gradient (A) and not eluted isocratically with either solvent B or C.

From this discussion it is now clear when to carry out the feed and production steps within the sequencing of the solvent lines shown in Fig. 6.1 for the case where the feed line is connected to inlet of column 1 and the product line connected to the

outlet of column 3: the two steps must take place somewhere in the time interval of the cycle spanned by steps *d*, *e*, and *f* of Fig. 6.1, because during these steps the effluent from column 3 is recycled to the upstream end of column 1. Given that steps *d* and *f* have the same duration, combining the collection of the target peak with step *e* is a simple and pragmatic solution that places the product collection in the middle of the recycling sequence. Moreover, by feeding in step *e* the mixture is injected into the correct column, which is the one that is afterwards eluted with the solvent gradient.

There is one last detail to take into account regarding the feed and production steps. If the feed step is shorter than the production step, column 1 should be frozen after the feed step while the product is still being withdrawn from column 3, so that when the mixed cut containing the trailing edge of the product is recycled to the upstream end of column 1 it is placed next to the feed cut.

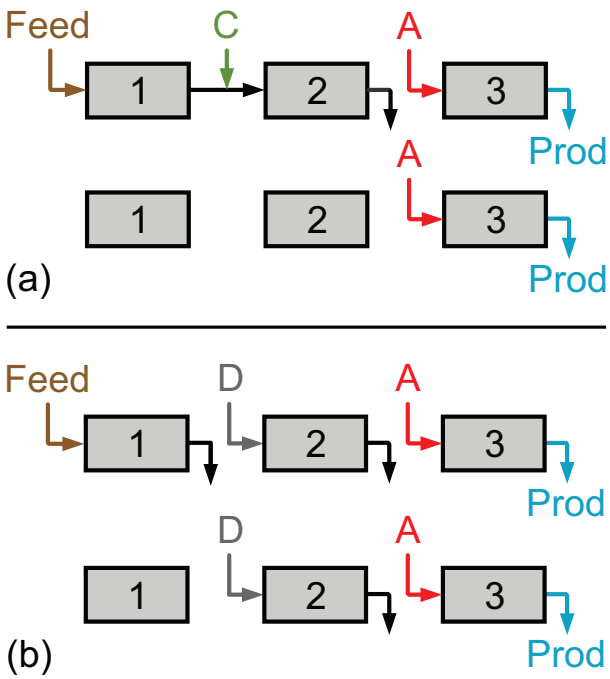

Figure 6.2: Flow diagrams of the feed and production steps for the case when they occur at the beginning of the third switching interval and when the product withdrawal takes longer than the injection of feed. Schematics (a) and (b) are for operations with and without on-line regeneration or cleaning in place, respectively. When the production step is finished the normal operation of the train of solvents is resumed.

Figure 6.2 shows the flow diagrams of the feed and production steps for the case when they occur at the beginning of the third switching interval, as discussed above, and when the product withdrawal takes longer than the injection of feed; the two sub-cases of operation with and without CIP must be handled separately

and require different flow diagrams. When the production step is finished the normal operation of the train of solvents is resumed. Other cases of placement of the feed and production steps in the GSSR cycle are discussed elsewhere [29].

Before concluding this section, it is worth noting that, in practice, the solvent gradient does not strictly follow the rules for simulating its counter-current movement around the ring of columns, but only approximately, due to the interference of the feeding and product collecting. The precise simulation of the counter-current movement of the solid is given up in favor of the extra flexibility provided by our cycle. Also, because the points of feeding and product collecting are fixed, each column can play a unique role in the separation. For the same reason, the N switching intervals that comprise a full GSSR cycle will not necessarily have the same length. This is different from multi-column systems adhering strictly to the simulated counter-current concept, where all columns undergo the same sequence of steps but phase out in time by multiples of the same switching interval, and opens up opportunities for a whole new range of cycles.

6.3 Pilot unit

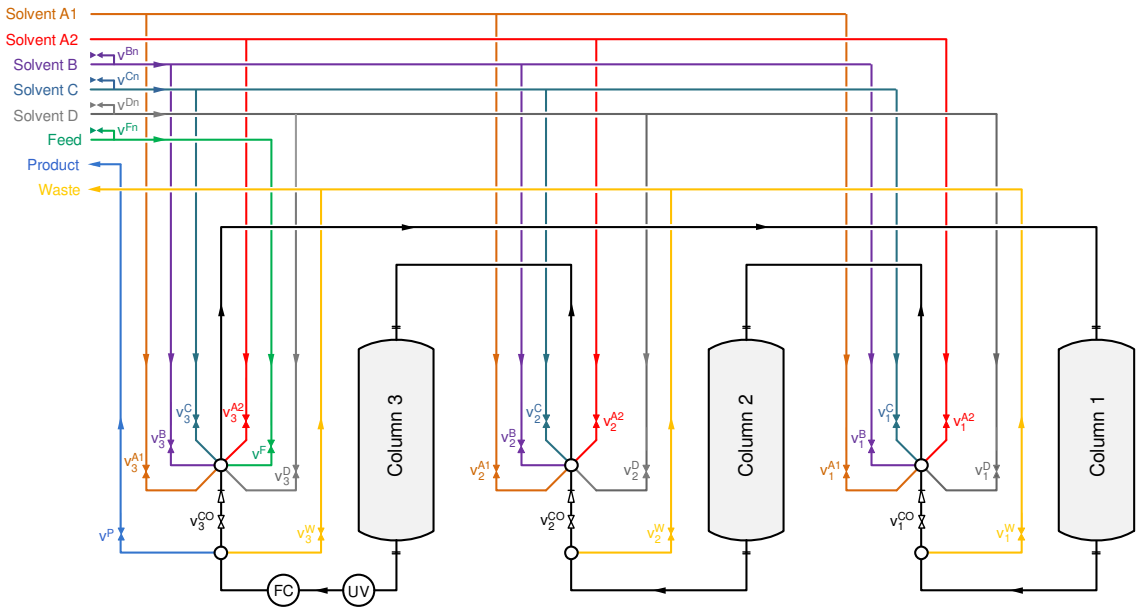

Figure 6.3: Schematic flowsheet of the GSSR pilot unit. v_j^{α}, two-way valve; UV, UV detector; FC, fraction collector.

Figure 6.3 shows a schematic flowsheet of the GSSR pilot unit. We use a distributed valve design based on two-way valves, since they are quite versatile and make it

possible to implement independent port switching. Two-way valves allow the flow either to go through or not to go through. The two-way valves are model SFVO from Valco International (Schenkon, Switzerland) with pneumatic actuation. Each valve is automated by means of a single computer-controlled, three-way solenoid: application of 50 psi opens the valve; venting the air allows the spring to return the valve to the closed position. Overall, the pilot unit employs 28 two-way valves.

Each set of six valves, $\{v^{\mathrm{CO}}, v^{\mathrm{A1}}, v^{\mathrm{A2}}, v^{\mathrm{B}}, v^{\mathrm{C}}, v^{\mathrm{D}}\}_j$ $(j = 1, 2, 3)$, is connected to a special tee with six inlets and one outlet; a check valve is placed in front of valve v^{CO} to prevent the occurrence of flow reversal. The other valves are attached to the transfers lines between columns by regular tees.

By simultaneously closing valve v_j^{CO} $(= 0)$ and opening valve v_j^{W} $(= 1)$, the effluent from column j is directed to the corresponding waste line; similarly, by simultaneously closing valve v_3^{CO} $(= 0)$ and opening valve v^{P} $(= 1)$, the effluent from column 3 is directed to the product line.

6.3.1 Inlet flow rates

The GSSR process employs three isocratic solvent streams—B, C, and D—with different solvent compositions, and one solvent-gradient stream, A. The composition of the solvent-gradient stream is τ-periodic in time and is continuously supplied into the process at constant flow rate Q_{A}. Solvents B and C are fed to the process at constant flow rates Q_{B} and Q_{C}, respectively; their flows, however, may have to be temporarily stopped while feeding or collecting product. Solvent D replaces solvent C during the desorption step of every switching interval; its flow rate, D, is constant. Finally, the feedstock fluid is injected once per cycle as a rectangular pulse with flow rate F. Overall, the inlet flow rates of the GSSR process are either constant or on/off; in the latter case, the flow rate is kept constant, at 0 or Q, over a given time interval before jumping discretely to the other value, Q or 0, over the next interval.

The HPLC pumps for the solvent lines B, C, and D, as well as that for the feed line, F, are operated under steady conditions at their prescribed flow rates to minimize disturbances in their operation. To interrupt the feed flow or the flow of one of the isocratic solvent streams, say stream B, the control software closes valve v_j^{B} and opens valve v^{Bn} to redirect the flow back to the solvent storage tank. Since for all purposes the valve switching is instantaneous, the net effect is a very good approximation of the sharp edge of the step change in the flow rate. To redirect the

flow of solvent B to column j, valve v^{Bn} is closed and valve v_j^{B} is open; the sharp edge of the step change in the flow rate is well reproduced again. The valves which are employed for redirecting the flow of an inlet line back to its source tank are v^{Fn}, v^{Bn}, v^{Cn}, and v^{Dn}.

Over each switching interval, the composition of solvent A changes linearly with time from $c_{\mathrm{A}}^{(0)}$ to $c_{\mathrm{A}}^{(\tau)}$,

$$c_{\mathrm{A}}(t) = c_{\mathrm{A}}^{(0)} + \frac{c_{\mathrm{A}}^{(\tau)} - c_{\mathrm{A}}^{(0)}}{\tau}\,(t \bmod \tau), \tag{6.1}$$

where $(\cdot \bmod \cdot)$ is the modulo operator, i.e., $(t \bmod \tau) \equiv t - \mathrm{int}\,(t/\tau)$. In the pilot unit, the solvent-gradient line is mimicked by the admixture of two isocratic solvent streams, A1 and A2, driven by two variable-velocity isocratic pumps, with two different solvent compositions, respectively, c_{A1} and c_{A2}, that satisfy $c_{\mathrm{A1}} \leq \min\{c_{\mathrm{A}}^{(0)}, c_{\mathrm{A}}^{(\tau)}\}$ and $c_{\mathrm{A2}} \geq \max\{c_{\mathrm{A}}^{(0)}, c_{\mathrm{A}}^{(\tau)}\}$. To reproduce the solvent gradient by the admixture of streams A1 and A2, the flow rates of the two HPLC pumps, Q_{A1} and Q_{A2}, are determined from the following material balances:

$$Q_{\mathrm{A1}} + Q_{\mathrm{A2}} \;=\; Q_{\mathrm{A}}, \tag{6.2}$$

$$Q_{\mathrm{A1}} c_{\mathrm{A1}} + Q_{\mathrm{A2}} c_{\mathrm{A2}} \;=\; Q_{\mathrm{A}} c_{\mathrm{A}}. \tag{6.3}$$

It is easily shown that $Q_{\mathrm{A1}}(t)$ and $Q_{\mathrm{A2}}(t)$ are τ-periodic, linear functions of time:

$$Q_{\mathrm{A1}}(t) \;=\; Q_{\mathrm{A1}}^{(0)} + \frac{Q_{\mathrm{A1}}^{(\tau)} - Q_{\mathrm{A1}}^{(0)}}{\tau}(\,t \bmod \tau), \tag{6.4}$$

$$Q_{\mathrm{A2}}(t) \;=\; Q_{\mathrm{A2}}^{(0)} + \frac{Q_{\mathrm{A2}}^{(\tau)} - Q_{\mathrm{A2}}^{(0)}}{\tau}(\,t \bmod \tau), \tag{6.5}$$

where

$$Q_{\mathrm{A1}}^{(0)} = Q_{\mathrm{A}} \frac{c_{\mathrm{A}}^{(0)} - c_{\mathrm{A2}}}{c_{\mathrm{A1}} - c_{\mathrm{A2}}}, \qquad Q_{\mathrm{A1}}^{(\tau)} = Q_{\mathrm{A}} \frac{c_{\mathrm{A}}^{(\tau)} - c_{\mathrm{A2}}}{c_{\mathrm{A1}} - c_{\mathrm{A2}}}, \tag{6.6}$$

$$Q_{\mathrm{A2}}^{(0)} = Q_{\mathrm{A}} \frac{c_{\mathrm{A}}^{(0)} - c_{\mathrm{A1}}}{c_{\mathrm{A2}} - c_{\mathrm{A1}}}, \qquad Q_{\mathrm{A2}}^{(\tau)} = Q_{\mathrm{A}} \frac{c_{\mathrm{A}}^{(\tau)} - c_{\mathrm{A1}}}{c_{\mathrm{A2}} - c_{\mathrm{A1}}}. \tag{6.7}$$

The six HPLC pumps employed in the pilot plant are model K-501 from Knauer (Berlin, Germany) with 10 mL and 50 mL pump heads, commanded by RS232 communication protocol.

6.3.2 Monitoring and fraction collection

A multi-wavelength UV detector (USB2000 from Ocean Optics, USA) with attenuator, connected to a DH-2000-S-DUV light source (Micropack, Ostfildern, Germany), is attached to the outlet of column 3. The communication between the UV detector and the control software is handled via a USB connection.

A fraction collector is also installed at the outlet of column 3, after the UV detector, for the periodic collection of internal samples that can be later analyzed by off-line HLPC. Each fraction is collected into a vial using an electrically driven, six-port, two-position valve, model K6 from Knauer (Berlin, Germany), commanded by RS232 communication protocol.

Most of the time, the effluent from column 3 flows through the UV measuring cell and through the injection loop of the six-port valve and is (i) directed to column 1, or (ii) collected as product, or (iii) removed as waste. At selected times the six-port valve is switched to inject position and valve v^{FC} is open, to place the injection loop within the flow path of mobile phase from a pressurized tank. The sample in the injection loop is thus pushed onto the vial for off-line HPLC analysis and the injection loop is washed with mobile phase. This occurs during a small, specified time interval at given instants of the cycle defined by the operator. During this time the effluent from column 3 bypasses the injection loop and is directly diverted into column 1. When the six-port valve is switched back to 'load' position and valve v^{FC} is closed, the mobile phase in the loop is pushed to the downstream column while the loop is being filled. Thus, the circulating flow in the pilot unit is not interrupted. The extra volumes in the pilot unit due to ancillary equipment, tubbing, detectors, and fraction collector were estimated to be 4.5 mL.

6.3.3 Process automation

The whole set-up, including pumps, two-way valves, UV detector, and fraction collector, is fully automated and driven by BioCTR [30]—our Labview-based software for process monitoring and control of multicolumn chromatographic processes.

A GSSR cycle is defined by a set of parameters, which are specified by the operator and can be changed while the pilot is running. Besides the number of columns, N, switching interval, τ, and the various flow rates, the set of operating parameters for a GSSR cycle includes other parameters that are described next. The start of the feed injection, t_{F}, is defined relative to the cycle time, $\tau_{\mathrm{cyc}} = N\tau$, as $t_{\mathrm{F}}/\tau_{\mathrm{cyc}}$, but the

duration of the injection, Δt_{F}, is defined in absolute time units. Product collection is defined similarly; hence, $t_{\mathrm{P}}/\tau_{\mathrm{cyc}}$ is the relative position of the start of collection and Δt_{P} specifies its duration.

The GSSR process can operate with a desorption zone where solvent C is replaced by a stronger solvent D. This step is applied once per switching interval and, therefore, is best defined with respect to that time interval. During the initial interval $0 \leq t/\tau < \Delta t_{\mathrm{D}}/\tau$ of every switching interval the system is operated with solvent D, whereas during the rest of the period, $\Delta t_{\mathrm{D}}/\tau \leq t/\tau < 1$, solvent D is replaced by normal solvent C. The solvent-gradient parameters Q_{A}, $c_{\mathrm{A}}^{(0)}$, and $c_{\mathrm{A}}^{(\tau)}$ are automatically converted by the control software into the flow rate parameters $Q_{\mathrm{A1}}^{(0)}$, $Q_{\mathrm{A1}}^{(\tau)}$, $Q_{\mathrm{A2}}^{(0)}$, and $Q_{\mathrm{A2}}^{(\tau)}$, using Eqs. (6.6) and (6.7).

6.4 Validation of moving solvent-gradient in the pilot unit

Before applying the GSSR process to the purification of the crude peptide mixture, the pilot unit underwent extensive testing in order to validate the automation of the valve sequencing, pump actuation, solvent-gradient implementation by the admixture of two isocratic pumps, pulsed feeding, and waste and product collecting. For example, some preliminary tests to validate the automation of the pumps and valves was carried out on the pilot unit using pure water and without the three chromatographic columns, which were simply replaced by capillary tee connections. The rate of accumulated mass from the waste and product lines was monitored in real time using a precision balance, model TE3102S from Sartorius (Goettingen, Germany). The rate of accumulated mass, dm/dt (g/min), is proportional to the flow rate, Q (cm^3/min), the scaling factor being the density ρ (g/cm^3) of the fluid: $\rho^{-1}(dm/dt) = Q$. The balance reading gives the mass accumulated over a given period of time, $m = \rho \int Q\, dt$.

In Fig. 6.4 a possible cycle configuration for the GSSR process is depicted. The proposed sequence was used to test the moving solvent-gradient implementation. The operating parameters for this scheme are shown in Table 6.1.

Although these tests were very successful (Fig. 6.5), they gave only a partial, and necessarily limited, validation of the practical implementation of the GSSR cycle on the pilot unit.

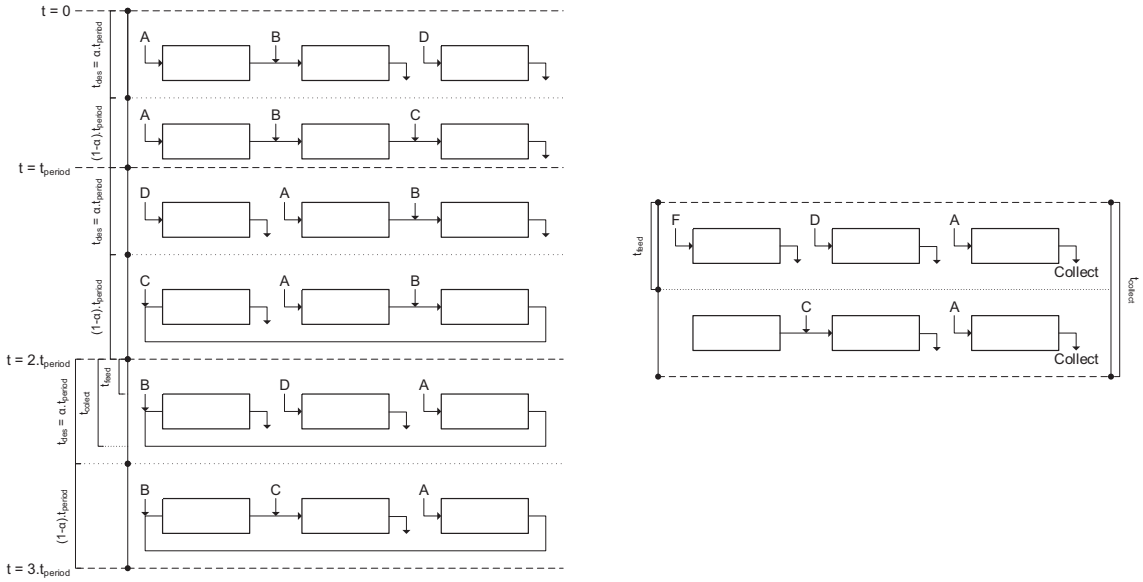

Figure 6.4: Cycle sequence chosen in the moving solvent-gradient implementation. The cycle depicted includes a desorption zone and injection in the 3rd period. The operating parameters are shown in Table 6.1.

Table 6.1: Operating parameters of the GSSR cycle. Second and third columns give, respectively, the blue dextran concentration, c_{Feed}, and the flow rate of the solvent line; solvent-gradient A increases c_A linearly from 0.24 g/L to 0.44g/L over every switching interval. Notation: N_C, number of columns; τ, switching interval; $\tau_{cyc} = N_C.\tau$, cycle time; t_{F} and Δt_{F}, position and duration of feed injection; t_{P} and Δt_{P}, position and duration of product collection; Δt_{D}, duration of desorption step.

	$(C_i - g/L)$	(mL/min)		(min)
Feed	0.00	0.5	τ	5.0
Solvent A	$0.24 - -0.44$	5.0	Δt_{D}	0.25τ
Solvent B	0.25	1.0	Δt_{F}	0.10τ
Solvent C	0.25	1.25	Δt_{P}	0.20τ
Solvent D	0.57	5.0	$t_{\mathrm{F}}, t_{\mathrm{P}}$	$2\tau/\tau_{\mathrm{cyc}}$

More realistic tests on the implementation of the moving solvent-gradient were performed on the pilot unit with three columns and a nonadsorbed tracer. The three chromatographic columns employed in these tests are Superformance 26-mm ID thermo-jacketed glass columns (Götec Labortechnik, Mühltal, Germany). Reversed-phase Source 30 RPC (30 μm particle size; GE Healthcare Amersham Biosciences, Uppsala, Sweden) was slurry packed into each column to a bed height of $L = 6$ cm with 5%-v/v ethanol/water at 25 ml/min, back-pressure of 30 bar, and 30 min packing time.

In these tests, changes in the solvent composition (say, changes in the water/ethanol ratio) were replaced by equivalent changes in the concentration of blue dextran

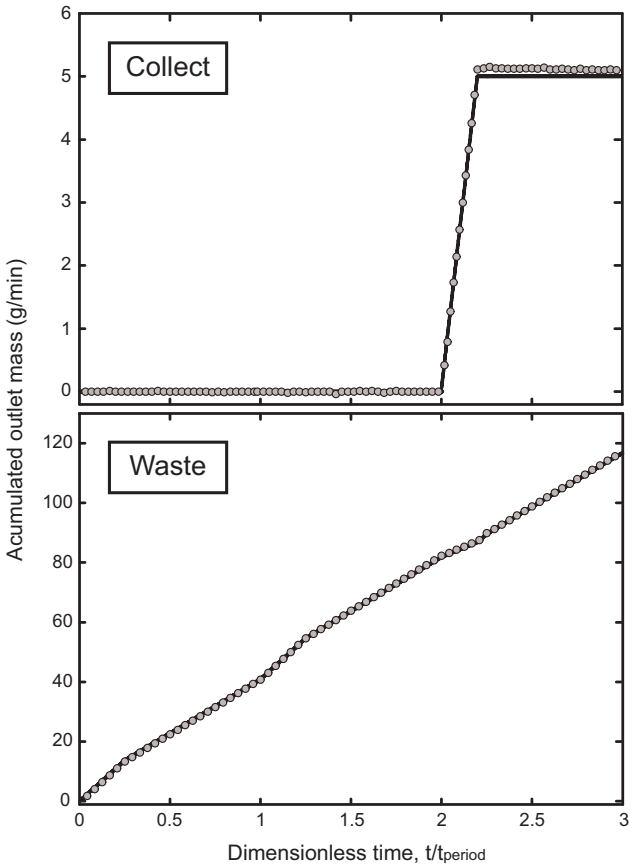

Figure 6.5: Accumulated mass from the product (top) and waste (bottom) outlets as function of elapsed time (t/τ) for one complete cycle of the GSSR process, with operating parameters defined in Table 6.1. Lines are the theoretical profiles and symbols the experimental data.

(BD) in an isocratic solvent. BD is a dextran polymer with an average molecule weight of 2×10^6. Its large molecular size prevents it from penetrating into the pore volume of the adsorbent particles; in practice, this tracer probes the interparticle void volume in the columns and extra-column dead volumes.

Figure 6.6 compares the BD's concentration profile measured by UV at the outlet of column 3 with the profile predicted by process simulation. In this tested GSSR cycle, feed is introduced into column 1 and product collected from column 3. The switching interval is $\tau = 5$ min and the feed (pure water) flow rate, $F = 0.5$ mL/min. The duration of the desorption zone is $\Delta t_{\mathrm{D}}/\tau = 0.25$; the instants, scaled by the cycle time, when feed is injected an the product is collected are the same and equal to $t_{\mathrm{F}}/\tau_{\mathrm{cyc}} = t_{\mathrm{P}}/\tau_{\mathrm{cyc}} = 0.667$ (beginning of the third switching interval); the duration of the feed pulse is $\Delta t_{\mathrm{F}} = 30$ s and the duration of the product withdrawal is $\Delta t_{\mathrm{P}} = 60$ s. The compositions and flow rates of the solvent lines are: solvent A1, 0.24 g/L, solvent A2, 0.44 g/L; $Q_{\mathrm{A1}} + Q_{\mathrm{A2}} = 5$ mL/min; solvent B, 0.25 g/L,

$Q_{\mathrm{B}} = 1$ mL/min; solvent C, 0.25 g/L, $Q_{\mathrm{C}} = 1.25$ gL/min; and solvent D, 0.57 g/L, $D = 5$ mL/min.

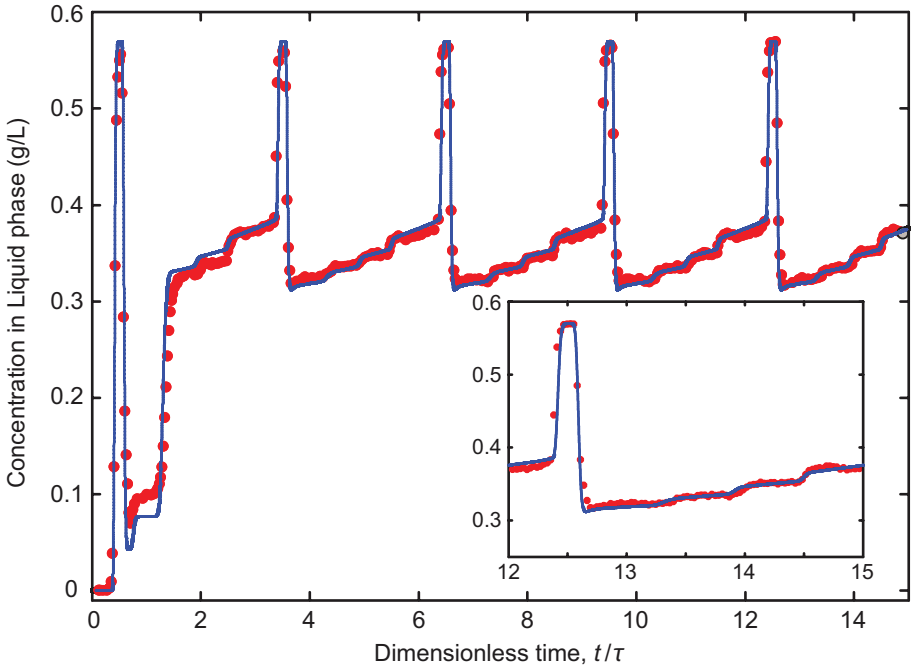

Figure 6.6: Temporal profile of blue dextran concentration at the outlet of column 3 for 5 cycles of a GSSR process. Lines are the theoretical predictions and symbols are the experimental UV data. The inset at lower-right zooms the profile for the 5th cycle.

The theoretical profile shown in Fig.6.6 was predicted by the GSSR model with interparticle porosity $\epsilon = 0.39$, intraparticle porosity $\epsilon_{\mathrm{p}} = 0$, and Péclet number $Pe = vL/D_{\mathrm{L}} = 700$, where v is the linear velocity of the fluid and D_{L} is the dispersion coefficient. The GSSR model was solved for $n_{\mathrm{c}} = 0$, since the solvent ($i = 0$) is the only component in the system (The default values $H_0' = 0$ and $n_0 = 0$ guarantee that it does not adsorb). The effect of dead volumes in the pilot unit was lumped into the value of ϵ; extra-column volumes represent roughly $100 \times (0.39 - 0.32) = 7\%$ of the volume of the packed beds. Figure 6.6 shows that there is good agreement between the experimental profile and the theoretical one. We can now tackle more confidently the difficult center-cut purification problem of the crude peptide mixture.

References

[1] Gary Walsh. Biopharmaceuticals: recent approvals and likely directions. *Trends in biotechnology*, 23(11):553–558, 2005.

[2] A Cecília A Roque, Christopher R Lowe, and M Ângela Taipa. Antibodies and genetically engineered related molecules: production and purification. *Biotechnology progress*, 20(3):639–654, 2004.

[3] R. Wooley, Z. Ma, and N.-H. L. Wang. A nine-zone simulating moving bed for the recovery of glucose and xylose from biomass hydrolyzate. *Industrial & Engineering Chemistry Research*, 37(9):3699–3709, 1998. doi: 10.1021/ie9800896.

[4] Phillip C. Wankat. Simulated moving bed cascades for ternary separations. *Industrial & Engineering Chemistry Research*, 40(26):6185–6193, 2001. doi: 10.1021/ie010075r.

[5] Alexandre Nicolaos, Laurence Muhr, Patrice Gotteland, Roger-Marc Nicoud, and Michel Bailly. Application of equilibrium theory to ternary moving bed configurations (four+ four, five+ four, eight and nine zones): I. linear case. *Journal of Chromatography A*, 908(1):71–86, 2001.

[6] Alexandre Nicolaos, Laurence Muhr, Patrice Gotteland, Roger-Marc Nicoud, and Michel Bailly. Application of the equilibrium theory to ternary moving bed configurations (4+ 4, 5+ 4, 8 and 9 zones): Ii. langmuir case. *Journal of Chromatography A*, 908(1):87–109, 2001.

[7] Anthony S. T. Chiang. Continuous chromatographic process based on smb technology. *AIChE Journal*, 44(8):1930–1932, 1998.

[8] Y. A. Beste and W. Arlt. Side-stream simulated moving-bed chromatography for multicomponent separation. *Chemical Engineering & Technology*, 25(10): 956–962, 2002.

[9] Jeung Kun Kim, Yifei Zang, and Phillip C Wankat. Single-cascade simulated

moving bed systems for the separation of ternary mixtures. *Industrial & engineering chemistry research*, 42(20):4849–4860, 2003.

[10] Stefanie Abel, Matthäus U Bäbler, Cordin Arpagaus, Marco Mazzotti, and Joachim Stadler. Two-fraction and three-fraction continuous simulated moving bed separation of nucleosides. *Journal of Chromatography A*, 1043(2): 201–210, 2004.

[11] Galatea Paredes, Stefanie Abel, Marco Mazzotti, Massimo Morbidelli, and Joachim Stadler. Analysis of a simulated moving bed operation for three-fraction separations (3f-smb). *Industrial & engineering chemistry research*, 43 (19):6157–6167, 2004.

[12] Weihua Jin and Phillip C Wankat. Two-zone smb process for binary separation. *Industrial & engineering chemistry research*, 44(5):1565–1575, 2005.

[13] Weihua Jin and Phillip C Wankat. Scaling rules and increasing feed rates in two-zone and four-zone simulated moving bed systems. *Industrial & engineering chemistry research*, 45(8):2793–2807, 2006.

[14] Rui CR Rodrigues, Tiago JSB Canhoto, João MM Araújo, and José PB Mota. Two-column simulated moving-bed process for binary separation. *Journal of Chromatography A*, 1180(1):42–52, 2008.

[15] Rui CR Rodrigues, Ricardo JS Silva, and José PB Mota. Streamlined, two-column, simulated countercurrent chromatography for binary separation. *Journal of Chromatography A*, 1217(20):3382–3391, 2010.

[16] João MM Araújo, Rui CR Rodrigues, Mário FJ Eusébio, and José PB Mota. Chiral separation by two-column, semi-continuous, open-loop simulated moving-bed chromatography. *Journal of Chromatography A*, 1217(33):5407–5419, 2010.

[17] Takayuki Masuda, Tohru Sonobe, Fumihiko Matsuda, and Masaharu Horie. Process for fractional separation of multi-component fluid mixture, March 30 1993. US Patent 5,198,120.

[18] Vera G Mata and Alírio E Rodrigues. Separation of ternary mixtures by pseudo-simulated moving bed chromatography. *Journal of Chromatography A*, 939(1):23–40, 2001.

[19] Eduardo A Borges da Silva and Alírio E Rodrigues. Design of chromatographic multicomponent separation by a pseudo-simulated moving bed. *AIChE journal*, 52(11):3794–3812, 2006.

[20] EA Borges da Silva and AE Rodrigues. Design methodology and performance analysis of a pseudo-simulated moving bed for ternary separation. *Separation Science and Technology*, 43(3):533–566, 2008.

[21] Jin Seok Hur and Phillip C Wankat. New design of simulated moving bed (smb) for ternary separations. *Industrial & engineering chemistry research*, 44 (6):1906–1913, 2005.

[22] Jin Seok Hur and Phillip C Wankat. Two-zone smb/chromatography for center-cut separation from ternary mixtures: Linear isotherm systems. *Industrial & engineering chemistry research*, 45(4):1426–1433, 2006.

[23] Lars Aumann, Michael Bavand, Thomas Müller-Späth, and Guido Ströhlein. Method for identification and purification of multi-specific polypeptides, March 15 2012. WO Patent App. PCT/EP2012/054,507.

[24] Guido Ströhlein, Lars Aumann, Marco Mazzotti, and Massimo Morbidelli. A continuous, counter-current multi-column chromatographic process incorporating modifier gradients for ternary separations. *Journal of Chromatography A*, 1126(1):338–346, 2006.

[25] Lars Aumann and Massimo Morbidelli. A continuous multicolumn countercurrent solvent gradient purification (mcsgp) process. *Biotechnology and bioengineering*, 98(5):1043–1055, 2007.

[26] Lars Aumann, Guido Stroehlein, and Massimo Morbidelli. Parametric study of a 6-column countercurrent solvent gradient purification (mcsgp) unit. *Biotechnology and bioengineering*, 98(5):1029–1042, 2007.

[27] Lars Aumann and Massimo Morbidelli. A semicontinuous 3-column countercurrent solvent gradient purification (mcsgp) process. *Biotechnology and bioengineering*, 99(3):728–733, 2008.

[28] Thomas Müller-Späth, Lars Aumann, Lena Melter, Guido Ströhlein, and Massimo Morbidelli. Chromatographic separation of three monoclonal antibody variants using multicolumn countercurrent solvent gradient purification (mcsgp). *Biotechnology and bioengineering*, 100(6):1166–1177, 2008.

[29] Eric Valery, Hector Osuna Sanchez, and Michel Bailly. Gradient-elution multi-column separation method, October 9 2009. WO Patent 2,009,122,281.

[30] Mário FJ Eusébio. Development of an universal interface for monitoring and control of chemical and biochemical processes, Ph.D. Thesis, Universidade Nova de Lisboa, 2006.

7

Gradient with Steady State Recycle process: Model-based analysis and experimental run

Proteins and peptides represent a growing sector in the pharmaceutical industry. Reversed-phase, high-performance liquid chromatography (RP-HPLC) has found wide use in the production of peptides for pharmaceutical formulations, due to its ability to provide high-resolution separation combined with good reproducibility. However, peptide mixtures can be complex, with significantly heterogeneous physico-chemical properties (including hydrophobic and highly hydrophilic compounds), thus rendering their efficient separation by RP-HPLC challenging [1]. Here, we demonstrate that the GSSR process is well suited for this task at preparative scale.

7.1 Materials and Methods

The selected packing material is Kromasil C18 (Eka Chemicals AB, Sweden), an octadecyl-bonded, reversed-phase silica, with high hydrophobicity, narrow pore size distribution (~ 100 Å), and very low content of metal impurities. Detrimental ionic interactions between basic peptides and residual ionized silanol groups in C18 phases often produce peak tailing [2, 3], which is undesirable when high

product purity is required; the Kromasil C18 phase has a high graft density and end-capping, and is therefore expected to exhibit a low silanol activity under the selected experimental conditions. The analytical experiments were performed with 5 μm Kromasil C18 purchased prepacked into a 0.46×15 cm column; the preparative experiments were performed with 25 μm Kromasil C18, packed into three 1×10 cm stainless steel columns by NOVASEP. The system was operated isothermally at 30°C.

The mobile phases used in this study are aqueous solutions of ethanol (EtOH) with a fixed residual amount of 0.1%-v/v terephthalic acid (TFA); the EtOH concentrations varied from 20% up to 50%-v/v. HPLC-grade EtOH and TFA were purchased from Panreac (Barcelona, Spain). The EtOH buffers were first prepared by diluting EtOH in deionized water, filtering through a 0.22-μm membrane, and adding TFA thereafter to prepare the final mobile phases. All solvents were degassed prior to use.

Figure 7.1 shows a chromatogram of the crude mixture for a 250 μL injection at 1 g/L into the Kromasil analytical column, eluted with water/ethanol/TFA (75/25/0.1, %-v/v) at 0.5 mL/min. The crude mixture is characterized by three main cuts: a weakly adsorbing (early eluting) cut containing three major impurities, an intermediate cut with the target product and at least four neighboring impurities, and a strongly adsorbing (late eluting) cut containing three impurities; the target product corresponds to the largest peak of the chromatogram, with roughly 50% of the total peak area. From the analysis of the chromatogram in Fig. 7.1, it is clear that the desired product is intermediate between nearby, weaker and stronger adsorbing impurities; a central cut is thus required to get the desired pure product.

7.2 Adsorption Equilibria

When dealing with the purification of a complex, multicomponent mixture, like the crude peptide mixture, it is convenient to minimize the number of solutes taken into consideration in the design procedure to make it numerically tractable. This is similar to the method often used in dealing with the design of distillation columns for the separation of petroleum fractions, where only a few selected key components are considered in the calculations. In the present case, five key components were selected: the most weakly adsorbed (earliest eluting) impurity ($i = 1$), the target product ($i = 3$) and its two closest impurities ($i = 2$ and $i = 4$), and the most strongly adsorbed (latest eluting) impurity ($i = 5$). The key components are

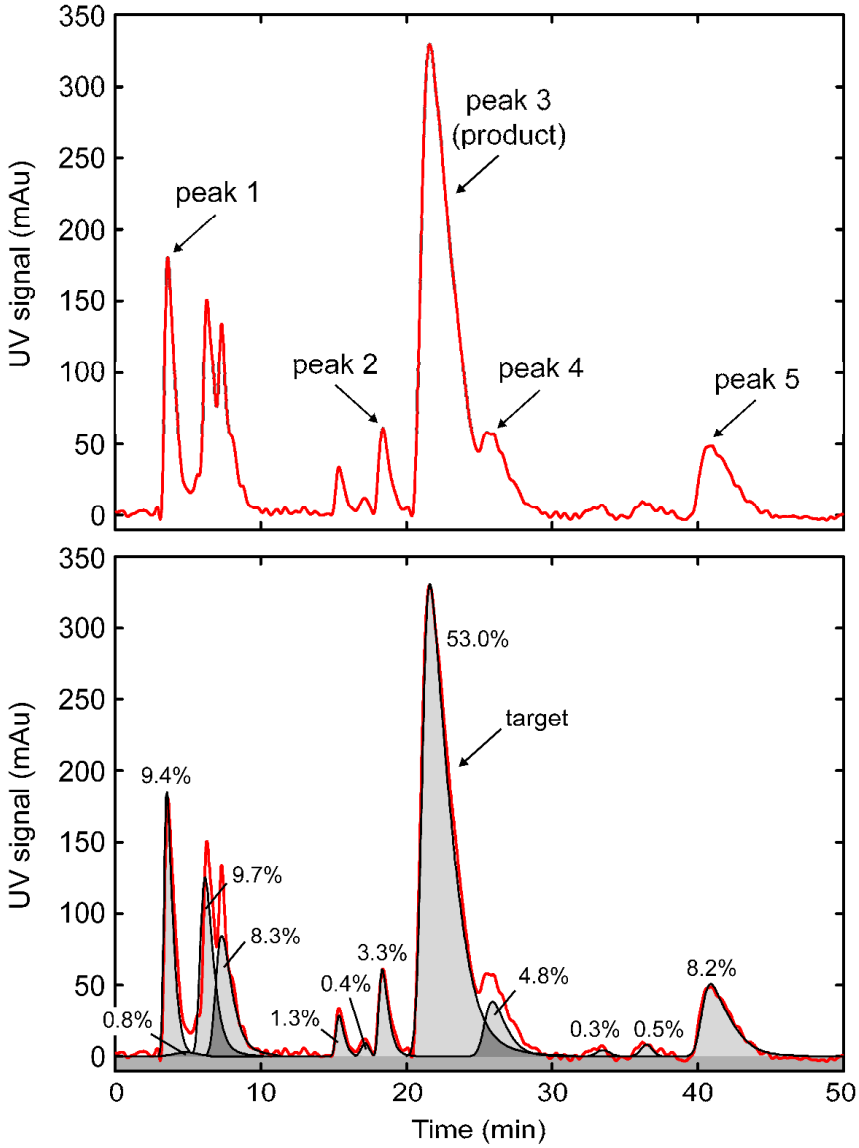

Figure 7.1: Peak deconvolution for an analytical chromatogram of the crude peptide mixture. Column: Kromasil C18, 5 μm, 100 Å, 0.46×15 cm; solvent: water/ethanol/TFA (75/25/0.1%-v/v); flow rate: 0.5 mL/min; concentration: 1 g/L; injected volume: 250 μL; detector: UV @ 220 nm.

identified by arrows pointing to their elution peaks in the analytical chromatogram of Fig. 7.1.

To determine the influence of the EtOH concentration, c_0, on the adsorption behavior of the peptide mixture, 250 μL pulses of the crude mixture at 1 g/L were injected into the analytical Kromasil column and eluted isocratically for various values of c_0; the flow rates in these experiments were in the range 0.3–0.6 mL/min (data not shown).

From the experimental chromatograms it is easy to determine the retention times

of the key components for each value of c_0. The retention time, t_i, for solute i, is related to the thermodynamic and elution parameters by

$$t_i = \frac{\epsilon + K_i}{Q/V}. \tag{7.1}$$

From the known value of t_i it is straightforward to determine the Henry's constant, K_i, or, more conveniently, the value of $\epsilon + K_i$:

$$\epsilon + K_i = \frac{t_i Q}{V}. \tag{7.2}$$

The calculated values of $\epsilon + K_i$ are listed in Table 7.1, where it is shown that for the least retained component, $\epsilon + K_1$ stabilizes at ≈ 0.61 as c_0 is increased.

Table 7.1: Values of $\epsilon + K_i$ for the key components of the peptide mixture, as a function EtOH concentration, c_0 (%-v/v), and their fitting to an expression of the form $K_i = K_i'/(c_0/100)^{n_i}$; data calculated from the retention times using Eq. 7.2.

	$\epsilon + K_i$				
c_0	Key component				
(%-v/v)	1	2	3	4	5
20	1.25	8.02	10.47	12.47	21.63
25	0.61	3.85	4.87	5.79	9.13
30	0.62	2.35	2.72	3.14	4.54
40	0.61	1.20	1.29	1.42	1.73
50	0.59	0.82	0.85	0.89	0.95
K_i'	8×10^{-7}	0.016	0.016	0.018	0.017
n_i	8.36	3.83	4.02	4.08	4.47

Since the value of ϵ [$= \epsilon_b + (1-\epsilon_b)\epsilon_p$] for a well-packed column chromatographic column is usually in the range 0.60–0.70, we take $\epsilon = 0.61$ and assume that for practical purposes the least retained solute does not adsorb for large values of c_0; this allows us to calculate the values of K_i [$= (1-\epsilon_b)H_i$] for all the key components.

The dependence of each K_i on c_0 was fitted to a function of the type $K_i = K_i'/c_0^{n_i}$, which is identical to the one used in the development of Eq. (7.5); the fitted values of K_i' and n_i are listed in the two bottom lines of Table 7.1.

The fitted curves are directly compared with the experimental data in Fig. 7.2, which shows that the dependence of K_i on c_0 is well described by an equation of the form $K_i = K_i'/c_0^{n_i}$.

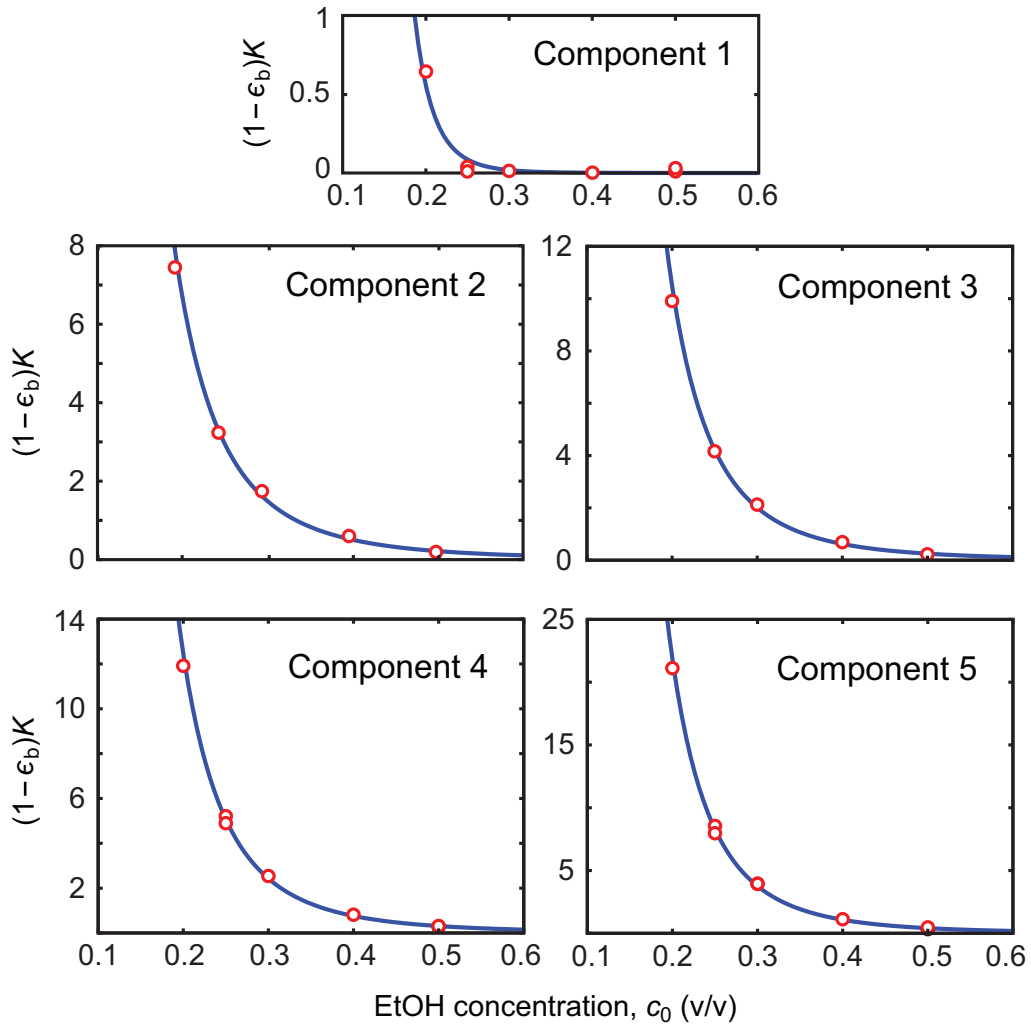

Figure 7.2: Henry constants, $K_i = (1 - \epsilon_b)H_i$, for the key components of the peptide mixture, as a function of EtOH concentration, c_0 (%-v/v). Symbols are experimental data and lines are plots of $K_i'/c_0^{n_i}$ with parameters taken from Table 7.1

To stress the difficulty of the peptide separation problem, the Henry constant of the target peptide ($i = 3$) and those of its two closest impurities ($i = 2$ and $i = 4$) are plotted against c_0 in Fig. 7.3 for comparison. When the K-curves are plotted together and compared, it is seen that the retention factors of the two impurities are very close to that of the target peptide. This makes the purification of the target peptide a difficult separation problem and, thus, a good case study for the GSSR process. Note also that the selectivities, $\alpha_{ij} = K_j/K_i = (H_j/H_i)c_0^{n_i - n_j}$, for the pair combinations (i, j) of the three solutes are weakly dependent on c_0 because $n_i - n_j \approx 0$. Thus, the solvent gradient must be properly placed along the three columns to effectively help at accomplishing the separation.

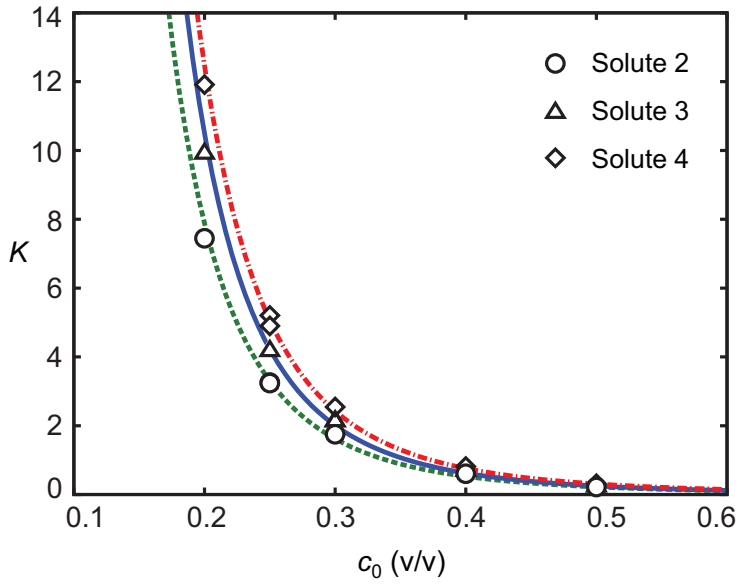

Figure 7.3: Henry constants, $K_i = (1 - \epsilon_b)H_i$, for the target peptide ($i = 2$) and its two closest impurities ($i = 2$ and $i = 3$), as a function of EtOH concentration, c_0 (%-v/v). Symbols are experimental data and lines are plots of $K_i'/c_0^{n_i}$ with parameters taken from Table 7.1.

7.3 Model-based analysis tools

For the sake of simplicity, we shall employ a linear adsorption model to help explain the operation of the GSSR process for the purification of the peptide crude mixture. A comprehensive, numerical study of the GSSR process, based on a more realistic multicomponent adsorption model of the peptide mixture, will be reported elsewhere.

The adsorption equilibrium of the competing solutes is the basis for the design or optimization of any chromatographic process governed by the thermodynamics of adsorption; this is the case of the peptide mixture on the 25 μm Kromasil C18 phase for the working range of linear velocities used in the preparative experiments. Mass transfer and axial dispersion certainly influence the composition fronts, by smearing the concentration profiles, but do not change their stoichiometric positions when the process is not limited by the adsorption kinetics. If the adsorption isotherms are known, suitable operating conditions can be determined through the application of design rules, such as those developed for the SMB process [4], or by computer-aided optimization. A short-cut method for designing the GSSR cycle is presented below.

7.3.1 Chromatographic column model

Under linear adsorption conditions, the equilibrium adsorbed concentrations can be expressed as

$$q_i = (\epsilon_\mathrm{p} + H_i)c_i, \tag{7.3}$$

where i is the solute index; c, the concentration in the liquid phase; q, the adsorbed concentration per unit volume of stationary phase; ϵ_p, the intraparticle porosity; and H, the Henry's constant. Henceforth index $i = 0$ shall denote the solvent modifier (EtOH) and $i = 1, \ldots, n_\mathrm{c}$, the n_c components of the peptide mixture.

The Henry's constant is strongly affected by the solvent composition; examples of expressions often used in the literature to model the dependence of H_i on c_0 are [5–7]

$$H_i = H_i'/c_0^{n_i} \quad \text{and} \quad H_i = H_i'/e^{n_i c_0}, \tag{7.4}$$

where H_i' and n_i are adjustable parameters.

For simplicity, we use the equilibrium-dispersed model for describing the dynamics of each chromatographic column [8]. If the dependence of H_i on c_0 is given by $H_i = H_i'/c_0^{n_i}$, the equilibrium-dispersed model can be written as

$$\left(\epsilon + \frac{V_\mathrm{e}}{V}\right)\frac{\partial c_i}{\partial t} + K_i\left(\frac{\partial c_i}{\partial t} - \frac{n_i c_i}{c_0}\frac{\partial c_0}{\partial t}\right) = \frac{Q}{V}\left(\frac{h_i}{2}\frac{\partial^2 c_i}{\partial x^2} - \frac{\partial c_i}{\partial x}\right), \quad \forall\, x \in]0,1[, \tag{7.5}$$

with boundary conditions

$$c_i - \frac{h_i}{2}\frac{\partial c_i}{\partial x} = c_i^\mathrm{in} \quad \text{for} \quad x = 0, \tag{7.6}$$

$$\frac{\partial c_i}{\partial x} = 0 \quad \text{for} \quad x = 1. \tag{7.7}$$

In these equations, $\epsilon = \epsilon_\mathrm{b} + (1-\epsilon_\mathrm{b})\epsilon_\mathrm{p}$ is the total bed porosity (ϵ_b is the interparticle void fraction); $K_i = (1-\epsilon_\mathrm{b})H_i$, the Henry's constant expressed per unit volume of column; t, the time coordinate; $x = z/L$, the dimensionless axial coordinate along the column; L and V, the length and volume of the column; V_e is the extra dead volume per column; Q, the flow rate through the column; h, the dimensionless plate height; and c^in, the solute concentration in the inlet effluent. The left-hand side of Eq. (7.5) is the expansion of $\epsilon_\mathrm{b}(\partial c_i/\partial t) + (1-\epsilon_\mathrm{b})(\partial q_i/\partial t)$. Note that for $i = 0$ (EtOH in the solvent), we have set $H_0' = 0$ and $n_0 = 0$.

The dimensionless plate height, h_i, governing band broadening for the ith component, can be expressed as [9]

$$\frac{h_i}{2} = \frac{1}{Pe} + \alpha_i \frac{Q}{V} + \gamma_i \frac{V}{Q}, \tag{7.8}$$

where

$$\alpha_i = \frac{\epsilon - \epsilon_\mathrm{b} + K_i}{k_i(\epsilon + K_i)^2}, \quad \gamma_i = \frac{\epsilon_\mathrm{b} D_{i\mathrm{m}}}{\alpha_\mathrm{b} L^2}. \tag{7.9}$$

Here, $Pe = vL/D_\mathrm{L}$ is the hydrodynamic Péclet number ($D_\mathrm{L} \propto d_\mathrm{p} v$ is the hydrodynamic dispersion coefficient and d_p the particle diameter); $k \propto d_\mathrm{p}^{-2}$, the linear-driving-force coefficient for lumped solid-diffusion mass transfer (including film diffusion); D_m, the molecular diffusion coefficient; and $\alpha_\mathrm{b} \approx 3$, the tortuosity factor of the packed bed. Note that γ measures the effect of bulk molecular diffusion on band broadening.

The $1+Q+Q^{-1}$ dependence of h in Eq. (7.8) gives the well-known van Deemter plot [8]. In the working range of linear velocity used in our preparative experiments, the γ's are negligible and Eq. (7.8) can be simplified to a linear relation between h and Q, because Pe is roughly constant and the α's are only weakly dependent on Q. For computational convenience, however, the γ's are assigned a small, but realistic value, in order to keep the boundary condition in Eq. (7.6) valid when $Q = 0$, i.e., when the flow through a column is halted.

7.3.2 Dynamic process model

The GSSR process's model is obtained by assembling N instances of the chromatographic column model, one for each of the N columns, and linking them through appropriate material balances written for the inlet nodes of the columns.

The node balances at each column inlet are written in a way that mimics our experimental implementation of the GSSR process. Binary variables (i.e., variables that can only take the values 0 or 1) are introduced to define the state of the two-way valves installed in the pilot unit (Fig. 6.3); if the variable is equal to 0, the valve is closed; if it is equal to 1, the valve is open.

The material balances on the flow rates at the N column inlets are

$$Q_1 = (1 - v_N^{\mathrm{W}} - v^{\mathrm{P}})Q_N + \sum_{s \in \mathcal{S}} v_1^s Q_s + v^{\mathrm{F}} F, \tag{7.10}$$

$$Q_j = (1 - v_{j-1}^{\mathrm{W}})Q_{j-1} + \sum_{s \in \mathcal{S}} v_j^s Q_s \quad (j = 2, \ldots, N), \tag{7.11}$$

where $\mathcal{S} = \{\mathrm{A}, \ldots, \mathrm{D}\}$ represents the train of solvents; the v's, the states of the corresponding two-way valves depicted in Fig. 6.3; Q_j, the volumetric flow rate through column j; Q_s, the flow rate of solvent s; and F, the feed flow rate. We recall that for our pilot unit, $N = 3$.

The balance for column 1 is different from the other two balances, because its inlet is connected to the feed line, and because the outlet of its upstream neighboring column (i.e., column 3) is connected to the product line. Note also that Eq. (7.10) is written under the assumption that v_N^{W} and v^{P} are never both set to 1 at the same time, because it is physically impossible to simultaneously collect waste and product from the same column outlet. To obtain a more robust mathematical balance, it suffices to replace $(1 - v_N^{\mathrm{W}} - v^{\mathrm{P}})$ by $(1 - \max\{v_N^{\mathrm{W}}, v^{\mathrm{P}}\})$.

The component material balances at the column inlets can be written a

$$(Qc_i^{\mathrm{in}})_1 = (1 - v_N^{\mathrm{W}} - v^{\mathrm{P}})(Qc_i^{\mathrm{out}})_N + \sum_{s \in \mathcal{S}} v_1^s Q_s c_i^s + v^{\mathrm{F}} F c_i^{\mathrm{F}}, \tag{7.12}$$

$$(Qc_i^{\mathrm{in}})_j = (1 - v_{j-1}^{\mathrm{W}})(Qc_i^{\mathrm{out}})_{j-1} + \sum_{s \in \mathcal{S}} v_j^s Q_s c_i^s \quad (j = 2, 3), \tag{7.13}$$

where c_{ij}^{in} and c_{ij}^{out} are the concentrations of component i at the upstream and downstream ends of column j, respectively; c_i^s, the concentration in solvent s; and c_i^{F}, the concentration in the feed.

Note that in Eqs. (7.12) and (7.13), i runs over the set of solutes and the solvent modifier ($i = 0$). Obviously, $c_i^s = 0$ for $i > 0$ and $s \in \{\mathrm{A}, \ldots, \mathrm{D}\}$ because the peptide mixture is not injected into the system via the train of solvents. The c_i^{F}, on the other hand, are different from zero for $i > 0$, because they define the feedstock composition; moreover, c_0^{F} defines the modifier concentration in the feed. The concentrations c_0^s for $s \in \{\mathrm{B}, \ldots, \mathrm{D}\}$ are constant (i.e., time independent), because they define the modifier concentrations in the isocratic solvents; but the modifier concentration, c_0^{A}, in the solvent-gradient line, A, is time variable according to piecewise-linear periodic profile given by Eq. (6.1).

7.3.3 Numerical solution

The GSSR's dynamic process model was solved using two different numerical solution strategies. In one case the model equations were solved directly for cyclic steady state (CSS) conditions to get the GSSR's steady periodic solution. To this end, each instance of the chromatographic column model—one for each column—was discretized both in time, $t \in [0, N\tau]$, and in the spatial coordinate, $z \in [0, 1]$, and the GSSR's CSS condition

$$c_{ij}(t + N\tau, z) = c_{ij}(t, z) \quad \forall\, z \in [0, 1] \tag{7.14}$$

was directly applied at $t = 0$ [this gives $c_{ij}(N\tau, z) = c_{ij}(0, z)$]. This full-discretization approach gives rise to a large sparse system of nonlinear equations that can be solved using a suitable solver.

Note that the GSSR's CSS condition is different from the CSS condition for multi-column, simulated counter-current adsorption processes [10–13]:

$$c_{i,j+1}(t + \tau, z) = c_{ij}(t, z). \tag{7.15}$$

This is because the GSSR's feed inlet and product outlet lines are attached to fixed columns and, therefore, do not advance their position by one column at the end of every switching interval as all other lines do.

The method above provides the steady periodic solution, but not the initial transient cycles until the CSS is attained, starting, e.g., from a clean system, nor the path followed by the process between two steady periodic states because of a change in an operating parameter. To determine the GSSR's cycle-to-cycle dynamics we employed a standard method-of-lines approach: the model was discretized in the spatial coordinate, $z \in [0, 1]$, to obtain a sparse system of differential-algebraic equations (DAE) for which robust and computationally efficient software is widely available to generate a numerical solution along the time coordinate.

7.3.4 GSSR cycle for purification of the peptide mixture

The GSSR cycle for the purification of the crude peptide mixture consists of a standard cycle with a desorption step ($\Delta t_{\mathrm{D}} > 0$), in which the feed and production steps start at the beginning of the third switching interval ($t_{\mathrm{F}} = t_{\mathrm{P}} = 2\tau$); this cycle is quite similar to the one tested with the blue dextran tracer.

Shortcut design procedure

The design procedure for a chromatographic process should not be too complicated or tedious, nor should it be time consuming, otherwise the process will be of limited use in industrial practice. Here, we briefly describe a simple shortcut procedure for designing a GSSR cycle, which is based only on the retention times of the key components.

The EtOH concentration in the solvents is restricted to the range 25–50% v/v; over this working range, the values of $\epsilon + K$ for the target peptide and its two closest impurities decrease by roughly 80%, thus giving a good extent of variation of the retention times. For simplicity, the EtOH concentrations in solvents B and C are fixed at 25% v/v and that in the stronger solvent D at 50% v/v. The gradient is applied somewhere in between these two values. The train of solvents are handled with only two solvent storage tanks: one with 25% v/v EtOH and the other with 50%. The solvent gradient (solvent line A) is built from the admixture of different amounts of solvent drawn from the two tanks.

Given that the HPLC pumps have 10 mL heads, we design the system with external flow rates of roughly 1–5 mL/min and a maximum internal flow rate around 8 mL/min, which for the GSSR cycle is given by $Q_{\mathrm{A}} + Q_{\mathrm{B}} + Q_{\mathrm{C}}$. Solvent A is responsible for doing most the separation, whereas the purpose of solvents B and C is to restrain the width of the central cut by adding a little more retention to the side parts of the target peak that are recycled. The mixed cut with the leading edge of the target peptide is diluted with solvent C during recycling (step *d* of Fig. 6.1), whereas the mixed cut with the trailing edge is diluted with solvent B (step *f* of Fig. 6.1). Thus solvent C should have a somewhat higher flow rate than solvent B, because the leading mixed cut is less retentive than the trailing one. If the flow rates of the isocratic solvents are fixed at $Q_{\mathrm{B}} = 1$ mL/min and $Q_{\mathrm{C}} = 1.25$ mL/min, the flow rate of the solvent gradient should be $Q_{\mathrm{A}} \approx 5.7$ mL/min to give a maximum internal flow rate of 8 mL/min.

The cycle time is fixed at ca. 10 min; this gives $\tau = 3 + 1/3$ min, which we round up to 3.5 min. We want the central cut to move from one column to the next over the duration of a switching interval by the injection of the solvent gradient. To achieve this, the retention time of the target solute in one column should be equal to the switching interval, i.e.,

$$[\epsilon + K_3(\bar{c}_0)]V + V_{\mathrm{e}} = Q_{\mathrm{A}}\tau. \tag{7.16}$$

Here, V is the column volume; V_{e}, the extra dead volume per column; K_3, the

Henry constant of the target peak; and $\bar{c}_0$, the EtOH concentration at which the gradient is centered around. Solving for $\bar{c}_0$ gives 34.0% v/v. Thus, working with 34%-v/v EtOH in the solvent will induce a retention time of the target peptide per column equal to the switching interval. By applying the same procedure to the two closest impurities, gives 32.4% v/v for the less retained one and 35.4% for the more retained. So as a first approximation, a total gradient from 32.4% to 35.4% v/v is to be expected.

Complete elution of the most retained impurity at 5 mL/min with solvent D (50%-v/v EtOH) gives $\Delta t_{\mathrm{D}} \approx 1.5$ min. The feedstock is diluted in 25%-v/v EtOH solvent at $c^{\mathrm{F}} = 0.53$ g/L, and 1 mL of feed solution is injected per cycle, which gives a feed pulse of $\Delta t_{\mathrm{F}} = 0.5$ min at $F = 2$ mL/min. This feed concentration is in the linear response range of the UV detector, well below its saturation limit. The width of the central cut, as measured by the positions of the two closest impurities, is about 1/3 of a column length; using an expression similar to Eq. 7.16, but with its l.-h.-s. multiplied by 0.33 and τ replaced by Δt_{P}, gives a collection time of about 1.1 min that we round down to $\Delta t_{\mathrm{P}} = 1$ min in order to introduce a small safety margin.

The set of operating parameters are summarized in Table 7.2 and were found to be adequate for exploratory experiments with the GSSR pilot unit.

Table 7.2: Operating parameters of the GSSR cycle. Second and third columns give, respectively, the EtOH concentration, c_0, and the flow rate of the solvent line; solvent-gradient A increases c_0 linearly from 32.4% to 35.4% v/v over every switching interval. Notation: τ, switching interval; t_{F} and Δt_{F}, position and duration of feed injection; t_{P} and Δt_{P}, position and duration of product collection; Δt_{D}, duration of desorption step.

	(%-v/v)	(mL/min)		(min)
Feed	0.25	2.0	τ	3.5
Solvent A	0.324–0.354	5.7	Δt_{D}	1.5
Solvent B	0.25	1.0	Δt_{F}	0.5
Solvent C	0.25	1.25	Δt_{P}	1.0
Solvent D	0.50	5.0	$t_{\mathrm{F}}, t_{\mathrm{P}}$	7.0

7.3.5 Step sequencing

To determine the sequencing of the inlet/outlet lines for the selected GSSR cycle, we resort to the schematics in Figs. 6.1 and 6.2. During the first two switching intervals of the cycle the train of solvents is unaffected by the feed and production steps, because these steps occur during the third switching interval. Thus, the

chronograms of port switching for the first two switching intervals of the cycle are taken directly from steps *a*–*d* in Fig. 6.1.

The feed and production steps start at the beginning of the third switching interval, but it must be noted that the production step is longer than the feed step ($\Delta t_{\mathrm{P}} > \Delta t_{\mathrm{F}}$); moreover, both steps occur while the desorption step is performed on the third column, because $\Delta t_{\mathrm{D}} > \max(\Delta t_{\mathrm{F}}, \Delta t_{\mathrm{P}})$. Thus, the third switching interval starts with the two bottom steps of Fig. 6.2; the duration of the first step is Δt_{F} and that of the second is $\Delta t_{\mathrm{P}} - \Delta t_{\mathrm{F}}$. Finally, the cycle ends with the sequencing of the solvent lines given by steps *e* and *f* of Fig. 6.1; but note that step *e* takes $\Delta t_{\mathrm{D}} - \Delta t_{\mathrm{P}}$ and is followed by step *f* for the remaining $\tau - \Delta t_{\mathrm{D}}$ of the switching interval.

7.3.6 Simulated cycle

The full GSSR cycle is shown in Fig. 7.4, along with snapshots of the simulated axial concentration profiles in the three columns taken at selected instants of the cycle when switching between some of the steps. For a better visualization, the concentration profiles have been scaled by the corresponding concentrations in the feed; this has the effect of magnifying the profiles for the impurities, which would, otherwise, be difficult to discern for some steps of the cycle. The axial solvent composition profile is represented by the dashed lines on a secondary y-axis with a linear scale ranging from 25% to 50%-v/v EtOH. The duration of each step of the cycle is given at the left of the corresponding flow diagram; thus the first step takes Δt_{D} time units, the second step takes $\tau - \Delta t_{\mathrm{D}}$ time units, and so forth.

Fresh feedstock fluid is injected into the upstream end of column 1 at the start of the third switching interval, while at the same time the target peptide contained in the feed pulse injected in the previous cycle is obtained in purified form at the downstream end of column 3. This way, each pulse of feed injected per cycle is forced to travel over the entire length of the system to get maximum separation between neighbor peaks.

Product withdrawal starts after the recycle of solute 2 and of the cut in which it is mixed with the leading edge of the product. The product collecting step continues until breakthrough of the target peptide's slower neighbor impurity. After product collection, the impure cut containing the trailing edge of the target peptide mixed with its slower neighbor impurity is recycled to the upstream end of column 1. Ideally, this cut should be injected into the upstream end of column 1 right after the injection of feed. To achieve this, and since the product collecting step is

longer than the feed step, the feed column (i.e., column 1) is frozen during the last $\Delta t_{\mathrm{P}} - \Delta t_{\mathrm{F}}$ time units of product collection to wait for the recycled cut.

The more weakly adsorbed impurity is pushed into column 2 during the third switching interval and then purged out of the system during the first switching interval of the following cycle. The most weakly adsorbed impurity is taken out of the system through column 2 during the last step of the cycle and the first step of the following cycle (these two steps are contiguous in time). The most strongly adsorbed impurity, which is the slowest traveling species in the system, is purged out of the system mostly during the strong desorption step applied to column 2, but with a delay of one cycle. The product's slower neighbor impurity is discarded from the system in three waste cuts taken from the three columns; the product's faster neighbor impurity is taken out of the system through columns 2 and 3.

7.3.7 Choice of manipulated variable for tuning the process

Whatever procedure is employed for process design, even a computer-aided one based on a detailed process model, it is always necessary to dynamically adjust some of the operating parameters during process operation to compensate for deviations from the target purity arising from imperfect design and experimental variability.

The switching interval, τ, was selected as manipulated variable for dynamically adjusting the GSSR process. The efficacy of this choice was verified by a parametric and sensitivity analysis of the process using the model-based tools described above, and is in line with methods proposed by some authors for controlling the SMB process [14].

Figure 7.5 shows an experimental study of the effect of τ on the UV signal at the outlet of column 3—the one from which product is collected—over a full GSSR cycle. The purified product cut is clearly identified by a broad peak in the UV signal. For $\tau = 2.61$ min the purified product exits column 3 after the collection has taken place, whereas for $\tau = 4.21$ min the purified cut exits column 3 before being diverted for product collection; for $\tau = 3.5$ min, the product peak seems to be well positioned with respect to the collecting interval, as can be seen by the simulated composition profiles which have been superposed on the experimental graphic.

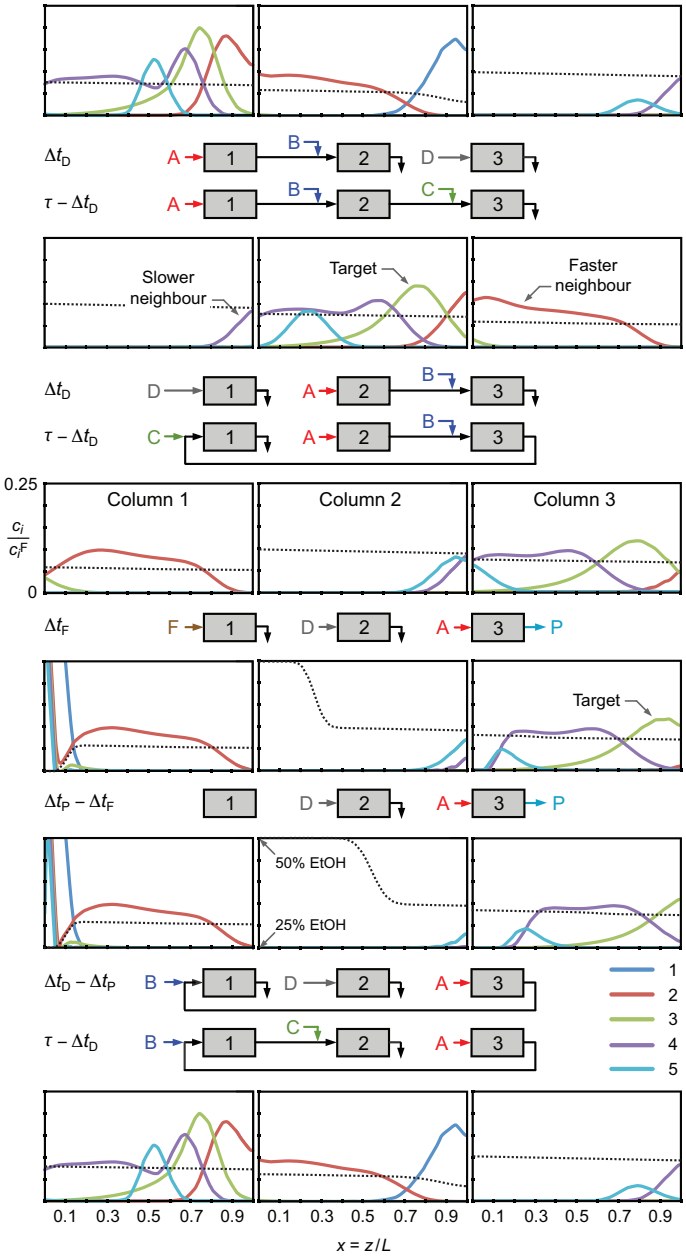

Figure 7.4: GSSR cycle for purification of the peptide mixture and snapshots of the simulated axial concentration profiles taken at selected instants of the cycle. The dashed lines represent the EtOH axial concentration profiles (%-v/v). The operating parameters are listed in Table 7.2.

7.4 Experimental GSSR run

As an experimental proof of concept of the GSSR process, the pilot unit was operated over a long period of time—30 full cycles—in order to attain the cyclic steady state conditions and to assess the reproducibility and stability of the pilot unit over a long period of operation.

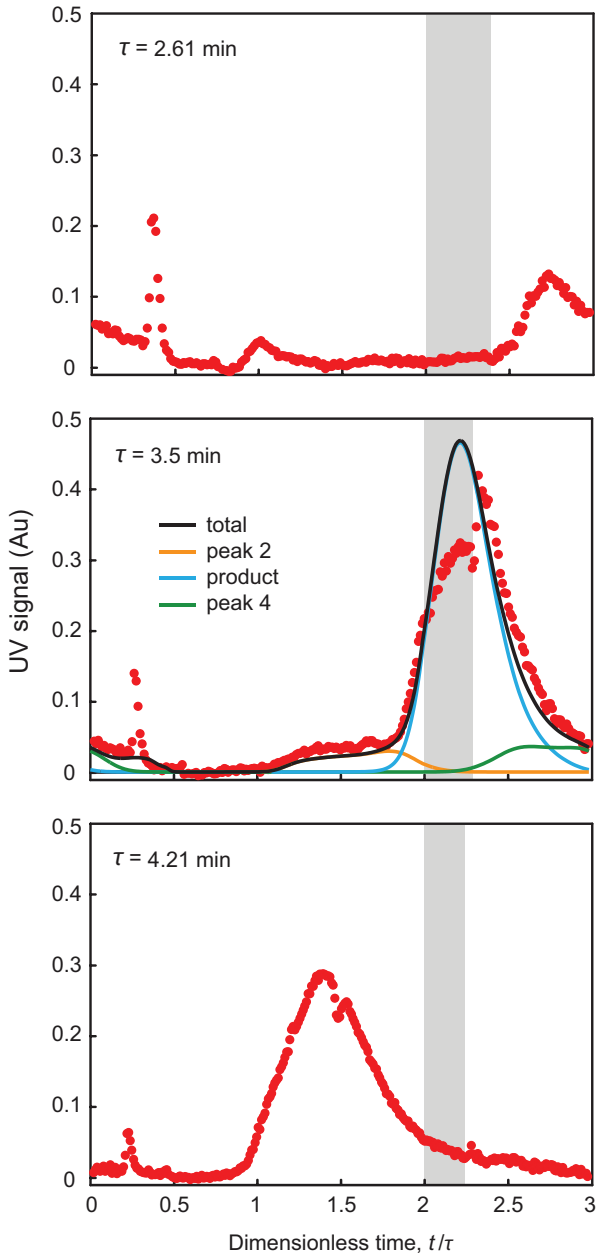

Figure 7.5: Effect of the switching interval, τ, on the elution time of the main product peak at the outlet of the column where the product fraction is collected. The experiment started with $\tau = 3$ min and then its value was changed every three cycles to one of the values shown in the graphics; the sequence was from top to bottom. Each graph shows the experimental UV profile at the column outlet before changing the value of τ. The gray area shows the time interval for product collection. The lines for $\tau = 3.5$ min are the simulated concentration profiles of the central key components of the peptide mixture (the product and its two nearest impurities); the black line is the simulated total concentration profile.

Figure 7.6 shows the temporal UV profile at the outlet of the third column for the 30-cycle GSSR experiment; in this figure the time scale is made dimensionless by dividing the process time by the value of the switching interval, τ; with this time

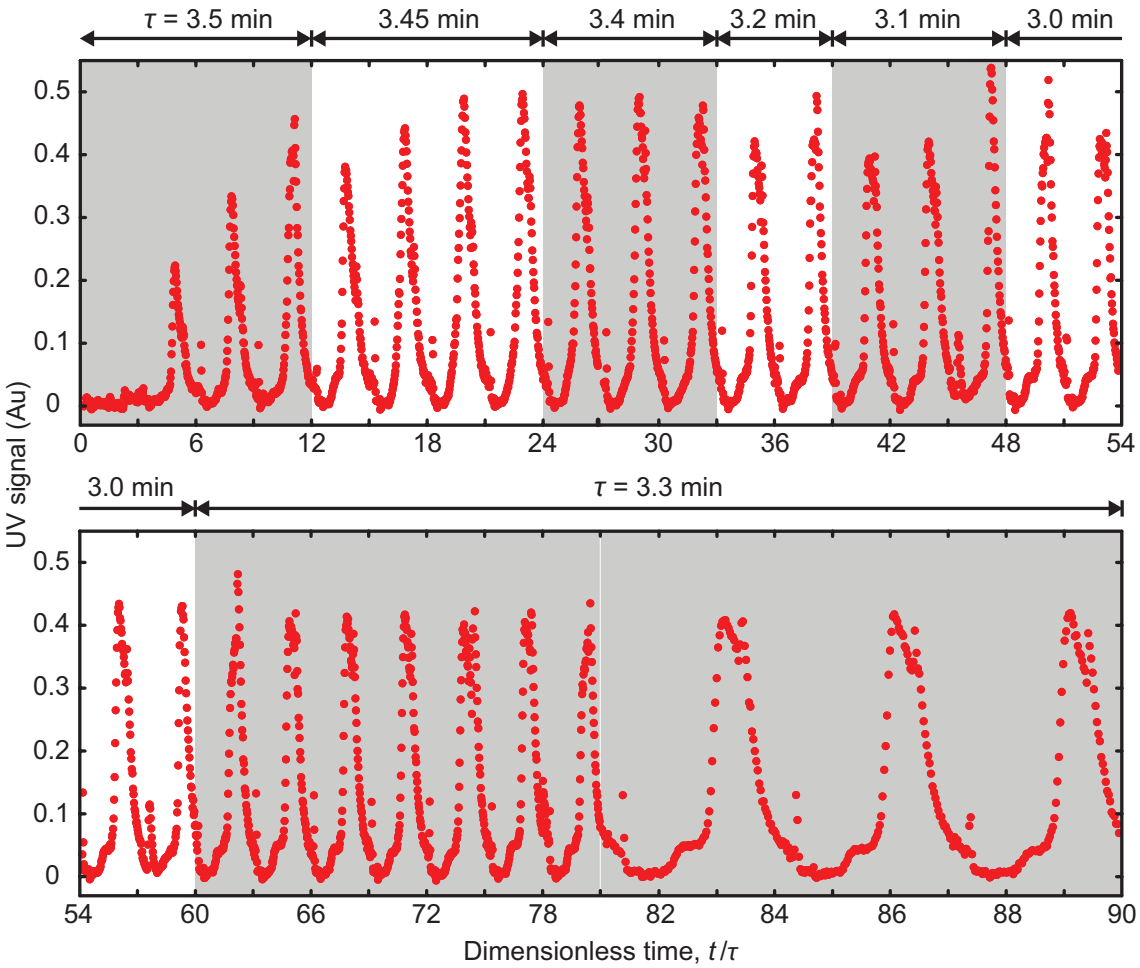

Figure 7.6: Temporal profile of the UV signal measured at the outlet of column 3 for the 30-cycle GSSR experiment.

scaling, a complete GSSR cycle takes three dimensionless time units, and the cycles start at $t/\tau = 0, 3, 6, 9$, and so forth.

As discussed above, τ was employed as a manipulated variable to adjust the relative position of the moving composition profile in the GSSR loop with respect to the outlet ports. The switching interval was initially set at $\tau = 3.5$ min. However, while monitoring the UV signal at the outlet of the third column, and using as a guide the position of the product peak with respect to the time frame for product collecting, the value of τ was ultimately decreased to 3.3 min; this action corrected the relative position of the moving composition profile in the GSSR loop.

The value of τ for each cycle is shown at the top of Fig. 7.6. The value of τ was initially set to 3.5 min over the first 4 cycles, but was then adjusted to 3.45 min over the following 4 cycles in an attempt to move the collected product fraction to the correct position. Based on the elution time of the product peak at the outlet

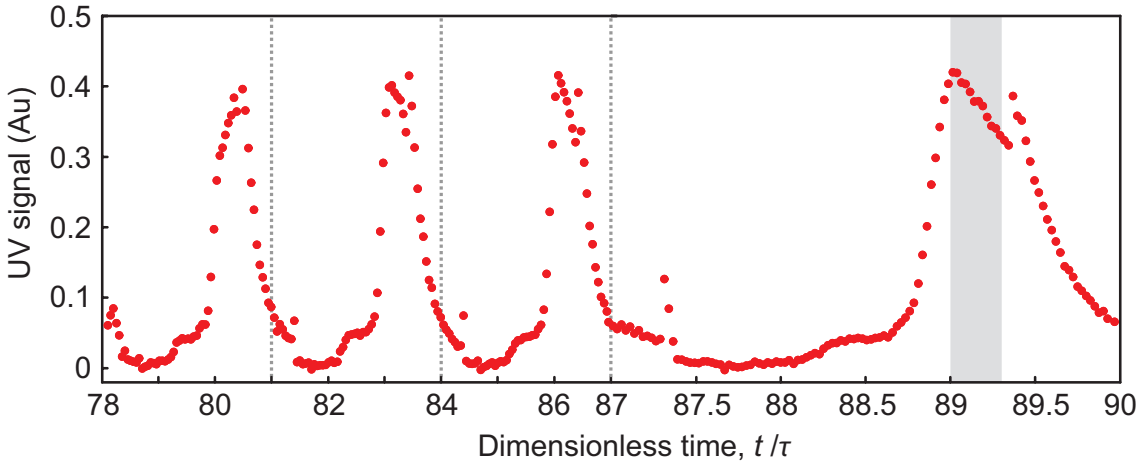

Figure 7.7: Temporal profile of the UV signal measured at the outlet of column 3 for the last four cycles of the 30-cycle GSSR experiment. The time scale for the 30th cycle is expanded to improve visual clarity. The grayed area shows the time interval during which product was collected in the 30th cycle.

of column 3, the initial reduction of τ to 3.45 min was found to be insufficient, so its value was further reduced to 3.4 min over the following 3 cycles, then changed to 3.2 min over another 3 cycles, further reduced to 3.1 min for another 3 cycles, and finally settled at 3.0 min for another 4 cycles. The elution times of the main product peak at the outlet of column 3 for values of τ equal to 3.0, 3.1, 3.2 and 3.4 min were fitted to a third-order polynomial, from which the optimum value of τ was determined to be ≈ 3.3 min. This value of τ was kept fixed over the last 16 cycles of operation.

Figure 7.7 shows the temporal UV profile at the outlet of column 3 for the last four cycles of the 30-cycle GSSR run, i.e., cycles 27 through 30. The time coordinate is scaled by the value of the switching interval and expanded for the 30th cycle for better visualization. The grayed rectangle shows the interval during which product is collected in the last cycle of the run; the peak in the UV signal appears to be well positioned by reference to Fig. 7.5.

Figure 7.8 shows the HPLC analysis of the product fraction collected over the 30th cycle; the analytical chromatogram of the product cut demonstrates that the product purity obtained experimentally meets the value originally aimed at, i.e., $pur_p \geq 98\%$. Actually, it is visually difficult to discern the existence of any trace of the faster neighbor impurity in the chromatogram of Fig. 7.8; however, our peak fitting procedure detects a small amount of impurity within the scatter of the UV signal's baseline, which is why we do not report 100% purity for the collected product fraction.

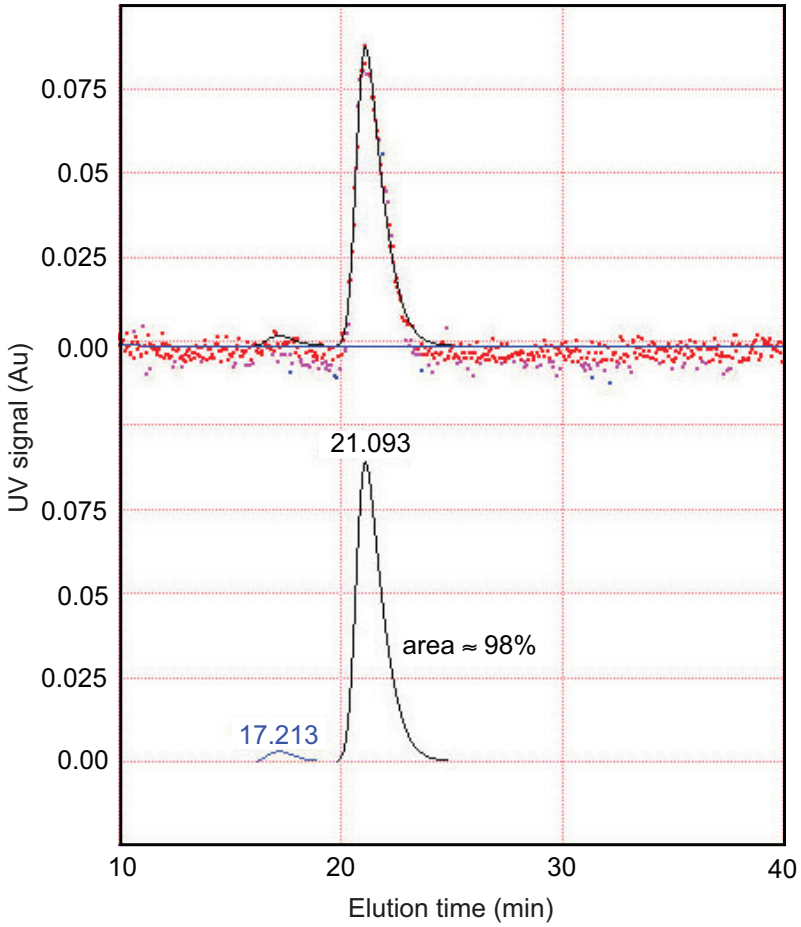

Figure 7.8: HPLC analysis of the product fraction collected during the last cycle of the 30-cycle GSSR experiment of Fig. 7.6.

Purity is not the only determining performance variable for the chromatographic separation of a high value-added bioproduct; recovery is also another important performance variable. The product recovery for the experimental GSSR run was determined by the following procedure. The concentration of the target peptide in the product fraction, c_p^{P}, can be determined by comparing the peak areas for the target peptide in two analytical chromatograms: one for the feed (top graph of Fig. 7.1) and the other for the collected product fraction (Fig. 7.8). Since the volumes of injected sample were the same in both chromatograms,

$$c_p^{\mathrm{P}} = \frac{A_p^{\mathrm{P}}}{A_p^{\mathrm{F}}} \frac{Q^{\mathrm{F}}}{Q^{\mathrm{P}}} c_p^{\mathrm{F}}, \tag{7.17}$$

where c_p^{F} is the solute concentration in the feed mixture, A_p^{F} is the peak area of the target solute in the analytical chromatogram of the feed mixture (Fig. 7.1), and Q^{F} is the flow rate at which the chromatogram was obtained; A_p^{P} is the peak area of the target peptide in the chromatogram of the product fraction from the

GSSR process (Fig. 7.8) and Q^{P} is the flow rate at which the corresponding chromatogram was obtained. In the present case, the values are $Q^{\mathrm{F}} = 0.558$ mL/min, $Q^{\mathrm{P}} = 0.631$ mL/min, $A_p^{\mathrm{F}} = 0.769$ mAU×min, $A_p^{\mathrm{P}} = 0.1145$ mAU×min, and $c^{\mathrm{F}} = 0.5295$ g/L. From Eq. (7.17), we get $c^{\mathrm{P}} = 0.089$ g/L. The amount of target solute injected per GSSR cycle is $f_p = c_p^{\mathrm{F}} F \Delta t_{\mathrm{F}} = (0.5295\ \text{g/L})(2\ \text{mL/min})(0.5\ \text{min}) = 0.529$ g and the amount of target solute collected per cycle in the purified cut is $m_p = c_p^{\mathrm{P}} Q_{\mathrm{P}} \Delta t_{\mathrm{P}} = (0.089\ \text{g/L})(5.7\ \text{mL/min})(1\ \text{min}) = 0.505$ g (note that for the GSSR cycle under analysis, $Q_{\mathrm{P}} = Q_{\mathrm{A}}$); therefore, the product recovery is $rec_p = m_p/f_p = 0.505/0.529 = 95.3\%$.

7.4.1 Comparison with single-column batch chromatography

We have determined by simulation the optimal operation of single-column batch chromatography with linear solvent gradient, and compared its performance with that of the 30-cycle GSSR experiment for the same amount of stationary phase and same amount of feed injected per cycle. The best solvent-gradient policy for the batch process that maximizes the recovery of the target peptide for purity specifications above 90% turns out to be isocratic elution. To see why this is so, first notice that the Henry constants given in Table 7.1 decrease monotonically with the EtOH concentration (c_0) in the solvent. But more importantly, however, is that the selectivities between the target peptide and its two neighbor impurities, α_{21} and α_{32}, where

$$\alpha_{ij} = \frac{1 + \beta K_i}{1 + \beta K_j} \tag{7.18}$$

and $\beta = (1 - \epsilon)/\epsilon$ is the phase ratio, also follow the same trend with respect to c_0. Since the batch process does not achieve baseline separation of the target product from its two neighbor impurities at the lowest EtOH concentration considered in the GSSR experiments ($c_{0,\min} = 0.25$ v/v), the three peaks will elute even closer to each other if the value of c_0 is increased. Thus, the optimal solvent-gradient policy for the batch process that maximizes the recovery is isocratic elution with $c_0 = c_{0,\min}$.

Figure 7.9 shows the numerical results of maximizing the recovery, rec_p, achieved by the batch process for purity specifications $pur_p \geq (pur_p)_{\min}$ in the range $0.9 \leq (pur_p)_{\min} \leq 0.98$. The amounts of stationary phase and feed injected per cycle are the same as those for the 30-cycle GSSR experiment. Figure 7.9 shows that the GSSR process performs considerably better than the batch process: in the experimental GSSR run 95.3% of the target product was recovered with 98% purity, whereas only

52% of the product would be recovered at the same purity with the batch process.

Since there is a single outlet in a one-column system, it is not possible to reject waste fractions—e.g., one containing the most weakly retained impurities—early in the cycle through intermediate waste outlets as in a multicolumn system. This imposes a constraint on the minimum length of the cycle for the batch process, which has a direct impact on its productivity. The GSSR process, on the other hand, is not limited by this constraint. As a result, the productivity achieved in the 30-cycle GSSR experiment is 4.2 times higher than the productivity that would be achieved with the batch process for the same purity specification of 98%.

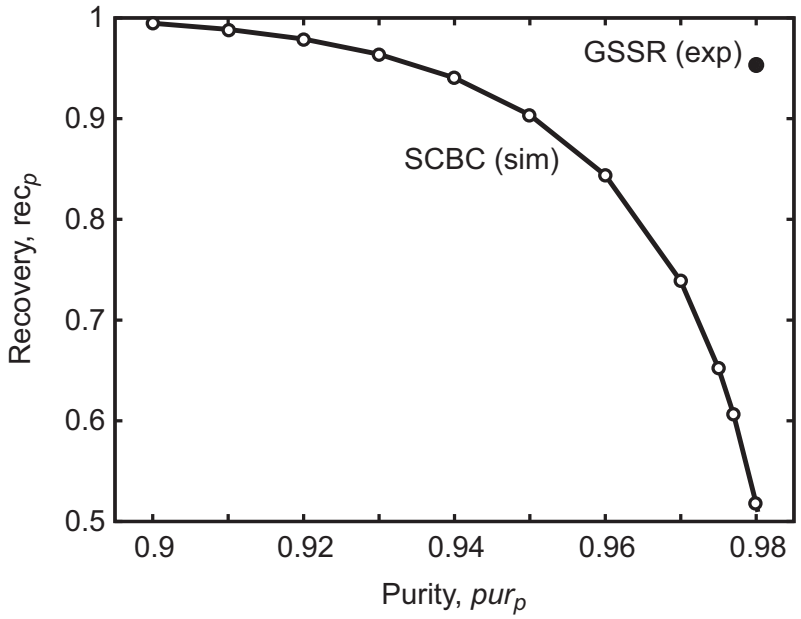

Figure 7.9: Simulated curve of optimal product recovery (rec_p) versus purity (pur_p) for single-column batch chromatography (SCBC) subject to the same amount of stationary phase and amount of feed injected per cycle as in the 30-cycle GSSR experiment. The open circles are the optimal numerical solutions of the maximization of rec_p for the batch process subject to the purity constraint $pur_p \geq (pur_p)_{\min}$, for various values of $(pur_p)_{\min}$; the closed circle gives the performance of the experimental GSSR run.

7.5 Conclusions

A new multicolumn, open-loop process for center-cut separation by solvent-gradient chromatography has been introduced. The process combines the simulated countercurrent operation of a moving solvent gradient with steps of pulsed feed injection and product withdrawal at fixed positions in a train of columns. With the use of multiple columns, better solvent gradients can be implemented and the cuts can be

manipulated more flexibly. Moreover, by means of the port switching it is possible to recycle some of the mixed cuts from the downstream end of the system to its upstream end, thereby increasing product recovery. We have shown that this can be done while working in a simple, open-loop system that resembles the batch system.

The experimental results presented here show that the GSSR process can separate an intermediate retained component from complex mixtures of biomolecules with nearby-eluting impurities, with high purity without sacrificing the product recovery. The GSSR experiments reported here were performed under diluted, linear conditions, which necessarily limits the assessment of the process performance to purity and recovery. For example, it is difficult to report on specific productivity and solvent consumption for a linear system; under those conditions, one cannot discuss about absolute values and the best we can do is to compare productivity and solvent consumption between processes for the same amount of stationary phase. For example, if the value of $F\Delta t_{\mathrm{F}} rec_p/\tau_{\mathrm{cyc}}$ is higher for process x than for process y, then the productivity of process x is higher than that of process y, and a similar reasoning can be applied to the solvent consumption; we have followed this procedure above to compare the performance of the GSSR process and that of the batch process.

The GSSR process also appears to be easy to control, as we have demonstrated by dynamically adjusting the value of the switching interval to correct the position of the moving composition profile in the GSSR loop with respect to the outlet ports. Upcoming research will provide further demonstrations that the GSSR process can perform difficult separations better and more efficiently than the current batch gradient process, and will compare its performance against those of other competing processes under conditions not limited by the feed concentration.

References

[1] A Abbood, C Smadja, C Herrenknecht, Y Alahmad, A Tchapla, and M Taverna. Retention mechanism of peptides on a stationary phase embedded with a quaternary ammonium group: A liquid chromatography study. *Journal of Chromatography A*, 1216(15):3244–3251, 2009.

[2] Fabrice Gritti and Georges Guiochon. Influence of a buffered solution on the adsorption isotherm and overloaded band profiles of an ionizable compound. *Journal of Chromatography A*, 1028(2):197–210, 2004.

[3] Fabrice Gritti and Georges Guiochon. Role of the buffer in retention and adsorption mechanism of ionic species in reversed-phase liquid chromatography: I. analytical and overloaded band profiles on kromasil-c18. *Journal of Chromatography A*, 1038(1):53–66, 2004.

[4] Marco Mazzotti, Giuseppe Storti, and Massimo Morbidelli. Optimal operation of simulated moving bed units for nonlinear chromatographic separations. *Journal of Chromatography A*, 769(1):3–24, 1997.

[5] Niklas Jakobsson, Marcus Degerman, and Bernt Nilsson. Optimisation and robustness analysis of a hydrophobic interaction chromatography step. *Journal of Chromatography A*, 1099(1):157–166, 2005.

[6] Marcus Degerman, Niklas Jakobsson, and Bernt Nilsson. Constrained optimization of a preparative ion-exchange step for antibody purification. *Journal of Chromatography A*, 1113(1):92–100, 2006.

[7] Marcus Degerman, Niklas Jakobsson, and Bernt Nilsson. Modeling and optimization of preparative reversed-phase liquid chromatography for insulin purification. *Journal of Chromatography A*, 1162(1):41–49, 2007.

[8] Georges Guiochon, Sadroddin Golshan Shirazi, and Anita M Katti. Fundamentals of preparative and nonlinear chromatography. 1994.

[9] Douglas Morris Ruthven. Principles of adsorption and adsorption processes. 1984.

[10] José PB Mota and João MM Araújo. Single-column simulated-moving-bed process with recycle lag. *AIChE journal*, 51(6):1641–1653, 2005.

[11] João MM Araújo, Rui CR Rodrigues, and José PB Mota. Use of single-column models for efficient computation of the periodic state of a simulated moving-bed process. *Industrial & engineering chemistry research*, 45(15):5314–5325, 2006.

[12] João MM Araújo, Rui CR Rodrigues, and José PB Mota. Optimal design and operation of a certain class of asynchronous simulated moving bed processes. *Journal of Chromatography A*, 1132(1):76–89, 2006.

[13] Rui CR Rodrigues, João MM Araújo, Mário FJ Eusébio, and José PB Mota. Experimental assessment of simulated moving bed and varicol processes using a single-column setup. *Journal of Chromatography A*, 1142(1):69–80, 2007.

[14] Eric Valery and Olivier Ludemann-Hombourger. Method and device for separating fractions of a mixture, February 2 2007. WO Patent 2,007,012,750.

8

Adenovirus purification by two-column, size-exclusion, simulated countercurrent chromatography

8.1 Introduction

Viral vectors are playing an increasingly important role in the vaccine and gene therapy fields. Adenoviruses (Ads), in particular, are considered one of the most suitable platforms for production of viral vaccines and gene therapy vectors; they are medium-sized (90–100 nm), nonenveloped, icosahedral viruses composed of a nucleocapsid and linear, non-segmented double stranded (ds) DNA genome that is about 36 kb long. Their broad tissue tropism and large transgene packing capacity make them attractive candidates for innovative virotherapies [1]. Adenoviruses can be produced in a complementary cell line in both adherent and suspension culture systems, such as HEK-293 or PER-C6 cells, or A549 for oncolytic therapies [2, 3].

The use of recombinant adenoviruses for vaccination and gene therapy requires fast and highly efficient purification protocols that yield high recoveries of infectious particles, maintain viral infectivity, and effectively remove contaminating DNA and host cell proteins, while also concentrating the viral samples for final delivery. The concentration of adenoviruses is critical not only to obtain high titer vector stocks, but also to reduce the handled volume; the latter accelerates the downstream

processing and keeps the scalability of the purification train at a manageable level.

The downstream processing of complex biopharmaceuticals, such as recombinant proteins, antibodies or vaccines, is gaining increasing importance in order to fulfil the requirements for a reliable production process with high purity and yield, and, also importantly, cost efficiency [4]. The downstream purification train of biopharmaceuticals has been extensively developed in the past years by combining different chromatography steps, namely ion-exchange and size-exclusion chromatography (and less frequently affinity chromatography), intermingled with concentration and ultra/diafiltration steps [1, 5–9].

Currently, the most frequently adopted approach is sequential, discontinuous processing of the clarified bioreaction bulk. Typically, the target product is separated from process-related impurities through a series of steps wherein a selected cut or fraction of the effluent from the previous step is selectively adsorbed and desorbed onto a given stationary phase using time and elution conditions as manipulated variables, until, ultimately, yielding the product purified to the desired level. Unlike other industries, biotechnology is late to embrace continuous processing, mainly due to the fact that innovation in this industry has traditionally been more product than process oriented [10]. However, the increasing interest in vaccines and gene therapy, together with the need to decrease the cost per dose, has led to the development of new chromatographic tools [11–14].

The classical approach for adenovirus purification consists of three major steps — clarification, concentration/purification, and polishing — applied sequentially: (i) clarification of the harvested bioreaction bulk to remove cell and cell debris; (ii) ultra/diafiltration; (iii) anion exchange; (iv) ultra/diafiltration step to concentrate the product; and (v) size-exclusion chromatography as a final polishing step. The size-exclusion chromatography step is carried out last mainly because of its low productivity and high product dilution. Usually in this final step the amount processed is reduced by 50 to 100 fold.

The purpose of the clarification is to efficiently remove cell debris and large aggregates (product- or process-related), while maintaining and protecting the product quality in the flow-through stream. The concentration step reduces the volume of clarified bulk by effectively removing low molecular weight HCP, fragmented HC DNA, and possibly fragmented, product-related impurities, e.g., viral proteins. This step is a key factor for decreasing the upfront investment in downstream equipment and materials. If detergent was used to disrupt the cells, the diafiltration removes the detergent and associated lipids from the cells.

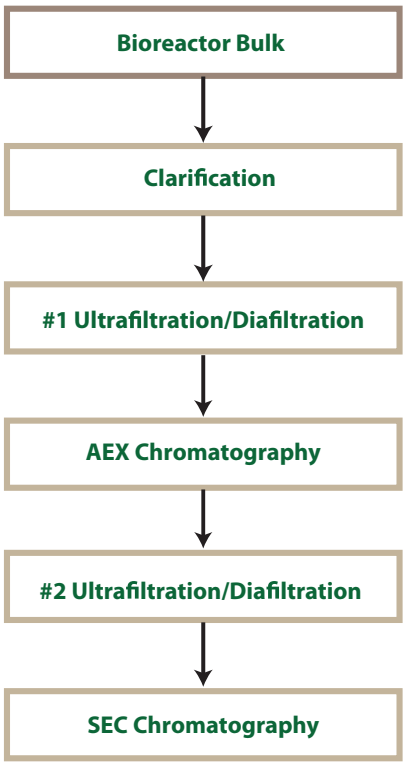

Figure 8.1: Standard batch downstream train for virus purification. The bioreactor bulk is treated with triton and benzonase and subsequently clarified. Two Ultra/diafiltration steps are required before of the chromatography unit operation.

Polishing is a critical step for the purification of biopharmaceuticals; purity is mandatory and product quality/potency must be as high as possible, or as defined in the corresponding requirements, so that its final clinical application is effective and safe. Therefore, this step is typically quite challenging as it should resolve impurities — either process- or product-related — very closely related to the product of interest.

It is often the case that IEX chromatography is used vertically within the DSP strategy, as it easily fits from early capture to final purification steps. IEX is typically operated in positive (bind-elute) mode: most of the impurities are collected in the flow-through pool, while the virus particles and some of the impurities are retained in the matrix. Due to the differences in charge of the different components, it is possible to use this process with high resolution elution gradients, separating the adsorbed materials into fractionated cuts, even though they are closely related. Size-exclusion chromatography (SEC) and ultra/diafiltration (usually by TFF) are two other widely used processes at the very latest stage for formulating the product. Both rely on molecule size, making them suitable for buffer exchange, the former permitting milder conditions. It is often argued that TFF scales more easily (by

increasing the membrane area) because in the latter case the load should not normally exceed 10% of the column bed volume.

Unlike the rather expensive affinity chromatography, which achieves good recovery yields based on immobilized metal affinity, heparin, or others, IEX chromatography is generally much more affordable at large scales and offers a broad spectrum of stationary phases for the capture of virus particles.

One process-based way to reduce the overall cost of the downstream chromatographic steps cost of goods (CoG) can be obtained by using continuous chromatography permitting higher throughput, lower buffer consume, higher capacity utilization and reducing column volume, hence increased productivity. Simulating moving bed is a practical implementation of the concept of the true moving-bed (TMB), where instead of one column with a moving solid phase, a series of several columns with fixed beds are used[15, 16]; its use is widely applied for small molecules and binary separations, in particular with chiral compounds under isocratic elution conditions[17–19].

Studies concerning continuous processing have been performed mostly with proteins and monoclonal antibody (mAb)[10, 20–22]; this is primarily because biopharmaceutical industry is dominate by those bioproducts. To date the purification of large biomolecules such as virus, has rarely been explored[23]. Despite the advantages of a continuous chromatography, biopharmaceutical industry is somehow sceptical in moving toward a multi-column chromatography. This is, in part, due to the increase in complexity in terms of process validation. However, the implementation of single use and ready-to-process technologies are mitigating these issues, therefore there is room for exploring a single compact and efficient multi-column chromatographic process.

In the present work the use of a simple semi-continuous, open-loop, two-column countercurrent chromatographic process was studied. The separation of adenovirus serotype 5 (Ad5) was established by using a size-exclusion resin under isocratic elution. Size-exclusion chromatography (SEC) is a well-known technique, widely used in biochromatography to separate smaller contaminants from large biomolecules while a gentle process without adsorption phenomena occurring between the stationary phase and the target product. SEC has been used for both polishing and intermediate purification of adenoviruses[1, 24–26]. However, it is often claimed that the main drawbacks of SEC are its low productivity and scale-up difficulties, thus a costly unit operation. Nevertheless, moving from a batch towards a semi-continuous process the earlier mentioned problems can be easily overcame.

In the present work the size-exclusion chromatography step is applied after the first ultra/diafiltration step. The reason is to challenge the size-exclusion unit operation in order to prove that, once productivity is no longer an issue, the classic scheme can be changed to meet specific needs in terms of reduction of cost of goods or purity requirements. Eglon et al. [1] showed that advantages of placing the size-exclusion chromatographic step earlier in the process, followed by anionic exchange, with the elimination of the intermediated concentration/buffer exchange step. It worth pointing out that the purity level required by the authorities is usually expressed as amount of DNA and HCP per dose; this implies that several purification steps may be required for applications whose therapeutic dose is very high (i.e., gene therapy), whereas for VLP or mucosa vaccine few steps may be sufficient to reach the desired purity level. For this reason, the performance of our process is always reported in terms of percentage of impurity clearance.

In Clearance of the contaminants, namely DNA and host cell protein (HCP) were assessed. The process performance were also evaluated concerning the productivity and buffer consumption compared to a standard batch process.

8.2 Material and Methods

8.2.1 Cell line and medium

Two hundred and ninety-three (293) cells purchased from ATCC (ATCC-CRL-1573) were adapted to suspension and grown in a commercial serum-free medium, Ex-Cell 293 (SAFC Biosciences, USA), supplemented with 4 mM of glutamine (Invitrogen, UK), in a humidified atmosphere of 8% CO_2 in air at 37°C using shake flasks (Corning, USA). The cells were routinely propagated twice a week using an inoculum of 0.5×10^6 cells/mL. Cell concentration and viability were determined by counting cells on a Fuchs-Rosenthal haemocytometer (Brand, Germany) using the trypan blue (Invitrogen, UK) dye exclusion method.

8.2.2 Virus production

We used a replication-defective adenovirus derived from serotype 5 adenovirus (Ad5) expressing GFP protein. The viruses were produced in a 2 L bioreactor with 1 L working volume (Sartorius-Stedim Biotech, Germany). The agitation rate

was set at 70 rpm and the dissolved oxygen was controlled at 50% air saturation by gas mixing and stirred cascade control with an airflow of 0.01 L/min; the pH was controlled at 7.2 by aeration with a gaseous CO_2 mixture and 1 M $NaHCO_3$; all infections were done at a cell concentration (CCI) of 10^6 cells/mL using a multiplicity of infection (MOI) of 5; the adenoviruses were harvested at 48 hpi (hours post-infection). The amount of infections particples (IP) in the bulk (before purification) was in the range 10^9–10^10 IP/mL.

8.2.3 Clarification and concentration

Upon harvesting, the bioreaction bulk was supplemented with 0.1% Triton X100 (Sigma Aldrich, MO, USA) and incubated for 2 hours at 37°C with 50 U/ml of Benzonase (Merck Millipore, Germany) to digest the DNA and to release the adenoviral vectors from the intracellular material by cell lysis.

Subsequently, the bulk was microfiltrated using a Sartopore 2 membrane capsule (Sartorius Stedim Biotech, Germany) comprising a 0.8 μm prefilter and a 0.45 μm filter, and concentrated up to 10 times and diafiltered up to 5 times with 20 mM Tris & 150 mM NaCl at pH 8 on a Sartorius Stedim Biotech cassette prototype with an average cut-off of 750 kDa. Before use, the capsules were washed with one capsule volume of Milli Q water and two capsule volumes of buffer. The bulk was stored in aliquots at -80°C until further use.

8.2.4 Analytics

The protocol for the quantification of total viral particles was a two-step procedure: DNA extraction according to the instructions on the “High Pure Viral Nucleic Acid Kit” (Roche) manual and real-time PCR. The number of viral DNA copies was determined by real-time PCR and LightCycler system (Roche Diagnostics) using a Fast Start DNA master SYBR Green I kit to track a specific Ad5 sequence (Roche Diagnostics). Internal plasmid of $4.15 \times 10^9/2\mu l$ was chosen as reference standard. The total particle concentrations were confirmed using Nanosight NS500 (NanoSight Ltd, UK), and the size distribution was determined. The average of the two measures was the value chosen for assessing the virus recovery yield. Protein profile analysis was performed in 4–12% NuPage gradient pre-cast gels (Invitrogen). The gels were stained by Coomassie Instant Blue (Expedeon Ltd, UK) and the protein concentration was determined using BCA kits (Pierce, Rockford,

USA) and bovine serum albumin (BSA) as the standard protein. The protein were precipitated using 99% ethanol and incubated overnight at -20°.C

The amount of host cell protein (HCP) was determined using a commercial available ELISA kit for HEK293 cell line (Cygnus Technologies, Inc.). The sample was diluted in PBS and the assay was performed according to the manufacture protocol, the 96 well plate was read by an absorbance microplate reader at 450/650 nm (SpectraMax 340). DNA was quantified by QuanT-iT Picogreen kit (Invitrogen). After 5 minutes of incubation, the fluorescence was measured by Luminometery (Turner BioSystems). Purified DNA was used as standard.

8.2.5 Chromatography

Size exclusion chromatography (SEC) is based on the well-established ability of size exclusion (SE) media — also referred to as gel filtration (GF) media — to separate molecules according to differences in molecular size as they pass through a GF medium packed in a column. The selected size-exclusion medium was Sepharose 4 Fast Flow (S4FF, GE Healthcare), which is supplied by the manufacturer with an average particle size of 90 μm (range of 45–165 μm). S4FF is based on a highly cross-linked 4% agarose matrix, which gives good physical stability and chromatographic qualities; its exclusion limit for globular proteins is ca. 3×10^7. The S4FF matrix enables processing of large volumes, making it suitable for use at process scale.

The very first data employed to design the process was the chromatogram for a small injection of the clarified bioreaction bulk on a XK 26/40 column (GE Healthcare; i.d. of 2.6 cm, maximum bed height of 40 cm) at a flow rate of 3 mL/min (data not shown). By noting that the resolution in SEC varies with the square root of bed height, we estimated that the total bed height could be reduced to around 20–25 cm while keeping a reasonable separation between the virus peak and its closest impurity. We thus aimed at packing two columns with a bed height of ca. 10–12 cm.

Two XK 26/20 chromatographic columns (i.d. of 2.6 cm, maximum bed height of 20 cm) were slurry packed with S4FF according to the manufacturer's specifications. The excess ethanol supplied with SF44 was decanted and replaced with working buffer (20 mM Tris, 150 mM NaCl, pH 8) before packing into the columns. The columns were initially filled with 70% slurry of S4FF and allowed to settle by gravity overnight. The flow rate was then increased in stepwise fashion up to

4 ml/min. The final, stabilized column lengths were 10.4 cm and 10.8 cm. No measures were taken to improve the balancing of the bed heights.

The UV absorbance of the effluent from each column was automatically monitored in real-time at 12 distinct wavelengths ranging from 230 nm to 300 nm using two USB4000 multiwavelength UV detectors (Ocean Optics, USA) with attenuator, sharing the same DH-2000-S-DUV light source (Micropack, Ostfildern, Germany) by means of a bifurcated optical fiber assembly. For each experiment, samples at every switches were collected and analyzed for virus and impurity contents.

After packing the columns, their efficiency was tested to check the quality of packing. The internal porosity was assessed using a high molecular weight (HMW) gel filtration calibration kit (GE Healthcare, Buckinghamshire, UK) containing 5 globular proteins with molecular weights in the range 44,000 to 669,000 and Blue Dextran (BD) 2000.

One should expect BD 2000 to be completely excluded from the S4FF's intraparticle porosity and the elution volume for BD 2000 should thus be equal to the column void volume, $V_\mathrm{o} = \epsilon_\mathrm{o} V_\mathrm{c}$, where V_c is the geometric column volume and ϵ_o is the interparticle porosity of the S4FF packing. We observed, however, that the elution volume for a short pulse of CsCl-purified Ad5 gave a smaller V_o than for BD. Therefore, the smaller of the two V_o values was taken as the better estimate of the true column void volume.

Table 8.1: Characterization of the two columns packed with Sepharose 4FF.

	Column 1	Column 2
V_c (cm^3)	55.2	57.3
L (cm)	10.4	10.8
V_o (cm^3)	16.8	15.2
N (–)	281	220

The total porosity, $\epsilon = \epsilon_\mathrm{o} + (1 - \epsilon_\mathrm{o})\epsilon_\mathrm{p}$, where ϵ_p is the intraparticle porosity, was estimated from the elution peak for a small injection of 2% acetone as tracer; for completeness, the number of theoretical plates (N) measured with this tracer was also calculated (Table 8.1). For a well-packed column of gel-filtration media the void volume V_o should be equivalent to approximately 30% of the total column volume V_c. Table 8.1 shows that this is indeed the case for our two columns.

Before each experiment the columns were sanitized with 1 M NaOH, washed with Milli Q water, and equilibrated with 5 bed volumes of running buffer (20 mM Tris, 150 mM NaCl, pH 8).

8.3 Mathematical Model

The perception of many practitioners is that (semi-)continuous multicolumn chromatography, such as the SEC process presented here, requires a lot of process data and modeling work to determine the design space, and, in many cases, careful fine tunning to make get the process working correctly. This has precluded the use of this technique in routine separation problems. While this may be true for the most challenging separation problems, say, those with complex solvent gradients operated under high loading conditions, it is certainly not the case for a SEC process.

We shall adopt a simple equilibrium-dispersive adsorption column breakthrough model for computer-aided design of the SEC step. The model can be written as

$$\epsilon_i \frac{\partial c_i}{\partial t} + \frac{Q}{V_\mathrm{c}} \left(\frac{\partial c_i}{\partial x} - \frac{h_i}{2} \frac{\partial^2 c_i}{\partial x^2} \right) = 0, \tag{8.1}$$

where t is the time coordinate, $x = z/L$ is the dimensionless axial coordinate along the packed bed, L and V_c are the length and volume of the column, i is the solute index, c is the solute concentration in the mobile phase, and Q is the volumetric flow rate of mobile phase.

The symbol ϵ_i denotes the volumetric fraction of the chromatographic column that is accessible to component i (i.e., the overall porosity of the packed bed that is probed by component i); ϵ_i can be expressed as

$$\epsilon_i = \epsilon_\mathrm{o} + (1 - \epsilon_\mathrm{o}) H_i, \quad H_i = \epsilon_\mathrm{p} \int_{d_{\mathrm{m},i}}^{\infty} \psi(\sigma)\, d\sigma, \tag{8.2}$$

where ϵ_o is the interparticle porosity, ϵ_p is the intraparticle porosity, and $\psi(\cdot)$ is the pore size distribution of the size exclusion medium,[1] i.e., $\psi(\sigma)\, d\sigma$ is the fraction of the porous volume of a Sepharex 4FF particle with pore diameters between σ and $\sigma + d\sigma$; $d_{\mathrm{m},i}$ is the size of the biomolecule (including any existing hydration layer). Equation 8.1 is subject to the following boundary conditions:

$$c_i - \frac{h_i}{2} \frac{\partial c_i}{\partial x} = c_i^{\mathrm{in}} \quad \text{for} \quad x = 0, \tag{8.3}$$

$$\frac{\partial c_i}{\partial x} = 0 \quad \text{for} \quad x = 1, \tag{8.4}$$

[1] The function $\psi(\cdot)$ is normalized distribution, $\int_0^\infty \psi(\sigma)\, d\sigma = 1$, and $\Psi(d_{\mathrm{m},i}) \equiv \int_{d_{\mathrm{m},i}}^\infty \psi(\sigma)\, d\sigma$ can be regarded as the exclusion factor for a biomolecule of size $d_{\mathrm{m},i}$.

where $c_i^{\mathrm{in}}(t)$ is the inlet concentration of component i.

In our simple model the column efficiency is measured by the dimensionless plate height, $h_i = L/N_i$, where N_i is the number of theoretical plates for component i. The approximate additivity of the effects of axial dispersion, external mass transfer resistance, and diffusion for linear systems was demonstrated long ago by various authors (e.g., by Haynes and Sarma [] using moments analysis). This means that in the modeling of chromatographic columns under inert or linear equilibrium conditions it is seldom worth modeling the band broadening using a more complex descriptor than an overall effective dispersion coefficient (or, alternatively, and overall effective rate coefficient) incorporating both effects of axial dispersion and the various mass transfer resistances. Using the additivity of linear resistances, the dimensionless plate height for a SEC column can be expressed as

$$\frac{h_i}{2} = \frac{1}{Pe_{\mathrm{o}}} + \left(\frac{vd_{\mathrm{p}}}{4L}\right)\frac{1}{\beta}\left(1-\frac{\epsilon_{\mathrm{o}}}{\epsilon_i}\right)^2\left(\frac{2}{3k_{\mathrm{f},i}} + \frac{d_{\mathrm{p}}}{15D_{\mathrm{p},i}}\right), \tag{8.5}$$

where $\beta = (1-\epsilon_{\mathrm{o}})/\epsilon_{\mathrm{o}}$ is the phase ratio, $k_{\mathrm{f},i}$ is the external film resistance coefficient, d_{p} is the particle diameter, and $D_{\mathrm{p},i}$ is the intraparticle diffusion coefficient; $Pe_{\mathrm{o}} = vL/D_{\mathrm{L}}$ is the hydrodynamic Péclet number, which under typical preparative flow rate conditions is inversely proportional to the particle diameter and independent of the fluid velocity, i.e., $Pe_{\mathrm{o}} \approx L/\gamma d_{\mathrm{p}}$, where γ is a constant with a value of about 0.5. If the biomolecule is completely excluded from the gel then $\epsilon_i = \epsilon_{\mathrm{o}}$ and $h_i/2 = 1/Pe_{\mathrm{o}}$.

To design the SEC process it is necessary to measure the retention volume of each component, to determine the value of ϵ_i, and the extent of band broadening at the working flow rate, to determine the value of h_i. We used PeakFit to quickly estimate the location, area, and broadening of the peaks. These data were then used as initial guess in a more accurate deconvolution procedure, which fits the superposition of multiple solutions of eq. 8.1 (one for each component) without neglecting the non-infinitesimal size of the injected sample.

The results of this approach are given in Fig. 8.2 which shows the chromatograms for injections of a small volume of the clarified bioreaction bulk into columns 1 and 2 separately and into the two columns coupled in series. Pulse experiments A and B refer to injections into column 2 and column 1, respectively. The black line is the experimental chromatogram (UV signal) whereas the colored lines are the deconvolution of the peaks. The blue line depicts the virus peak. Figures C and D show the experiments performed on the two columns arranged in series. The

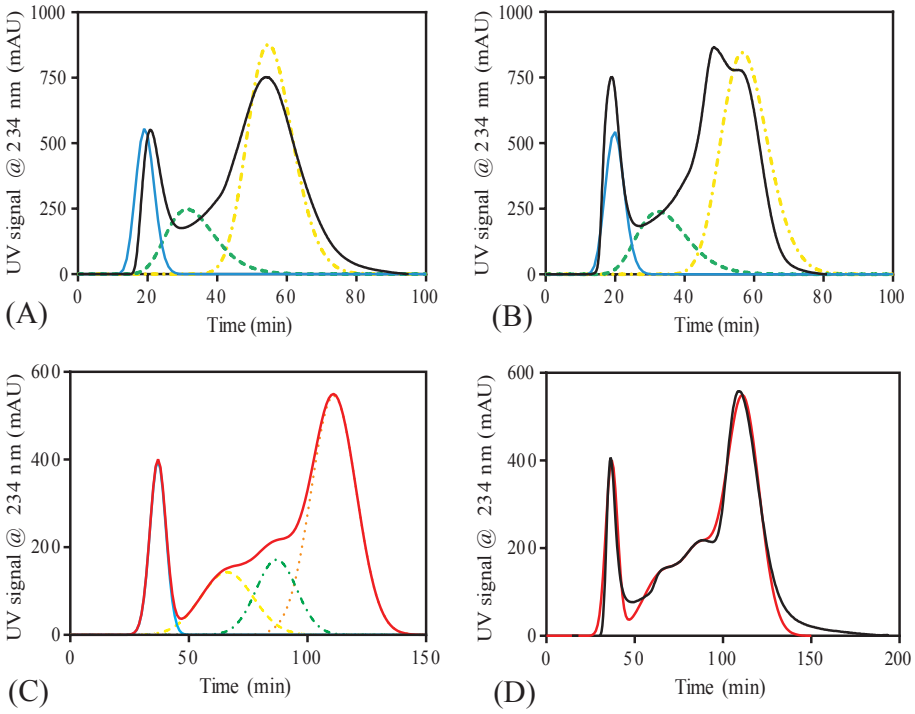

Figure 8.2: Pulse experiments A and B represent columns 2 and 1 respectively. The black line correspond to the experimental chromatogram while the color line indicate the deconvolution of the peaks. The blue line depicts the virus peak. Figure C and D shows the two columns in series, impurity were gathered into three main groups and modeled according. The red line represent the modeled chromatogram, whereas the black line is the experimental one.

complex multicomponent mixture in the bioreaction bulk impurity is modeled as a simpler mixture of fours key components: (1) the virus, which is the largest species and, hence, the earliest eluting species; (2) a large impurity that elutes close to the virus; (3) an intermediate impurity that elutes after the larger impurity; (4) and a small impurity that is the last eluting species. The red line represent the modeled chromatogram, obtained by superposing the individual chromatograms for the four key components.

Table 8.2 lists the model parameters derived from analysis of pulse experiments performed on the two columns placed in series.

8.4 Cycle Design

Fig. 8.3 shows a schematic of the set of feasible flow diagrams for designing the operating cycle for the class of two-column, open-loop SEC processes considered in the present work; they represent the alternative configurations that can be

Table 8.2: Model parameters derived from analysis of pulse experiments performed on the two columns placed in series. i is the component index, c^{F} is the feed concentration, which is assumed to be proportional to the area under the UV absorbance peak (arbitrary units s.t. $\sum_i c_i^{\mathrm{F}} = 1$), ϵ is the accessible porosity, and N is the number of theoretical plates per column.

i	1	2	3	4
c_i^{F}	0.140	0.165	0.154	0.541
ϵ_i	0.306	0.564	0.750	0.945
N_i	61	18	51	69

considered for the implementation of any given step of the cycle. The set includes the following configurations: (a) directing the flow to the next column; (b) adding an external stream to the circulating flow; (c) freezing one column (temporarily stopping the flow through the column); and (d) withdrawing the effluent from one column while injecting an external stream into the other column. In this class of two-column, open-loop SEC processes the flow through a column is always in one of three states: (i) frozen, (ii) completely directed to the next column, or (iii) entirely diverted to either the product line or the waste line.

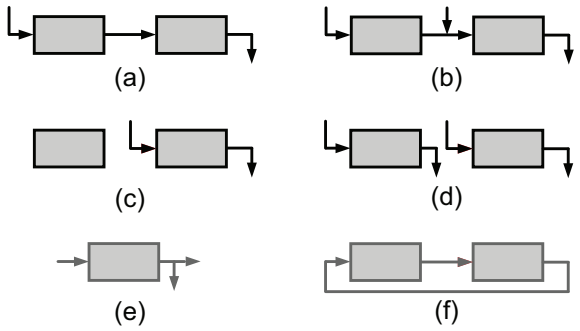

Figure 8.3: Set of suitable flow-path configurations for the design of a two-column, open-loop SEC process without partial splitting of exit streams: (a) complete direction of flow to the next column; (b) flow addition to circulating stream; (c) frozen bed; (d) complete withdrawal and flow injection at the same node. Partial splitting of an exit stream and closed-loop recirculation are given by configurations e and f, respectively.

We have purposively excluded from the set of feasible configurations those in which the flow exiting one column is split into two or more streams — schematic *e* illustrates what is meant by split flow — or in which the flow is recirculated in closed loop (schematic *f*). The reason for discarding these configurations is to avoid the use of flow controllers or an extra pump; our objective is to design a SEC process that is physically realizable with simple two- or three-way valves to control the flow paths in the system and requires a minimum number of pumps — one for injecting the feed and another for injecting the mobile phase.

In a two-column SEC process the cycle is divided into two equal-length time intervals, which we shall henceforth refer to as switch intervals. To design the cycle it suffices to define the sequence of flow-line configurations for one of the switch intervals; the sequence for the other twin switch interval is similar, but the positions of the two columns are exchanged. The sequence for a switch interval is defined as a serial arrangement of flow-line configurations taken from the set shown in Fig. 8.3. To each flow-path configuration one has to assign (i) the positions of columns 1 and 2, (ii) the nature of each inlet (feed or eluent), and (iii) the nature of each outlet (product or waste). Although this picture may sound too theoretical to the downstream processing engineer, we advocate that this process-systems-engineering view of the downstream process, and of the SEC step in particular, is very helpful, as it very clearly establishes the

In practice, it is easier to keep the columns fixed in space and to move the positions of the inlet and outlet lines by means of an automated arrangement of two- or three-way valves.

A rigorous model-based optimization approach was employed to determine the optimal operating parameters. The purpose of the nonlinear programming problem (NLP) is to guarantee the fulfillment of product and process specifications, such as minimal purities and maximal operating flow rates, while optimizing process performance in terms of productivity and eluent consumption. Using the parameters in Tables 1 and 2 we designed the cycle depicted in Fig. 8.4. Each switching interval is divided into four sub-steps:

Step 1. The upstream column is eluted while the effluent of the downstream column is diverted to the waste line.

Step 2. The upstream column is eluted but its effluent is diverted to the waste line instead of being directed to the downstream column. The downstream column is fed with the clarified bioreaction bulk while is effluent is collected as purified product.

Step 3. The system is operated as in step 1 but the effluent of the downstream column is collected as product.

Step 4. The upstream column is eluted but its effluent is again diverted to the waste line instead of being directed to the downstream column. The downstream column is kept frozen, that is, the flow through the column is temporarily halted.

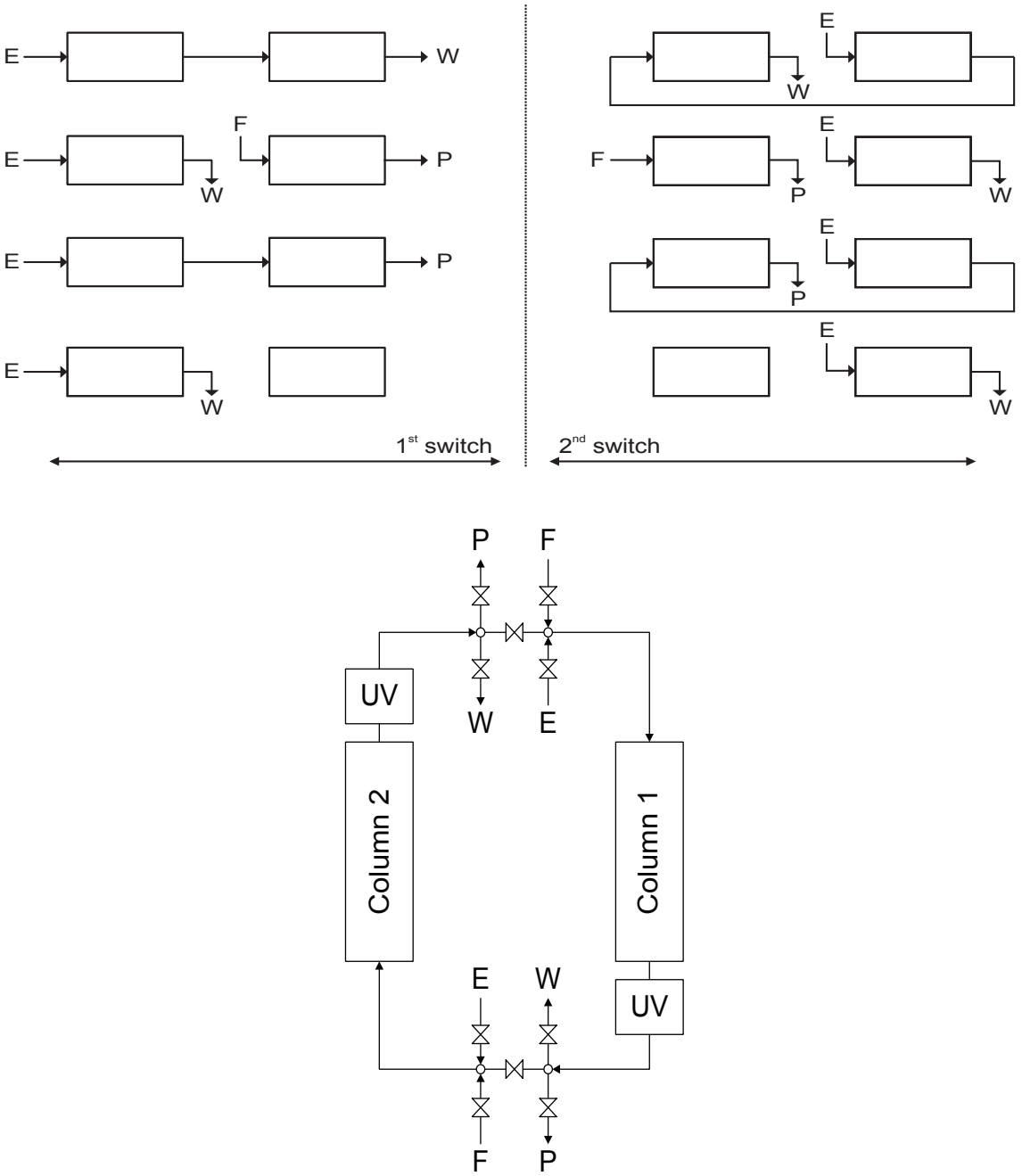

Figure 8.4: Top figure, show a schematic representation of operating cycle for the two-column, semi-continuous open loop process. E denotes the eluent inlet; F,the feed inlet,P and W present the product and waste outlet respectively. On the bottom the scheme of the two-column unit is shown. For each column 5 switching valves are associated with.UV detectors are present at the outlet of the columns.

Figure 8.5 shows the simulated axial concentration profiles of the key components in the two columns at the start of each sub-step of the switching interval.

Figure 8.6 shows the simulated temporal profiles of the key components at the outlet of each column during the first switching interval of the cycle.

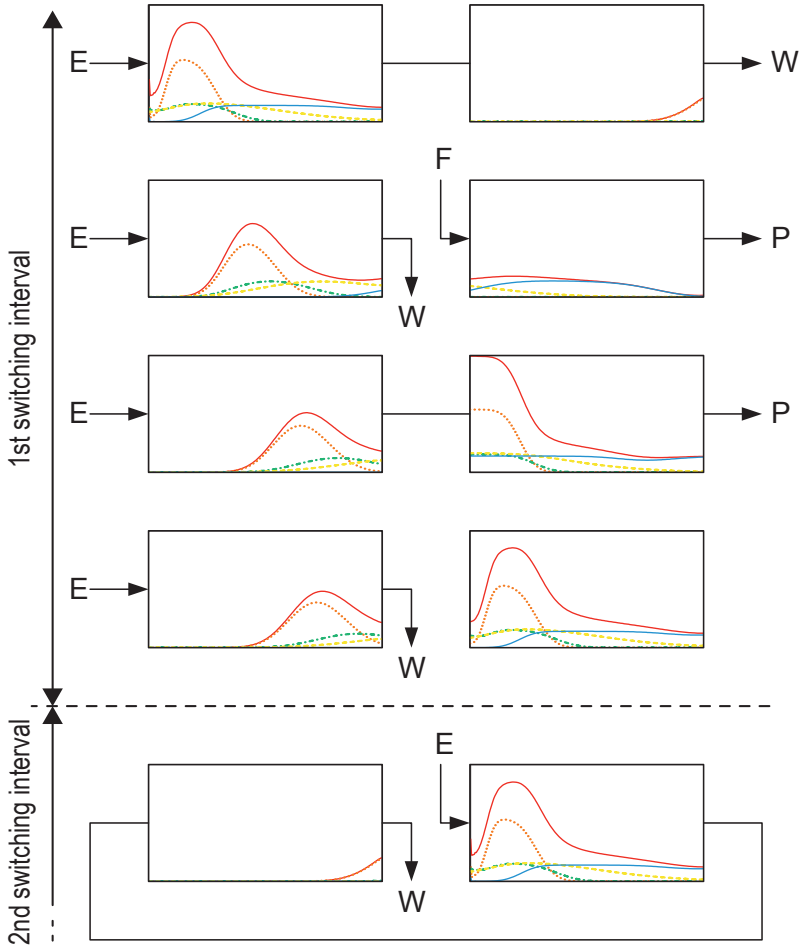

Figure 8.5: Steady state profile at the inlet/outlet of the first switching interval of the two columns operating according to the scheme in figure 2. Over the second interval the columns undergo the same steps but their positions is exchanged.Blue lines denotes the virus as less retain product. Yellow line represent the most retained product, most likely DNA fragments.

8.5 Results and Discussion

The cycle was implemented experimentally in laboratory prototype unit. The unit was operated for five cycles, which was more than enough to attain the cyclic steady state. Fig. 8.7 compares the temporal profile of the UV signal measured experimentally at the outlet of column 2 and the simulated profile. The agreement between the experimental and simulated profiles is fairly good.

Table 8.1 shows the evaluated process performance for the two-column system compared to the standard single-column batch process for the same amount of gel permeation medium. The virus recovery yield was determined by RT-PCR and Nanosight quantification. The protein profile analyzed by SDS-PAGE. The products (P1 and P2) from the operational point for the cycle 4 and 5 were analyzed. For

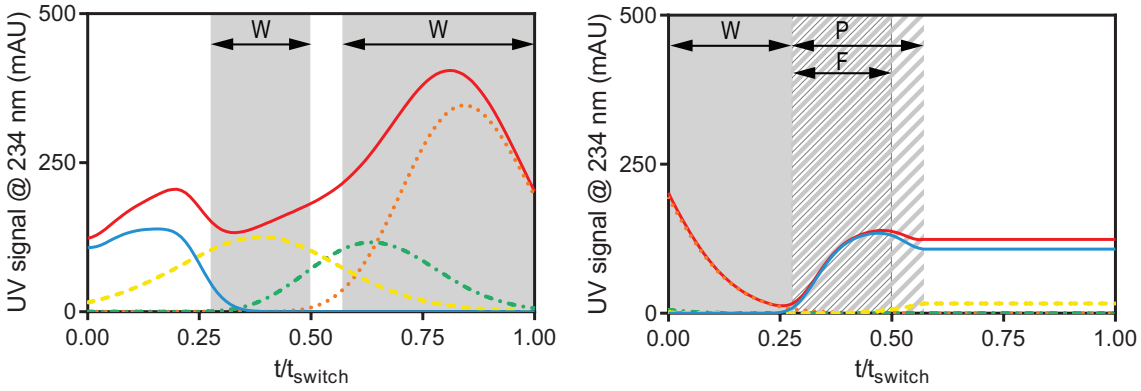

Figure 8.6: Modeled profile of the two-column during the semi-continuous cycle. The figure on the left displays the profile at the outlet of the second column, whereas the profile of the outlet of the fist column is displayed on the right. The waste fractions are indicated in gray while product is evidenced by the strips pattern.The blue and red lines denote the virus and the overall predicted UV signal, respectively.

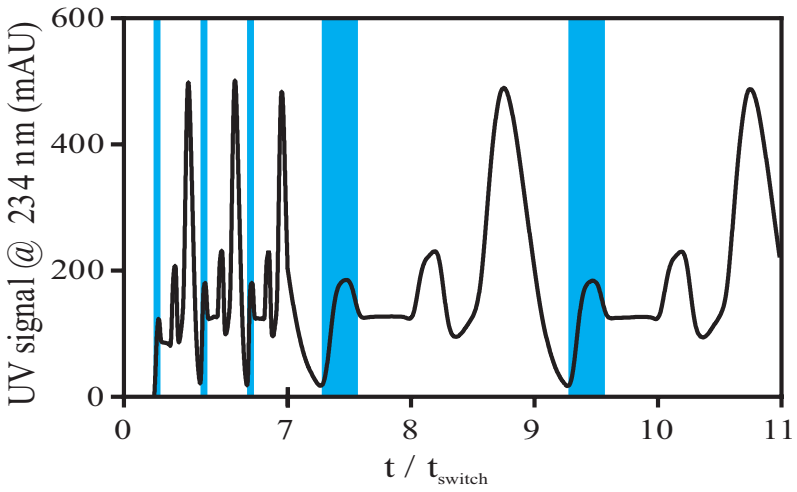

Figure 8.7: Experimental chromatogram representing the automatic column cycling during the continuous SEC purification. The window in gray displays the virus fraction.

each line 15μg of protein were loaded. The protein related to the adenovirus capside, namely hexon, penton and core are marked within the red boxes.

It is seen that DNA clearance and HCP clearance achieved with our two-column process are identical to those obtained with the traditional process. However, the virus recovery yield is increased from 57% to 86% and the productivity is boosted by 6-fold. This is a clear demonstration that with this increased productivity, size exclusion can do much more than just final polishing and buffer exchange in the downstream train of a biopurification. It worth to point out that the purity level required by the authorities is usually expressed as amount of DNA and host cell protein per dose, this implies that for application where the theraputic dose is very

Table 8.3: Process performance for the two-column system compared to a batch process. Virus recovery yield was determined by RT-PCR and Nanosight quantification.

Productivity L min^{-1}	Virus Recovery Yield [%]	DNA Clearance [%]	HCP Clearance [%]
2-columns process			
0.67	86.3	90	89
Batch process			
0.11	57.4	94	94

high (i.e gene therapy) several steps can be required, whereas for VLP or mucose vaccine few steps can be enough to reach the desired purity level. For this reason in the work presented the performance of the 2-column simulated chromatography is always indicated in terms of % clearance.

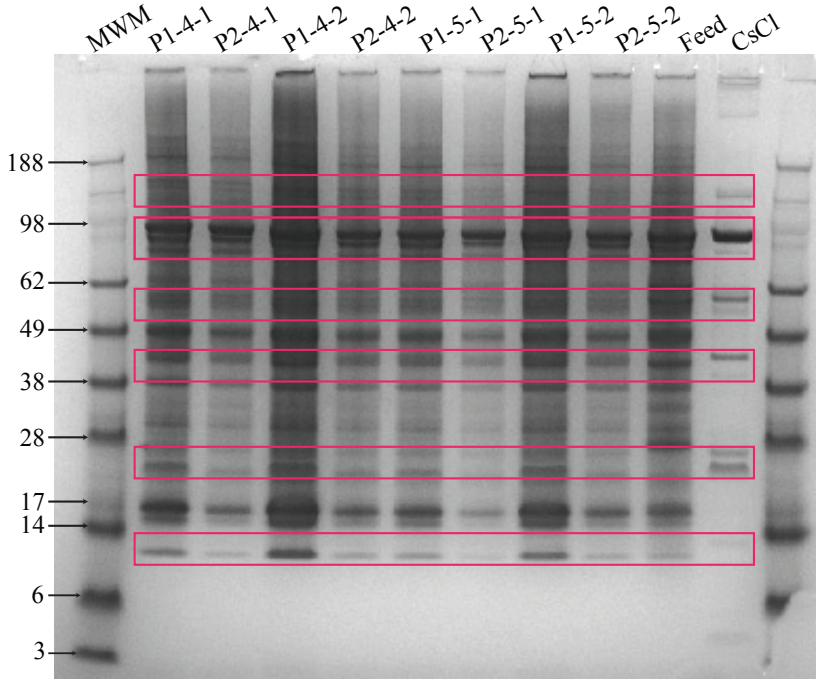

Figure 8.8: Protein profile analyzed by SDS-PAGE. The products (P1 and P2) from the operational point for the cycle 4 and 5 were analyzed. For each line 15μg of protein were loaded.The protein related to the adenovirus capside, namely hexon, penton and core are marked within the red boxes.

8.6 Conclusions

In the present work, we report on the successful separation of adenovirus serotype 5 (Ad5) by size exclusion chromatography using a simple, yet efficient, two-column, semi-continuous, simulated moving-bed process operated in an open-loop configuration. Clearance of impurities, namely DNA and host cell protein (HCP), were experimentally assessed. Our results showed a virus recovery yield of 86%, and a clearance of 90% and 89% for DNA and HCP, respectively. These figures compare very favorably against single-column batch chromatography for the same volume of size-exclusion resin. In conclusion, the main drawbacks of size-exclusion chromatography, namely lower productivity and product dilution, and scale up difficulties, were easily overcome by an innovative two-column configuration that keeps the mixed fractions inside the system at all times.

References

[1] Marc N. Eglon, Aoife M. Duffy, Timothy O'Brien, and Padraig M. Strappe. Purification of adenoviral vectors by combined anion exchange and gel filtration chromatography. *J.Gene Med.*, 11(11):978–989, 2009.

[2] Maria M Segura, Raul Alba, Assumpcio Bosch, and Miguel Chillon. Advances in helper-dependent adenoviral vector research. *Curr. Gene Ther.*, 8(4):222–235, 2008.

[3] Amine Kamen and Olivier Henry. Development and optimization of an adenovirus production process. *J.Gene Med.*, 6(S1):S184–S192, 2004.

[4] Jun Wang, Rene Faber, and Mathias Ulbricht. Influence of pore structure and architecture of photo-grafted functional layers on separation performance of cellulose-based macroporous membrane adsorbers. *J. Chromatogr. A*, 1216 (37):6490–6501, 2009.

[5] John O. Konz, Ann L. Lee, John A. Lewis, and Sangeetha L. Sagar. Development of a purification process for adenovirus: controlling virus aggregation to improve the clearance of host cell dna. *Biotechnol. Prog.*, 21(2):466–472, 2005.

[6] John O. Konz, Rebecca C. Livingood, Andrew J. Bett, Aaron R. Goerke, Michael E. Laska, and Sangeetha L. Sagar. Serotype specificity of adenovirus purification using anion-exchange chromatography. *Hum. Gene Ther.*, 16(11):1346–1353, Nov 2005.

[7] E. Burova and E. Ioffe. Chromatographic purification of recombinant adenoviral and adeno-associated viral vectors: methods and implications. *Gene Ther.*, 12 Suppl 1:S5–17, Oct 2005.

[8] C. Peixoto, T. B. Ferreira, M J T. Carrondo, P. E. Cruz, and P. M. Alves. Purification of adenoviral vectors using expanded bed chromatography. *J. Virol. Methods*, 132(1-2):121–126, Mar 2006.

[9] Aaron R. Goerke, Brian C S. To, Ann L. Lee, Sangeetha L. Sagar, and John O. Konz. Development of a novel adenovirus purification process utilizing selective precipitation of cellular dna. *Biotechnol. Bioeng.*, 91(1):12–21, Jul 2005.

[10] Rahul Godawat, Kevin Brower, Sujit Jain, Konstantin Konstantinov, Frank Riske, and Veena Warikoo. Periodic counter-current chromatography – design and operational considerations for integrated and continuous purification of proteins. *Biotechnol. Journal*, 7(12):1496–1508, Dec 2012.

[11] Milos Barut, Ales Podgornik, Peter Brne, and Ales Strancar. Convective interaction media short monolithic columns: enabling chromatographic supports for the separation and purification of large biomolecules. *J. Sep. Sci.*, 28(15): 1876–1892, Oct 2005.

[12] William Riordan, Steve Heilmann, Kurt Brorson, Kannan Seshadri, Yi He, and Mark Etzel. Design of salt-tolerant membrane adsorbers for viral clearance. *Biotechnol. Bioeng.*, 103(5):920–929, Aug 2009.

[13] Tiago Vicente, René Fáber, Paula M Alves, Manuel JT Carrondo, and José PB Mota. Impact of ligand density on the optimization of ion-exchange membrane chromatography for viral vector purification. *Biotechnology and bioengineering*, 108(6):1347–1359, 2011.

[14] Dong-Sop Lee, Byong-Moon Kim, and Dai-Wu Seol. Improved purification of recombinant adenoviral vector by metal affinity membrane chromatography. *Biochem. Biophys. Res. Commun.*, 378(3):640–644, Jan 2009.

[15] Ricardo JS Silva, Rui CR Rodrigues, and José PB Mota. Relay simulated moving bed chromatography: Concept and design criteria. *J. Chromatogr. A*, 1260:132–142, 2012.

[16] Andreas Seidel-Morgenstern, LC Keßler, and Malte Kaspereit. New developments in simulated moving bed chromatography. *Chem. Eng. Tech.*, 31(6): 826–837, 2008.

[17] Arvind Rajendran, Galatea Paredes, and Marco Mazzotti. Simulated moving bed chromatography for the separation of enantiomers. *J. Chromatogr. A*, 1216(4):709–738, 2009.

[18] Eric R Francotte and Paul Richert. Applications of simulated moving-bed chromatography to the separation of the enantiomers of chiral drugs. *J. Chromatogr. A*, 769(1):101–107, 1997.

[19] Pedro Sá Gomes, Mirjana Minceva, and Alírio E Rodrigues. Simulated moving bed technology: old and new. *Adsorption*, 12(5-6):375–392, 2006.

[20] Martin Kratli, Thomas Muller-Spath, and Massimo Morbidelli. Multifraction separation in countercurrent chromatography (mcsgp). *Biotechnol. Bioeng.*, 10.1002/bit.24901, 2013.

[21] Veena Warikoo, Rahul Godawat, Kevin Brower, Sujit Jain, Daniel Cummings, Elizabeth Simons, Timothy Johnson, Jason Walther, Marcella Yu, Benjamin Wright, Jean McLarty, Kenneth P. Karey, Chris Hwang, Weichang Zhou, Frank Riske, and Konstantin Konstantinov. Integrated continuous production of recombinant therapeutic proteins. *Biotechnol. Bioeng.*, 109(12):3018–3029, Dec 2012.

[22] Lars Aumann and Massimo Morbidelli. A continuous multicolumn countercurrent solvent gradient purification (mcsgp) process. *Biotechnol. Bioeng.*, 98 (5):1043–1055, Dec 2007.

[23] D. A. Homeman, M. Ottens, L. A. M. Van der Wielen, D. Van Roosmalen, L. J. P. Van der Broeke, and J. T. F. Keurentjes, EP1461246 (2004).

[24] E Burova and E Ioffe. Chromatographic purification of recombinant adenoviral and adeno-associated viral vectors: methods and implications. *Gene Ther.*, 12: S5–S17, 2005.

[25] Bernd Kalbfuss, Michael Wolff, Robert Morenweiser, and Udo Reichl. Purification of cell culture-derived human influenza a virus by size-exclusion and anion-exchange chromatography. *Biotechnol. Bioeng.*, 96(5):932–944, 2007.

[26] Vladimir Slepushkin, Nancy Chang, Reuben Cohen, YUXIANG Gan, BING Jiang, E Deausen, D Berlinger, G Binder, K Andre, L Humeau, et al. Large-scale purification of a lentiviral vector by size exclusion chromatography or mustang q ion exchange capsule. *Bioprocess J.*, 2:89–95, 2003.

9

Conclusions and Future Work

9.1 Conclusions

In the present thesis we have exploited several simulated counter-current adsorption based processes both experimentally and theoretically.

A two-column open-loop system previously proposed by our group was assessed experimentally and numerically with a nonlinear enantiomeric separation while exploring two different elution strategies. The results have proven the effectiveness of the presented scheme for the chosen binary separation. The two-column SMB process demonstrated to be a real alternative to single-column batch chromatography with recycling. This new unit couples the simplicity of the batch system with the high performance of the continuous process. It has a minimum equipment requirement, since it uses only two pumps to supply feed and desorbent into the system, while the flow rates of liquid withdrawn from the system are controlled by material balance using simple two-way valves. This type of operation implicitly discards the flow splitting at an active outlet, in this sense, the product, waste or recycling fractions are always obtained by completely directing the effluent over a certain period of the cycle to the appropriate destination.

This strategy of handling the product outlets was also explored in the Relay SMB. For this class of processes we derive a SMB analog — the R-SMB process and demonstrate, under the framework of the equilibrium theory, that this process

has the same separation region as the classical SMB for linear adsorption systems. In the framework of equilibrium theory is was possible to show that the R-SMB process consists of two distinct cycles that differ only in their intermediate sub-step depending on the selectivity of a given separation. The analogy with the standard SMB in terms of displaced volumes of fluid per switch interval could be maintained in the R-SMB process while using simple two-way valves to control the flow-rates of liquid withdrawn from the system by material balance.

Despite the advantages of a continuous chromatography, biopharmaceutical industry is somehow skeptical about moving to multi-column chromatography. This is, in part due to the increase in complexity in terms of process validation. In this sense the current thesis shows two different approaches possible to the biopurification challenges. The GSSR process, particularly suited for ternary separations, exploits the advantages of a countercurrent adsorption process combined with a cyclic solvent gradient operation. This process was experimentally validated in a pilot unit, using a test-case of a crude mixture of peptides. The two-column open-loop system presented in the last chapter of this thesis aimed at the purification of adenovirus. The designed process was successfully applied in a size exclusion system under isocratic elution conditions. The simplicity of the design cycle and ease of operation are comparable to common batch chromatographic operation, with the additional advantage of incorporating the benefits of coutercurrent operation.

9.2 Suggestions for future work

In the last decade the paradigm for chromatographic separation has substantially changed, mostly due to an emerging area of opportunity for continuous chromatography in the field of biotechnological downstream processing. Here, the productions demands represents the kilogram to low ton range at best, for compounds with high added value, such as recombinant proteins or monoclonal antibodies. The developed tools and schemes have proved to be powerful instruments at the research level and seem suitable for this low level of production scale. Following this line of opportunity, further developments should be investigated.

The application of gradient elution profiles in the developed two-column schemes is a possibility not yet exploited and could lead to an important process in the biotechnology world as well the evolution of the process from binary separation to a center-cut behavior can also be an important path for further developments.

Another subject that could be of interest is the operation with different types of packed beds. This could lead to a process intensification of the downstream separation processes, where usually it is necessary to perform several steps of purification, each one with a characteristic yield.

Regenerative medicine based on stem cells has been changing the way medicine is practiced today and hopefully will revolutionize healthcare over the next years. Although there has been significant research focused on the optimization of current cell culture systems, much less has been targeted at the development of efficient and scalable downstream processes in order to obtain a significant number of these cells for cell therapy in a cost-effective approach, while maintaining their bioactivity.

The separation of cells by phenotype from heterogeneous mixtures (e.g. whole blood) has applications in a wide range of fields in medicine and biology. One of the major challenges for tissue engineering will be the separation of stem cells in large scale. On this subject there is a huge need for novel cost-effective scalable separation processes with high resolution. Among the many stem cell separation methods, affinity-based approaches are the most efficient and reliable due to the high specificity of antibodies that recognize stem cell surface markers. For positive cell isolation, cells of interest are labeled and bind to the column while unlabeled cells pass through. For negative cell isolation, unwanted cells are labeled for depletion and bind to the column while cells of interest pass through and are untouched.

As we have seen, although nowadays the chromatographic processes are available for different fields and scales, there is still room for the application and improvement of this technology, either by the creation of new markets, like in the case of the growing interest in biotechnological products, or by the appearance of new technologies that can change the spectrum of the possible compounds obtained by chromatography.